Bayerische
Julius-Maximilians-Universität
Würzburg

Fakultät für Chemie und Pharmazie

Theoretical investigations on the spectroscopy of molecular aggregates

Dissertation

zur Erlangung

des naturwissenschaftlichen Doktorgrades

der Julius-Maximilians-Universität Würzburg

vorgelegt von

Joachim Seibt

Würzburg, 2009

Eingereicht am: .....

bei der Fakultät für Chemie und Pharmazie

1. Gutachter: .....

2. Gutachter: .....

der Dissertation

1. Prüfer: .....

2. Prüfer: .....

3. Prüfer: .....

des öffentlichen Promotionskolloquiums

Tag des öffentlichen Promotionskolloquiums: .....

Doktorurkunde ausgehändigt am: .....

Contents

Chapter 1

Introduction

The properties of functional organic materials strongly depend on intermolecular interactions [1]. As the applications for those materials in organic solar cells and molecular electronics [2–5] are of great importance, research activities in this area are increasingly promoted. In this context, the contribution of theoretical chemistry, especially quantum dynamics, consists of the investigation of intermolecular interactions on energy transfer processes in molecular aggregates. In the so-called "diabatic" representation [6], the potential energy surfaces, which belong to different electronic states describing a localized excitation, are coupled by off-diagonal potential matrix-elements. The latter lead to a splitting of the excited state potential curves in an adiabatic picture. Depending on the relative orientation of the transition dipole moments of the monomer units within the molecular aggregate, different relative intensities for spectroscopic vibronic transitions are found, which lead to characteristic band-structures in the absorption spectrum. If only the energetically lowest or highest band is excited, the system is specified as a J- and H-aggregate, respectively [7]. As the excitation energy is delocalized and movable within the aggregate in general, it is called a molecular exciton [8].

For the quantum dynamical description of molecular aggregates, both electronic couplings and vibrational degrees of freedom have to be included. Numerical investigations on the absorption spectroscopy of such systems have first been performed by Fulton and Goutermann [9,10], where two electronic states including one vibrational degree of freedom for each monomer unit were regarded. This model was used later by Scherer and Fischer to simulate various experiments [11]. It was noted [12] that it is equivalent to the Jaynes-Cummings model describing a two level system interacting with a quantized electromagnetic field [13]. Also trimer systems have already been discussed [14]. The aggregate model can be extended, within further approximations, to larger polymers. Examples are given in the early work of Herzenberg and Briggs [15] and also more recent papers [16, 17]. All mentioned studies employed methods of time-independent quantum mechanics. This work takes another approach in applying wave-packet propagation techniques to describe the interaction of aggregates with an electromagnetic field. A time-dependent calculation of absorption-spectra [18–21] has the advantage that spectral features can be related to dynamical processes and in particular to the exciton migration within the aggregate. This connection is of central importance in the context of the present studies. Besides absorption spectroscopy, circular dichroism (CD) spectroscopy is also helpful to investigate the structure of molecular aggregates [22]. This underlying effect correlates to the difference in absorbance of a substance from right versus left circular polarized light [23]. The theory of optical activity, i. e., the property of matter to rotate the polarization vector of an incoming field, and its relation to CD has been summarized, e.g., by Condon [24], Cadwell and Eyring [25]. Although formulated about ten years ago [26], a time-dependent approach has not been applied to the calculation of CD-spectra

until recently [27].

Emission spectra provide an insight into the excited state properties and allow conclusions about exciton trapping effects. Such processes compete against exciton migration and therefore limit the exciton mobility [28]. Nevertheless, investigations on emission spectra of molecular aggregates are rare (see e.g. [29]).

The application of nonlinear electronic 2D-spectroscopy on molecular aggregates is a new interesting research field. Two dimensional spectroscopic techniques have first been developed in the context of NMR spectroscopy [30], where they are used to extract structural and dynamical information about molecules and solid state systems [31]. The employed pulse sequence schemes have been transferred to vibrational spectroscopy in the infrared [32–34] and electronic spectroscopy in the optical spectral range [35–39]. Theoretical aspects of femtosecond 2D-spectroscopy have been extensively discussed by Mukamel and co-workers [40–42]. The explicit treatment of vibrations in 2D-spectroscopy has been performed by Gallagher, Faeder and Jonas [43], and more recently by Egorova et al. [44]. The role of the relative orientation of the monomer transition dipole-moments in aggregates has been studied by Szoecs et al. for a two- [45], and also a four chromophore system [46]. All the mentioned studies relay on density-matrix approaches and mostly vibrations are not included. In this work, the results of wave function based calculations are presented with the aim to elucidate basic principles of vibronic 2D-spectroscopy.

The present dissertation is structured as follows: The first two chapters review the employed theoretical (chapter 2) and numerical (chapter 3) methods.

In chapter 4, the application of these methods to molecular aggregates is discussed.

Chapter 5 contains investigations on the dimer problem in terms of a reflexion principle.

The dependence of linear spectra on the geometry of molecular aggregates is discussed in chapter 6. For dimer and trimer systems, absorption-, CD- and emission-spectra are calculated by varying the relative orientations of the monomer units and the intermolecular coupling constants. Thereby the connection between the resulting spectra and the underlying quantum dynamics is illustrated. Furthermore, the theoretical investigations are applied to measured data of merocyanine and perylene bisimide aggregates.

As the preliminary dimer model includes no intermolecular degrees of freedom, which cannot be neglected, if a consistent picture of both absorption and emission spectra is to be found, an intermolecular torsional coordinate is introduced in chapter 7. The corresponding potential curves stem from quantum chemical calculations.

In chapter 8, vibronic 2D-spectra of monomers and dimers are investigated. Besides the general properties of 2D-spectra, the appearing features are related to the relative orientation of the monomer subunits in the dimer and the coupling between them.

The aim of this work is to provide a better insight in the spectroscopic properties of molecular aggregates using the time-dependent approach. It can be considered as a basis for further investigations within the GRK 1221.

Chapter 2

Theoretical basics

2.1 Quantum dynamical description of molecules

The description of time-dependent processes in molecules is based on the solution of the time-dependent Schrödinger equation

$$\hat{H}_{mol}\Psi\left(\vec{q},\vec{r},t\right)=i\hbar\frac{\partial\Psi\left(\vec{q},\vec{r},t\right)}{\partial t}, \tag{2.1}$$

where the molecular Hamiltonian

$$\hat{H}_{mol}=\hat{T}_{nuc}+\left(\hat{V}_{nuc-nuc}+\hat{T}_{el}+\hat{V}_{el-el}+\hat{V}_{nuc-el}\right)=\hat{T}_{nuc}+\hat{H}_{el} \tag{2.2}$$

contains the kinetic and potential energy contributions of nuclei ($\hat{T}_{nuc}+\hat{V}_{nuc-nuc}$) and electrons ($\hat{T}_{el}+\hat{V}_{el-el}$) as well as the interaction $\hat{V}_{nuc-el}$ between them. The nuclear and electronic coordinates are collectively denoted as $\vec{q}$ and $\vec{r}$, respectively. If an adiabatic expansion is applied to the total wave function

$$\Psi(\vec{q},\vec{r},t) = \sum_n \chi_n(\vec{q},t)\,\phi_n(\vec{r},\vec{q})\,, \tag{2.3}$$

and the electronic wave functions $\phi_n(\vec{r},\vec{q})$ fulfill the electronic Schrödinger equation

$$\hat{H}_{el}\phi_n(\vec{r},\vec{q}) = \hat{V}_n(\vec{q})\,\phi_n(\vec{r},\vec{q})\,, \tag{2.4}$$

electronic and nuclear motion can be separated under the assumption that derivatives of the electronic wave functions with respect to the nuclear coordinates can be neglected [47]. Then, the corresponding Schrödinger equation for the nuclear wave functions in the fixed electronic state (n)

$$\hat{H}_{nuc}\,\chi_{n,m}(\vec{q}) = \left(\hat{T}_{nuc} + \hat{V}_n(\vec{q})\right)\chi_{n,m}(\vec{q}) = E_{n,m}\chi_{n,m}(\vec{q}) \tag{2.5}$$

yields the vibrational eigenfunctions evolving in time as

$$\chi_{n,m}(\vec{q},t) = \chi_{n,m}(\vec{q},0)\exp\left(-\frac{iE_{n,m}t}{\hbar}\right). \tag{2.6}$$

A superposition of these eigenfunctions leads to the wave-packet

$$\psi(\vec{q},t) = \hat{U}_n(t)\,\psi(\vec{q},0) = \sum_m a_m\chi_{n,m}(\vec{q},0)\exp\left(-\frac{iE_{n,m}t}{\hbar}\right). \tag{2.7}$$

where the propagator $\hat{U}_n(t) = \exp(-i\hat{H}_n t)$ is employed and a_m are coefficients. In what follows, all operators act in the subspace of the nuclei if not specified otherwise.

2.2 Time-dependent calculation of linear spectra

According to time-dependent perturbation theory, the first-order expression for the excitation of a molecular system from the electronic ground state to an electronic excited state induced by an electric field $\vec{E}$, which interacts with the electric transition dipole moment $\vec{\mu}$, can be written as

$$\left|\psi_{\mu}^{(1)}\right\rangle \sim \int_{-\infty}^{t} dt'\, \hat{U}_e(t-t')\, W_{\mu}(t')\, \hat{U}_g(t')\, |\psi_0\rangle = |\psi_{\mu}(t)\rangle\,. \tag{2.8}$$

In this formula, $\hat{U}_g(t')$ and $\hat{U}_e(t-t')$ are the propagators in the electronic ground and excited state, respectively. The lowest vibrational eigenstate in the electronic ground state is denoted as $|\psi_0\rangle$. Furthermore, the interaction $W_{\mu}(t') = -\vec{\mu}\vec{\epsilon}f(t)$ appears in this expression, where $\vec{\epsilon}$ is the polarization vector and $f(t) = \frac{1}{2}\exp(-iEt)$ describes the time-dependence of the field. As the interaction starts at $t = 0$, negative times can be neglected in the integral. On this basis, the transition probability

$$P_{abs}(t) = \left\langle \psi_{\mu}^{(1)}(t) | \psi_{\mu}^{(1)}(t) \right\rangle \tag{2.9}$$

can be defined leading to the transition rate

$$\begin{aligned} R_{abs}(t) &= \frac{d}{dt} P_{abs}(t) \qquad (2.10)\\ &= \frac{d}{dt} \int_0^t dt_1 \int_0^t dt_2 \exp(i(E+E_g)(t_1-t_2)) \\ &\quad \left\langle \hat{U}_e(t-t_1)\, \vec{\epsilon}\, \vec{\mu}\, \psi_{g,0} | \hat{U}_e(t-t_2)\, \vec{\epsilon}\, \vec{\mu}\, \psi_{g,0} \right\rangle \\ &= \int_0^t dt_1 \exp(i(E+E_g)(t_1-t)) \left\langle \hat{U}_e(t-t_1)\, \vec{\epsilon}\, \vec{\mu}\, \psi_{g,0} |\, \vec{\epsilon}\, \vec{\mu}\, \psi_{g,0} \right\rangle \\ &+ \int_0^t dt_2 \exp(i(E+E_g)(t-t_2)) \left\langle\, \vec{\epsilon}\, \vec{\mu}\, \psi_{g,0} | \hat{U}_e(t-t_2)\, \vec{\epsilon}\, \vec{\mu}\, \psi_{g,0} \right\rangle, \end{aligned}$$

which depends on the energy E and contains the ground state energy E_g. Changing the variables of integration to $\tau = t_1 - t$ and $\tau = t - t_2$ in the first and second time integral, respectively, leads to

$$\begin{aligned} R_{abs}(t) &= \int_{-t}^{0} d\tau \exp(i(E+E_g)\tau) \left\langle \hat{U}_e(-\tau)\ \vec{\epsilon}\,\vec{\mu}\ \psi_{g,0}\right| \vec{\epsilon}\,\vec{\mu}\ \psi_{g,0}\Big\rangle \\ &+ \int_{0}^{t} d\tau \exp(i(E+E_g)\tau) \left\langle\ \vec{\epsilon}\,\vec{\mu}\ \psi_{g,0}|\hat{U}_e(\tau)\ \vec{\epsilon}\,\vec{\mu}\ \psi_{g,0}\right\rangle, \end{aligned} \quad (2.11)$$

so that in the limit of $t \to \infty$, the absorption-spectrum

$$\sigma_{abs}(E) \sim \int_{-\infty}^{\infty} dt \exp(i(E+E_g)t)\ c_{abs}(t). \quad (2.12)$$

is obtained [18,48], which corresponds to a Fourier transformation of a time-correlation function

$$c_{abs}(t) = \left\langle \vec{\epsilon}\,\vec{\mu}\ \psi_{g,0}\ |\ \hat{U}_e(t)\ \vec{\epsilon}\,\vec{\mu}\ \psi_{g,0}\right\rangle. \quad (2.13)$$

The standard, time-independent expression for the absorption-spectrum is obtained by introducing a complete set of final states $|f\rangle$ of energies E_f in the excited state and using the identity

$$\hat{U}_e(t) = \sum_f |f\rangle \exp(-iE_f t) \langle f|, \quad (2.14)$$

so that

$$\begin{aligned} \sigma_{abs}(E) &\sim \int_{-\infty}^{\infty} dt \exp(i(E+E_g)t) \\ &\quad \left\langle \vec{\epsilon}\,\vec{\mu}\ \psi_{g,0}\ |\ \sum_f |f\rangle \exp(-iE_f t) \langle f|\ \vec{\epsilon}\,\vec{\mu}\ \psi_{g,0}\right\rangle \\ &= \sum_f \langle \vec{\epsilon}\,\vec{\mu}\ \psi_{g,0}\ |f\rangle \langle f|\ \vec{\epsilon}\,\vec{\mu}\ \psi_{g,0}\rangle \int_{-\infty}^{\infty} dt \exp(i(E+E_g-E_f)t) \\ &\sim \sum_f \langle \vec{\epsilon}\,\vec{\mu}\ \psi_{g,0}\ |f\rangle \langle f|\ \vec{\epsilon}\,\vec{\mu}\ \psi_{g,0}\rangle\ \delta(E-(E_f-E_g)), \end{aligned} \quad (2.15)$$

where a property of the δ -function is used [49]. In order to take broadening effects into account [50], a Gaussian function $\exp\left(-\beta t^2\right)$ is introduced in the final expression for the absorption-spectrum

$$\sigma_{abs}(E) \sim \int_{-\infty}^{\infty} dt \exp\left(i(E+E_g)t\right) c_{abs}\left(t\right) \exp\left(-\beta_{abs} t^2\right). \tag{2.16}$$

For the emission-spectrum, the corresponding formula

$$\sigma_{em}(E) \sim \int_{-\infty}^{\infty} dt \exp\left(-i(E+E_e)t\right) c_{em}\left(t\right) \exp\left(-\beta_{em} t^2\right), \tag{2.17}$$

is obtained, which contains the vibrational ground state energy in the electronic excited state E_e and the time-correlation function

$$c_{em}(t) = \left\langle \psi_{e,0} \middle| \, \vec{\epsilon}\, \vec{\mu}\, \hat{U}_g(t)\, \vec{\mu}\, \vec{\epsilon} \, \middle| \psi_{e,0} \right\rangle \tag{2.18}$$

with the vibrational ground state in the electronic excited states $|\psi_{e,0}\rangle$ as the initial function.

According to the theory of optical activity [51], in the case of CD-spectra an additional interaction term

$$W_m(t) = -\vec{m}\vec{B}(t) = -\vec{m}\left(\vec{k} \times \vec{\epsilon}\right) f(t) \tag{2.19}$$

has to be taken into account, which describes the interaction between the magnetic transition dipole moment $\vec{m}$ and the magnetic field $\vec{B}$. The wave vector is denoted as $\vec{k}$, while the other symbols are identical with the ones that have already been introduced above. The magnetic dipole interaction results in the first order state $\left|\psi_m^{(1)}(t)\right\rangle$, see Eq. (2.8) with $W_\mu(t)$ replaced by $W_m(t)$. The total wave function (to first order in the field-matter interaction) is then

$$\left|\psi^{(1)}(t)\right\rangle = \left|\psi_\mu^{(1)}(t)\right\rangle + \left|\psi_m^{(1)}(t)\right\rangle \tag{2.20}$$

giving rise to the transition probability

$$\begin{aligned} P(t) &= \left\langle\psi^{(1)}(t)|\psi^{(1)}(t)\right\rangle = \left\langle\psi_\mu^{(1)}(t)|\psi_\mu^{(1)}(t)\right\rangle + \left\langle\psi_m^{(1)}(t)|\psi_m^{(1)}(t)\right\rangle \\ &+ \left\langle\psi_m^{(1)}(t)|\psi_\mu^{(1)}(t)\right\rangle + \left\langle\psi_\mu^{(1)}(t)|\psi_m^{(1)}(t)\right\rangle . \end{aligned} \tag{2.21}$$

The first and second term correspond to an electric and magnetic dipole transition, respectively. Additionally, there is an interference term, which is important for CD-spectroscopy. This can be shown by specifying the polarization vector as

$$\vec{\epsilon} = \alpha_1\vec{\epsilon_1} + i\alpha_2\vec{\epsilon_2}, \tag{2.22}$$

where left and right polarized light are characterized by $\alpha_1 = \alpha_2 = 1$ and $\alpha_1 = 1, \alpha_2 = -1$, respectively. The first two terms in Eq. (2.21) correspond to the electronic and magnetic dipole transition and are of the form

$$\begin{aligned} \langle\vec{\epsilon}\,\vec{\mu}\;||\;\vec{\mu}\,\vec{\epsilon}\,\rangle &= |\alpha_1|^2\,\langle\vec{\epsilon_1}\,\vec{\mu}\;||\;\vec{\mu}\,\vec{\epsilon_1}\,\rangle \\ &+ |\alpha_2|^2\,\langle\vec{\epsilon_2}\,\vec{\mu}\;||\;\vec{\mu}\,\vec{\epsilon_2}\,\rangle\,, \\ \left\langle\left(\vec{k}\times\vec{\epsilon}\right)\,\vec{m}\;||\;\vec{m}\,\left(\vec{k}\times\vec{\epsilon}\right)\right\rangle &= |\alpha_1|^2\left\langle\left(\vec{k}\times\vec{\epsilon_1}\right)\,\vec{m}\;||\;\vec{m}\,\left(\vec{k}\times\vec{\epsilon_1}\right)\right\rangle \\ &+ |\alpha_2|^2\left\langle\left(\vec{k}\times\vec{\epsilon_2}\right)\,\vec{m}\;||\;\vec{m}\,\left(\vec{k}\times\vec{\epsilon_2}\right)\right\rangle, \end{aligned} \tag{2.23}$$

where $\vec{\mu}$ is real and $\vec{m}$ is imaginary. Also, the detailed form of the states like in Eq. (2.8) is not explicitly written down, which is indicated in writing the scalar product $\langle|\rangle$ as $\langle||\rangle$. The two terms (Eqs. 2.23) are identical for left and right polarization. On the other hand, the cross terms contain the expression

$$\left\langle \vec{\epsilon}\,\vec{\mu}\,||\,\left(\vec{k}\times\vec{\epsilon}\right)\,\vec{m}\right\rangle \tag{2.24}$$

and its conjugate complex. Inserting the form (Eq.(2.22)) for $\vec{\epsilon}$ and using the fact that $\vec{k}$ and $\vec{\epsilon}_{1,2}$ are orthogonal, one finds:

$$\begin{aligned}\left\langle \vec{\epsilon}\,\vec{\mu}\;||\;\vec{m}\;\left(\vec{k}\times\vec{\epsilon}\right)\right\rangle &= |\alpha_1|^2\,\langle\vec{\epsilon}_1\;\vec{\mu}\;||\;\vec{m}\;\vec{\epsilon}_2\,\rangle - |\alpha_2|^2\,\langle\vec{\epsilon}_2\;\vec{\mu}\;||\;\vec{m}\;\vec{\epsilon}_1\,\rangle \\ &- i\alpha_1\alpha_2\left(\langle\vec{\epsilon}_1\;\vec{\mu}\;||\;\vec{m}\;\vec{\epsilon}_1\,\rangle - \langle\vec{\epsilon}_2\;\vec{\mu}\;||\;\vec{m}\;\vec{\epsilon}_2\,\rangle\right). \end{aligned}\tag{2.25}$$

In calculating the sum of this expression and its conjugate complex, the terms with $|\alpha_n|^2$ cancel out and the result is:

$$\begin{aligned}&\left\langle \vec{\epsilon}\,\vec{\mu}\;||\;\vec{m}\;\left(\vec{k}\times\vec{\epsilon}\right)\right\rangle + \left\langle\vec{m}\;\left(\vec{k}\times\vec{\epsilon}\right)\;||\;\vec{\epsilon}\,\vec{\mu}\,\right\rangle \\ = \;& i\alpha_1\alpha_2\left[\langle\vec{\epsilon}_1\;\vec{m}\;||\;\vec{\mu}\;\vec{\epsilon}_1\,\rangle + \langle\vec{\epsilon}_2\;\vec{m}\;||\;\vec{\mu}\;\vec{\epsilon}_2\,\rangle\right. \\ - \;& \left.\langle\vec{\epsilon}_1\;\vec{\mu}\;||\;\vec{m}\;\vec{\epsilon}_1\,\rangle - \langle\vec{\epsilon}_2\;\vec{\mu}\;||\;\vec{m}\;\vec{\epsilon}_2\,\rangle\right] \\ = \;& i\alpha_1\alpha_2\left[\langle\vec{m}\,||\,\vec{\mu}\rangle - \langle\vec{\mu}\,||\,\vec{m}\rangle\right]. \end{aligned}\tag{2.26}$$

The remaining difference in the excitation probability of left and right polarized light is given as

$$P_{CD}(t) = P_L(t) - P_R(t) = -i\left(\langle\psi_m|\psi_\mu\rangle - \langle\psi_\mu|\psi_m\rangle\right) = 2\Im\left(\langle\psi_m|\psi_\mu\rangle\right), \tag{2.27}$$

where ($\Im$) denotes the imaginary part. As in the case of absorption the transition rate (i. e. the derivative of the transition probability with respect to time) in the limit of infinite times yields a CD-spectrum of the form

$$\lim_{t\to\infty} R_{CD}(t) = \sigma_{CD}(E) \sim \int_{-\infty}^{\infty} dt\exp(i(E+E_g)t)\;c_{\mu m}(t), \tag{2.28}$$

where the time-correlation-function reads

$$\begin{aligned} c_{\mu m}(t) &= \frac{1}{2i}\Big(\langle\psi_{g,0}|\ \vec{m}\,\hat{U}_e(t)\,\vec{\mu}\ |\psi_{g,0}\rangle \\ &- \langle\psi_{g,0}|\ \vec{\mu}\,\hat{U}_e(t)\,\vec{m}\ |\psi_{g,0}\rangle\Big). \end{aligned} \tag{2.29}$$

At $t = 0$, the propagator $\hat{U}_e(t)$ corresponds to the unity operator, and as the scalar products in Eq. (2.26) commutate with respect to a basis containing canonical basis vectors, the expression vanishes. Then it can be easily seen that

$$\begin{aligned} &\int_{-\infty}^{\infty} dE\ \sigma_{CD}(E) = \int_{-\infty}^{\infty} dt\ c_{\mu m}(t)\exp(iE_g t)\int_{-\infty}^{\infty} dE\exp(iEt) \\ = &\int_{-\infty}^{\infty} dt\ c_{\mu m}(t)\exp(iE_g t)\delta(t) = c_{\mu m}(0) = 0. \end{aligned} \tag{2.30}$$

This means that the CD-spectrum must posses negative and positive branches with equal area. Furthermore, the property

$$c_{\mu m}(-t) = c^*_{\mu m}(t) \tag{2.31}$$

ensures that the spectrum is real. Also, from a practical point of view, it means that the calculation of the time-correlation function $c_{\mu m}(t)$ has to be performed for either positive or negative times only.

2.3 Calculation of two-dimensional nonlinear spectra

Two-dimensional optical spectra originate from the interaction of three laser pulses with a material system. The total electric field is described as

$$\vec{E}\left(\vec{q},t\right)=\sum_{n=1}^{3}\vec{\epsilon}_{n}f_{n}\left(t-T_{n}\right)\cos\left(\omega_{n}\left(t-T_{n}\right)-\vec{k}_{n}\vec{x}\right), \tag{2.32}$$

where $\vec{\epsilon}_n$, $\vec{k}_n$ are the polarization and wave vectors and ω_n denote the laser frequencies. The envelope functions of the pulses ($f_n\left(t-T_n\right)$) are localized around the times T_n. The electric field induces a polarization in the medium [6, 52], which is

$$\vec{P}\left(t\right)=\left\langle \psi\left(t\right)\right|\vec{\mu}\left|\psi\left(t\right)\right\rangle , \tag{2.33}$$

with $\left|\psi\left(t\right)\right\rangle$ being the state vector of the system and $\vec{\mu}$ its dipole operator. In order to calculate third order nonlinear spectra, the corresponding polarization expansion term is needed, which is of the form

$$\vec{P}^{(3)}\left(t\right)=\left\langle \psi^{(0)}\left(t\right)\right|\vec{\mu}\left|\psi^{(3)}\left(t\right)\right\rangle +\left\langle \psi^{(1)}\left(t\right)\right|\vec{\mu}\left|\psi^{(2)}\left(t\right)\right\rangle +c.c., \tag{2.34}$$

where c.c. denotes the conjugate complex. The states appearing in the latter equation emerge from perturbation theory and have the general form

$$\left|\psi^{(0)}\left(t\right)\right\rangle = \hat{U}(t)\left|\psi_{i}\right\rangle \tag{2.35}$$

$$\left|\psi^{(1)}\left(t\right)\right\rangle = i\int_{-\infty}^{t}dt_{1}\,\hat{U}(t-t_{1})\left[\vec{E}(t_{1})\vec{\mu}\right]\hat{U}(t_{1})\left|\psi_{i}\right\rangle \tag{2.36}$$

$$\begin{aligned}\left|\psi^{(2)}\left(t\right)\right\rangle = {} & (i)^{2}\int_{-\infty}^{t}dt_{2}\int_{-\infty}^{t_{2}}dt_{1}\,\hat{U}(t-t_{2})\left[\vec{E}(t_{2})\vec{\mu}\right]\\ & \hat{U}(t_{2}-t_{1})\left[\vec{E}(t_{1})\vec{\mu}\right]\hat{U}(t_{1})\left|\psi_{i}\right\rangle \end{aligned} \tag{2.37}$$

$$\begin{aligned}\left|\psi^{(3)}\left(t\right)\right\rangle = {} & (i)^{3}\int_{-\infty}^{t}dt_{3}\int_{-\infty}^{t_{3}}dt_{2}\int_{-\infty}^{t_{2}}dt_{1}\,\hat{U}(t-t_{3})\left[\vec{E}(t_{3})\vec{\mu}\right]\\ & \hat{U}(t_{3}-t_{2})\left[\vec{E}(t_{2})\vec{\mu}\right]\hat{U}(t_{2}-t_{1})\left[\vec{E}(t_{1})\vec{\mu}\right]\hat{U}(t_{1})\left|\psi_{i}\right\rangle .\end{aligned} \tag{2.38}$$

In these equations, the initial state of energy E_i is denoted as $\left|\psi_i\right\rangle$. Below, only the case is taken into account, where the signals are detected in the

$\vec{k}_s = -\vec{k}_1 + \vec{k}_2 + \vec{k}_3$ direction. Therefore, the respective terms in the third-order polarization $\vec{P}^{(3)}(t)$ have to be determined. Under specific assumptions it is possible to reduce the number of terms essentially. In the analytical considerations presented below, a pulse overlap between f_1 and f_2, and also between f_1 and f_3 is excluded. The carrier frequencies of the pulses are taken to be equal, i. e. $\omega_n = \omega$. Furthermore, only resonant contributions are included, so that in the case of absorption $(+)$ and emission $(-)$ the fields are replaced by:

$$\vec{E}_n^{+}(\vec{q},t) = \frac{1}{2} f_n(t-T_n)\, e^{-i\omega_n(t-T_n)} e^{+i\vec{k}_n\vec{x}}, \tag{2.39}$$

$$\vec{E}_n^{-}(\vec{q},t) = \frac{1}{2} f_n(t-T_n)\, e^{+i\omega_n(t-T_n)} e^{-i\vec{k}_n\vec{x}}. \tag{2.40}$$

The number of terms contributing to the third-order polarization strongly depends on the model employed. In the most simple case, a monomer with two electronic states $(|g\rangle, |e\rangle)$, having a single vibrational degree of freedom q, is taken into account. In this case, the Hamiltonian reads

$$\hat{H}_M = |g\rangle \hat{H}_g(q) \langle g| + |e\rangle \hat{H}_e(q) \langle e|, \tag{2.41}$$

where the ground and excited state Hamiltonians are taken as

$$\hat{H}_g(q) = -\frac{1}{2}\frac{d^2}{dq^2} + \frac{1}{2}\omega_{vib} q^2, \tag{2.42}$$

$$\hat{H}_e(q) = -\frac{1}{2}\frac{d^2}{dq^2} + \frac{1}{2}\omega_{vib}(q-q_e)^2 + \Delta E \tag{2.43}$$

with the vibrational frequency ω_{vib}, the displacement q_e and the energy shift ΔE. The dipole moment connecting the ground with the excited state is:

$$\vec{\mu} = |e\rangle \vec{\mu}_{eg} \langle e| + cc, \tag{2.44}$$

where c.c. denotes the adjoint operator and $\vec{\mu}_{eg}$ is the transition dipole vector. Under the assumptions formulated above (and in particular that the pulses $\vec{E}_2$ and $\vec{E}_3$ are identical), the polarization into direction $\vec{k}_s = -\vec{k}_1 + \vec{k}_2 + \vec{k}_3$ (see Fig.(2.1)) contains two identical terms, so that

$$\vec{P}^{(3)}(t) = 2\left\langle \psi(21,t)\right| \vec{\mu} \left|\psi(3,t)\right\rangle . \tag{2.45}$$

The (nuclear) wave functions appearing in this expression are

$$\left|\psi(3,t)\right\rangle = i\int_{-\infty}^{t} dt_1\, \hat{U}_e(t-t_1)\left[\vec{E}_3^{+}(t_1)\vec{\mu}\right]\hat{U}_g(t_1)\left|\psi_i\right\rangle \tag{2.46}$$

$$\begin{aligned}\left|\psi(21,t)\right\rangle = {} & (i)^2\int_{-\infty}^{t} dt_2 \int_{-\infty}^{t_2} dt_1\, \hat{U}_g(t-t_2)\left[\vec{E}_2^{-}(t_2)\vec{\mu}\right] \\ & \hat{U}_e(t_2-t_1)\left[\vec{E}_1^{+}(t_1)\vec{\mu}\right]\hat{U}_g(t_1)\left|\psi_i\right\rangle ,\end{aligned} \tag{2.47}$$

for an interpretation see Fig.(2.2).

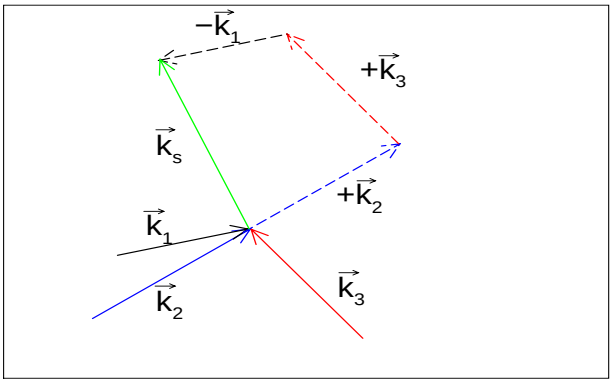

Figure 2.1: *Illustration of the wavevector linear combination resulting in the detection direction* $\vec{k}_s$.

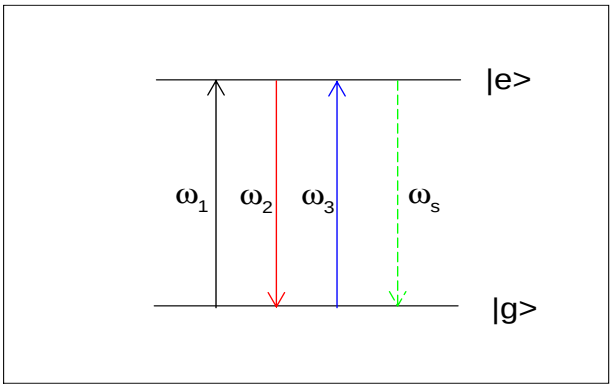

Figure 2.2: *Illustration of the corresponding transition scheme in the case of a two-level system.*

To evaluate the third-order polarization, the propagators in the ground and excited state are represented employing complete sets of vibrational eigenstates $|n_g\rangle$ and $|n_e\rangle$ with eigenenergies E_{n_g} and E_{n_e}, so that

$$\hat{U}_g(t) = \sum_{n_g} |n_g\rangle\, e^{-iE_{n_g}t}\, \langle n_g|\,, \tag{2.48}$$

$$\hat{U}_e(t) = \sum_{n_e} |n_e\rangle\, e^{-iE_{n_e}t}\, \langle n_e|\,. \tag{2.49}$$

Regarding times t after the interaction, this yields the expression

$$\begin{aligned} &\langle \psi\,(21,t)|\,\mu\,|\psi\,(3,t)\rangle \\ = &\left(\frac{i}{2}\right)^3 \sum_{n_e}\sum_{n_g}\sum_{m_e} a\,(i,n_e,n_g,m_e)\,b\,(\tau,i,n_e,n_g,m_e)\,. \end{aligned} \tag{2.50}$$

Thereby it is assumed that the polarization vectors of all three fields are parallel, so that the projection of the transition dipole moment on the field is equal in each case ($\vec{\mu}_{eg}\vec{\epsilon}_n = \mu_{eg}$). Furthermore, the coefficients are defined as

$$a\left(i,n_e,n_g,m_e\right)=\left\langle\psi_i\right|\mu_{ge}\left|n_e\right\rangle\left\langle n_e\right|\mu_{eg}\left|n_g\right\rangle\left\langle n_g\right|\mu_{ge}\left|m_e\right\rangle\left\langle m_e\right|\mu_{eg}\left|\psi_i\right\rangle \quad (2.51)$$

and

$$\begin{aligned} b\left(\tau,i,n_e,n_g,m_e\right)&=\int_{-\infty}^{\infty}dt_3\int_{-\infty}^{\infty}dt_2\int_{-\infty}^{t_2}dt_1\\ &f_1\left(t_1\right)e^{i\omega t_1}f_2\left(t_2-\tau\right)e^{-i\omega(t_2-\tau)}f_3\left(t_3-\tau\right)e^{-i\omega(t_3-\tau)}\\ &e^{i(E_i-E_{n_e})t_1}e^{i\left(E_{n_e}-E_{n_g}\right)t_2}e^{i(E_{m_e}-E_i)t_3}e^{i\left(E_{n_g}-E_{m_e}\right)t}. \end{aligned} \quad (2.52)$$

In an experiment, the emitted field is detected after the delay-time τ, i. e., the time origin occurs at $t=\tau$. This is illustrated in Fig. (2.3).

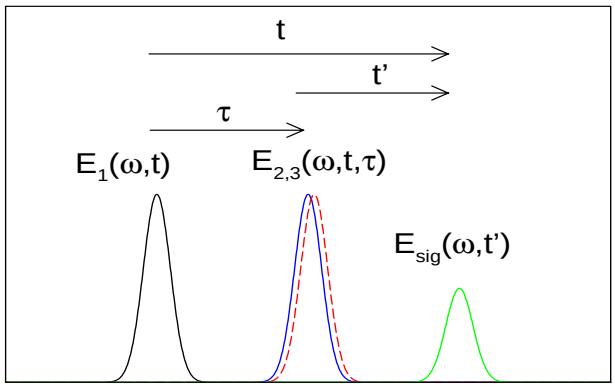

Figure 2.3: *Three ultrashort pulses of equal frequency interact at different times to induce a time-dependent polarization $P(t)$ in an ensemble of molecules. The second and third pulse (E_2, E_3) are identical and time-delayed by time τ with respect to the first pulse (E_1). The time-variable t' is defined to have its origin at the delay-time τ.*

Formally, this results in the replacements ($t'=t-\tau, t_2'=t_2-\tau, t_3'=t_3-\tau$) in the expression for the coefficient $b\left(\tau,i,n_e,n_g,m_e\right)$. Because the time-integral over t_1 does not depend on the delay-time and a time-separation of the first

pulse and the others excluding a temporal overlap is assumed, the variable remains the same, i. e. $t_1^{'} = t_1$. As a result one finds:

$$b\left(\tau, i, n_e, n_g, m_e\right) = e^{i(E_{n_e} - E_i)\tau} e^{i\left(E_{n_g} - E_{m_e}\right)t'} \tilde{b}\left(i, n_e, n_g, m_e\right) \tag{2.53}$$

with the definition

$$\begin{aligned} \tilde{b}\left(i, n_e, n_g, m_e\right) = & \int_{-\infty}^{\infty} dt_3^{'} \int_{-\infty}^{\infty} dt_2^{'} \int_{-\infty}^{t_2^{'}+\tau} dt_1^{'} \\ & f_1\left(t_1^{'}\right) e^{i\omega t_1^{'}} f_2\left(t_2^{'}\right) e^{-i\omega t_2^{'}} f_3\left(t_3^{'}\right) e^{-i\omega t_3^{'}} \\ & e^{i(E_i - E_{n_e})t_1^{'}} e^{i\left(E_{n_e} - E_{n_g}\right)t_2^{'}} e^{i(E_{m_e} - E_i)t_3^{'}}, \end{aligned} \tag{2.54}$$

where the delay-time dependence drops out for the non-overlapping pulse sequence illustrated in Fig. (2.3). One finally obtains

$$\begin{aligned} \vec{P}^{(3)}\left(t', \tau\right) &= 2\left(\frac{i}{2}\right)^3 \sum_{n_e} \sum_{n_g} \sum_{m_e} a\left(i, n_e, n_g, m_e\right) \tilde{b}\left(i, n_e, n_g, m_e\right) \\ & \quad e^{i(E_{n_e} - E_i)\tau} e^{i\left(E_{n_g} - E_{m_e}\right)t'}, \end{aligned} \tag{2.55}$$

which directly shows the dependence of the polarization on the delay-time τ and on time t'. In what follows, the variable t' is renamed as t, keeping in mind that this time refers to the origin at the delay-time τ (see Fig. (2.3)). The 2D-spectrum is obtained as a Fourier-transform of the polarization with respect to the variables t and τ. There are various conventions to convert the time-dependent polarization into the two-dimensional energy-dependent signal. They differ in the origin of the energy variables ω_t and ω_τ appearing in the Fourier-transform. Here, a forward and a backward Fourier-transformation is employed in order to locate the spectrum exclusively at positive energies:

$$\begin{aligned} S\left(\omega_\tau,\omega_t\right) &= (2\pi)^2 \int d\tau \int dt\; e^{i\omega_t t} e^{-i\omega_\tau \tau}\; P^{(3)}(t,\tau) \\ &= -\frac{i}{4}\sum_{n_e}\sum_{n_g}\sum_{m_e} a\left(i,n_e,n_g,m_e\right)\tilde{b}\left(i,n_e,n_g,m_e\right) \\ &\quad \delta\left(\omega_t - \left(E_{m_e} - E_{n_g}\right)\right)\delta\left(\omega_\tau - \left(E_{n_e} - E_i\right)\right). \end{aligned} \tag{2.56}$$

The real part of the spectrum exhibits the same peak structure as the imaginary part. The difference is that in varying either one of the two energies over a peak position, the spectrum changes sign. This is well known [43] and can be understood by inspection of Eq. (2.55). The polarization, in general, does not oscillate forever. Rather, it decays via interaction with a surrounding. In the calculation, the polarization is damped by multiplying it with a window function $w(t,\tau)$. For an exponentially decay as represented by a function $w(t,\tau) = exp(-\beta_t t - \beta_\tau \tau)$, one finds

$$\begin{aligned} S(\omega_t,\omega_\tau) &= \int dt \int d\tau\; e^{i(\omega_t + i\beta_t)t}\;\; e^{-i(\omega_\tau - i\beta_\tau)\tau}\; P^{(3)}(t,\tau) \\ &\sim -\sum_{n_e}\sum_{n_g}\sum_{m_e} a(i,n_e,n_g,m_e)\;\tilde{b}(i,n_e,n_g,m_e) \\ &\quad \left(\frac{\beta_t(\omega_t - (E_{m_e} - E_{n_g})) + \beta_\tau((E_{n_e} - E_i) - \omega_\tau)}{[(\omega_t - (E_{m_e} - E_{n_g}))^2 + \beta_t^2][((E_{n_e} - E_i) - \omega_\tau)^2 + \beta_\tau^2]}\right. \\ &+ \left. i\frac{(\omega_t - (E_{m_e} - E_{n_g}))((E_{n_e} - E_i) - \omega_\tau) + \beta_t\beta_\tau}{[(\omega_t - (E_{m_e} - E_{n_g}))^2 + \beta_t^2][((E_{n_e} - E_i) - \omega_\tau)^2 + \beta_\tau^2]}\right). \end{aligned} \tag{2.57}$$

Regarding resonance conditions, the coefficients $\tilde{b}(i,n_e,n_g,m_e)$ and the product of matrix elements $a(i,n_e,n_g,m_e)$ are real. Real and imaginary part of the spectrum are called dispersion- and absorption- signals, respectively [31]. If the energy ω_t is fixed to be equal to an energy difference $(E_{m_e} - E_{n_g})$, and ω_τ is varied over a resonance $(\omega_\tau = E_{n_e} - E_i)$, the imaginary part exhibits a maximum, whereas the real part shows a change of sign. The same happens

if a cut through the 2D-landscape is taken in the other direction. In the numerical calculation, it is convenient to employ a Gaussian window function instead of the exponentially decaying functions as discussed above. However, the structure of the imaginary and real part of the 2D-spectra remains the same if one or the other damping function is employed. This stems from the fact that the polarizations are not symmetric with respect to the time origins, but decay to zero for negative times within the ultrashort widths of the overlapping pulses.

The numerical calculation of the third-order polarization can be performed employing schemes, which rely on the numerically exact solution of the time-dependent Schrödinger equation for the vibrational dynamics in the coupled electronic states. Here, the method of Seidner, Stock and Domcke is employed, which originatively was used for a two-pulse scheme [53], and was extended to a three-pulse scenario later [54], see also Ref. [55]. An alternative method is proposed in Sec. (A.3). The polarization is expanded as

$$P(t,\tau,\phi_1,\phi_2,\phi_3) = \sum_{lmn} P_{lmn}(t,\tau)\, e^{i(l\phi_1+m\phi_2+n\phi_3)}, \tag{2.58}$$

where $P_{lmn}(t,\tau)$ corresponds to the emitted field in $l\vec{k}_1 + m\vec{k}_2 + n\vec{k}_3$ direction. The ϕ_j are phases which are attached to the three pulses. In order to determine the component emitted in a given direction, the respective term from the total polarization emerging from a numerically exact calculation has to be extracted. By symmetry, under the assumption of weak fields, and taking only resonant contributions into account, the number of terms in the sum Eq. (2.58) can be restricted to 12 [54]. A calculation of the polarization for 12 different choices of phases $\vec{\phi}_s = (\phi_{s,1}, \phi_{s,2}, \phi_{s,3})$ allows to set up an inhomogeneous system of equations as

$$\begin{pmatrix} c_{1,1} & . & . & . & c_{1,12} \\ . & & & & . \\ . & & & & . \\ . & & & & . \\ c_{12,1} & . & . & . & c_{12,12} \end{pmatrix} \begin{pmatrix} P_1(t) \\ . \\ . \\ . \\ P_{12}(t) \end{pmatrix} = \begin{pmatrix} P(t, \phi_{1,1}, \phi_{2,1}, \phi_{3,1}) \\ . \\ . \\ . \\ P(t, \phi_{1,12}, \phi_{2,12}, \phi_{3,12}) \end{pmatrix}, \quad (2.59)$$

where the coefficients are defined as

$$c_{s,q} = e^{i(\vec{\phi}_s \vec{r}_q)}. \quad (2.60)$$

The choice of the phases is not unique and one possible combination of values, together with the corresponding values for the combinations $\vec{r}_q = (l_{q,1}, m_{q,2}, n_{q,3})$, are collected in Tab. 2.1.

$\phi_{s,i}$	s=1	2	3	4	5	6	7	8	9	10	11	12
i=1	0	0	$\frac{\pi}{2}$	$\frac{\pi}{2}$	π	π	$\frac{3\pi}{2}$	0	0	$\frac{\pi}{2}$	$\frac{3\pi}{2}$	$\frac{3\pi}{2}$
2	0	0	0	0	0	0	0	0	0	0	0	0
3	0	$\frac{\pi}{2}$	π	$\frac{\pi}{2}$	0	$\frac{\pi}{2}$	$\frac{3\pi}{2}$	$\frac{3\pi}{2}$	π	$\frac{3\pi}{2}$	π	$\frac{\pi}{2}$
$r_{q,i}$	q=1	2	3	4	5	6	7	8	9	10	11	12
i=1	1	0	0	1	1	-1	2	2	-1	0	-1	0
2	0	1	0	-1	1	1	-1	0	2	2	0	-1
3	0	0	1	1	-1	1	0	-1	0	-1	2	2

Table 2.1: Phases for the calculation of the third order polarization.

In praxis, the third order polarization is calculated 12 times employing the respective phases. This is done by solving the time-dependent Schrödinger equation for the vibrational motion in the field coupled electronic states. In

the case of a monomer system with an electronic ground state and one excited state, the Hamiltonian

$$\hat{H}^M = \begin{pmatrix} H_g^M(q) & W_{ge}^{(s)} \\ W_{eg}^{(s)} & H_e^M(q) \end{pmatrix} \tag{2.61}$$

includes the interaction term $(T_1 = 0, T_2 = T_3 = \tau)$

$$W_{eg}^{(s)} = W_{ge}^{(s)} = -\mu_{eg} \sum_{n=1}^{3} f_n(t - T_n) \cos\left[\omega_n(t - T_n) - \phi_{s,n}\right]. \tag{2.62}$$

Chapter 3

Numerical methods

3.1 The Split-Operator-Method

The numerical solution of the time-dependent Schrödinger equation is performed by iterative application of the short time propagator

$$\hat{U}(\Delta t) = \exp\left(-\frac{i}{\hbar}\hat{H}\Delta t\right) \tag{3.1}$$

to a wave function:

$$\psi(q, t_n + \Delta t) = \hat{U}(\Delta t)\psi(q, t_n). \tag{3.2}$$

The propagator is split up into a product of terms containing either the kinetic or the potential energy contribution to the Hamiltonian [56]. In order to keep the numerical error in the range of $O(\lambda^2)$ with $\lambda = \frac{-i\Delta t}{\hbar}$, it is essential to use a splitting scheme

$$\begin{aligned} \hat{U}(\lambda) &= \exp\left(-\frac{i}{\hbar}\Delta t\hat{H}\right) = \exp\left(-\frac{i}{\hbar}\Delta t\left(\hat{T}+\hat{V}\right)\right) \\ &\approx \exp\left(-\frac{i\hat{V}\Delta t}{2\hbar}\right)\exp\left(-\frac{i\hat{T}\Delta t}{\hbar}\right)\exp\left(-\frac{i\hat{V}\Delta t}{2\hbar}\right). \end{aligned} \tag{3.3}$$

While the potential propagation can be performed by pointwise multiplication of the wave function with a phase factor in coordinate space, the kinetic part is more difficult to handle. A practicable method includes a Fourier-transformation to momentum-space, where the wave-packet can be represented as

$$\tilde{\psi} = \sum_m a_m \exp(ik_m q), \tag{3.4}$$

and the application of the operator to the wave-packet

$$\exp\left(\lambda \hat{T}\right) \tilde{\psi}(\vec{q}) = \sum_m a_m \left(\exp\left(\frac{\lambda}{2M} k_m^2\right)\right) \exp(ik_m q) \tag{3.5}$$

corresponds to a multiplication with a phase factor at each grid point. In this formula, the mass is denoted as M. Afterwards a backward-transformation has to be performed.

In the case of the dimer (see Sec. (4)), the split operator method formalism has to be extended by the inclusion of the coupling matrix into the splitting scheme

$$\begin{aligned} &\exp\left\{\tfrac{\lambda}{2}\begin{pmatrix} V_{e1} & J \\ J & V_{e2} \end{pmatrix}\right\} \\ \approx &\exp\left\{\tfrac{\lambda}{4}\begin{pmatrix} 0 & J \\ J & 0 \end{pmatrix}\right\} \exp\left\{\tfrac{\lambda}{2}\begin{pmatrix} V_{e1} & 0 \\ 0 & V_{e2} \end{pmatrix}\right\} \exp\left\{\tfrac{\lambda}{4}\begin{pmatrix} 0 & J \\ J & 0 \end{pmatrix}\right\} \quad , \end{aligned} \tag{3.6}$$

which implies an error of the magnitude $O(\lambda^3)$, see Ref. [57]. As the propagator, which contains the coupling matrix elements, is not diagonal, it can be evaluated using the common formula

$$\exp(-i\hat{J}\Delta t) \;=\; \hat{S}\ \exp(-i\ \Delta t\ \hat{S}^T\ \hat{J}\ \hat{S})\ \hat{S}^T \tag{3.7}$$

$$= \hat{S}\ \left(diag\left(\exp(-i\lambda_1\frac{\Delta t}{4}),...,\exp(-i\lambda_n\frac{\Delta t}{4})\right)\right)\ \hat{S}^T.$$

Thereby $diag\,(\exp(-i\lambda_1\Delta t),...,\exp(-i\lambda_n\Delta t))$ denotes a diagonal matrix containing the eigenvalues λ_n of $\hat{J}$ in the argument of the exponential function. The corresponding eigenvectors appear as the columns of the matrix $\hat{S}$. In the case of the dimer, this expression can be evaluated analytically, yielding the result

$$\exp(-i\frac{\Delta t}{4}\hat{J}) = \begin{pmatrix} \cos(\frac{\Delta t}{4}J) & -i\sin(\frac{\Delta t}{4}J) \\ -i\sin(\frac{\Delta t}{4}J) & \cos(\frac{\Delta t}{4}J) \end{pmatrix}. \tag{3.8}$$

For larger systems, the diagonalization is performed numerically using the Jacobi method [58].

3.2 The Relaxation-Method

The ground state wave function of a molecular system can be determined using a relaxation algorithm. For this aim, the split operator technique is employed, where the real time-step Δt is replaced by $-i\Delta t$ [59]. As the wave-packet $\psi(\vec{q})$ can be represented as a linear combination

$$\psi(\vec{q}) = \sum_i \langle\phi_i(\vec{q})|\psi(\vec{q})\rangle\,\phi_i(\vec{q}), \tag{3.9}$$

which contains the eigenfunctions ϕ_i of the respective Hamiltonian, time-propagation yields the expression

$$\psi(\vec{q},t) = \sum_i \langle\phi_i(\vec{q})|\psi(\vec{q})\rangle\,\phi_i(\vec{q})\exp\left(-\frac{E_i t}{\hbar}\right), E_i > 0. \tag{3.10}$$

Starting from an arbitrary wave function, the contributions of the excited states are damped much faster than the ground state. If the wave-packet is

normalized after each time step, only the ground state remains in the limit of $t \to \infty$ and the square of its norm can be specified as

$$\lim_{t\to\infty} ||\psi(\vec{q}, t+\Delta t)||^2 = \exp\left(-2\frac{E_0}{\hbar}\Delta t\right) ||\psi_0(\vec{q})||^2. \tag{3.11}$$

Accordingly, the corresponding ground state energy results from the evaluation of the expression

$$E_0 = -\frac{\hbar}{2\Delta t} \ln\left(\lim_{t\to\infty} \frac{||\psi(\vec{q}, t+\Delta t)||^2}{||\psi(\vec{q}, t)||^2}\right). \tag{3.12}$$

The calculation of vibrational excited states demands that the normalized vibrational ground state $\left|\tilde{\psi}_0\right\rangle$ is already known. Starting from an initial function $\left|\psi_n^{(0)}\right\rangle$, the n -th eigenfunction can be determined using the iteration scheme

$$\left|\psi_n^{(m)}\right\rangle = \hat{U}(\Delta t)\left(1 - \sum_{k=0}^{n-1} \left|\tilde{\psi}_k\right\rangle \left\langle\tilde{\psi}_k\right|\right) \left|\tilde{\psi}_n^{(m-1)}\right\rangle, \tag{3.13}$$

where a normalization

$$\left|\tilde{\psi}_n^{(m)}\right\rangle = \frac{1}{\left\langle\psi_n^{(m)}|\psi_n^{(m)}\right\rangle} \left|\psi_n^{(m)}\right\rangle \tag{3.14}$$

is performed after each time step. This leads to the result

$$|\psi_n\rangle = \lim_{m\to\infty} \left|\psi_n^{(m)}\right\rangle. \tag{3.15}$$

The corresponding eigenenergy is obtained from the evaluation of the expression

$$E_n = -\frac{\hbar}{2\Delta t} \ln\left(\lim_{m\to\infty} \frac{||\psi_n^{(m+1)}||^2}{||\psi_n^{(m)}||^2}\right). \tag{3.16}$$

In order to calculate the ground state of a coupled system, the propagator

$$\exp\left(-\hat{J}\frac{\Delta t}{4}\right) = \hat{S}\ \left(diag\left(\exp(-\lambda_1\frac{\Delta t}{4}), ..., \exp(-\lambda_n\frac{\Delta t}{4})\right)\right)\ \hat{S}^T. \quad (3.17)$$

has to be determined, see Eq. (3.7). For a dimer system, the analytical result

$$\exp(-i\frac{\Delta t}{4}\hat{J}) = \begin{pmatrix} \cosh(\frac{\Delta t}{4}J) & -\sinh(\frac{\Delta t}{4}J) \\ -\sinh(\frac{\Delta t}{4}J) & \cosh(\frac{\Delta t}{4}J) \end{pmatrix}. \quad (3.18)$$

is obtained.

3.3 The MCTDH-Method

The MCTDH method [60] is based on a basis set, where the infinite-dimensional quantum mechanical Hilbert space is replaced by a numerical one with finite dimension. Assuming that a system has f degrees of freedom described by nuclear coordinates $q_1, ..., q_f$, this can be accomplished by establishing an $N_1 \times ... \times N_f$ -dimensional time-independent orthonormal product basis set $\left\{\chi_{j_1}^{(1)}(q_1), ..., \chi_{j_f}^{(f)}(q_f)\right\}$. By representing the Hamiltonian H in this basis one obtains the matrix

$$H_{i_1...i_f j_1...j_f} = \left\langle \chi_{i_1}^{(1)} ... \chi_{i_f}^{(f)} \right| H \left| \chi_{j_1}^{(1)} ... \chi_{j_f}^{(f)} \right\rangle. \quad (3.19)$$

The ansatz for the time-dependent total wave function reads

$$\psi\left(q_1, ..., q_f, t\right) = \sum_{j_1=1}^{n_1} ... \sum_{j_f=1}^{n_f} A_{j_1...j_f}(t) \prod_{\kappa=1}^{f} \phi_{j_\kappa}^{(\kappa)}(q_\kappa, t), \quad (3.20)$$

where $A_{j_1...j_f}$ denote the MCTDH expansion coefficients and $\phi_{j_\kappa}^{(\kappa)}$ are the expansion functions for each degree of freedom, also called single particle functions. The latter are represented as linear combinations of the primitive basis:

$$\phi_{j_\kappa}^{(\kappa)}(Q_\kappa, t) = \sum_{i_\kappa=1}^{N_\kappa} c_{i_\kappa j_\kappa}^{\kappa}(t)\chi_{i_\kappa}^{\kappa}(Q_\kappa) \tag{3.21}$$

The MCTDH equations of motion are then derived by variationally optimizing the coefficients and single particle functions employing the Dirac-Frenkel variational principle

$$\langle\delta\psi| H - i\frac{\partial}{\partial t}|\psi\rangle = 0. \tag{3.22}$$

In order to simplify the notation, the abbreviations $A_J = A_{j_1\ldots j_f}$ and $\Phi_J = \prod_{\kappa=1}^{f} \phi_{j_\kappa}^{(\kappa)}$ are used in the following. Furthermore, the projector

$$P^{(\kappa)} = \sum_{j=1}^{n_\kappa} \left|\phi_j^\kappa\right\rangle \left\langle\phi_j^\kappa\right| \tag{3.23}$$

on the space spanned by the single-particle functions for the κ -th degree of freedom is introduced. The single hole functions $\psi_l^{(\kappa)}$ are defined as the linear combination of Hartree products of $(f-1)$ single particle functions that do not contain the single particle function for the coordinate q_κ,

$$\psi_l^{(\kappa)} = \left\langle\phi_l^{(\kappa)}|\psi\right\rangle = \sum_{J}^{\kappa} A_{J_l^\kappa}\phi_{j_1}^{(1)}\ldots\phi_{j_{\kappa-1}}^{(\kappa-1)}\phi_{j_{\kappa+1}}^{(\kappa+1)}\phi_{j_f}^{(f)}, \tag{3.24}$$

where the integration in the intermediate expression runs only over q_κ and where J_l^κ denotes a composite index J with the κ -th entry set at l and $\sum_{J}^{\kappa}$ is the sum over the indices of all degrees of freedom including the κ -th. Using the single-hole functions, the mean fields

$$\langle H\rangle_{jl}^{\kappa} = \left\langle\psi_j^\kappa\right| H \left|\psi_l^\kappa\right\rangle \tag{3.25}$$

and the density matrices

$$\rho_{jl}^{\kappa} = \left\langle\psi_j^\kappa|\psi_l^\kappa\right\rangle = \sum_{J}^{\kappa} A_{J_j^\kappa}^* A_{J_l^\kappa}. \tag{3.26}$$

are defined. Thus, the Dirac-Frenkel variational principle leads to the equations of motion

$$i\dot{A}_J = \sum_L \langle \Phi_J | \, H \, | \Phi_L \rangle \, A_L \tag{3.27}$$

and

$$i\dot{\phi}_j^{(\kappa)} = \sum_{lm} \left(1 - P^{(\kappa)}\right) \left((\rho^{(\kappa)})^{-1}\right)_{jl} \langle H \rangle_{lm}^{(\kappa)} \, \phi_m^{(\kappa)} \tag{3.28}$$

Concerning the calculation effort, the MCTDH method is more appropriated than the split-operator method for systems with many vibrational degrees of freedom such as large molecular aggregates.

Chapter 4

Molecular aggregates

As dimer systems are the smallest molecular aggregates and thus easiest accessible for a theoretical investigation, the dimer model will be discussed first. This model is built from the combination of two monomer systems, which include the Hamiltonians $H_g^M(q_n)$ and $H_e^M(q_n)$ in order to describe the motion within the electronic ground state and the excited state along the vibrational coordinates $q_n, n = 1, 2$. For the ground state of the dimer, the Hamiltonian reads

$$H_g^D(q_1, q_2) = |g(1), g(2)\rangle \left(H_g^M(q_1) + H_g^M(q_2)\right) \langle g(2), g(1)| , \qquad (4.1)$$

where $g(1)$ and $g(2)$ denote the ground states of the respective monomer units. Upon the generally closed electron configuration of molecules in the electronic ground state only van-der-Waals-interaction exists, which leads to a relatively weak coupling and is therefore neglected. Within the 1-exciton-model, excitations of the dimer-system are taken into account where only one of the monomer units is excited, respectively [9, 10]. The coupling between these states is much stronger, as due to the binding interaction between the two configurations a closed electron configuration arises. The corresponding

Hamiltonian is written as

$$H_e^D(q_1,q_2) = |e(1),g(2)\rangle\, H_{e1}^D(q_1,q_2)\, \langle e(1),g(2)| + |g(1),e(2)\rangle\, J\, \langle e(1),g(2)| + |e(1),g(2)\rangle\, J\, \langle g(1),e(2)| + |g(1),e(2)\rangle\, H_{e2}^D(q_1,q_2)\, \langle g(1),e(2)|\,, \tag{4.2}$$

using the notation $|e(1),g(2)\rangle$ for the direct product of the electronic excited state of the first monomer and the electronic ground state of the second monomer. In the case of $|g(1),e(2)\rangle$, the roles of the monomer units are changed. This simplified description neglects exchange effects. The Hamiltonian for the excited state is represented in the electronic basis $\{|g(1),e(2)\rangle\,, |e(1),g(2)\rangle\}$ as

$$\hat{H}_e^D = \begin{pmatrix} H_{e1}^D(q_1,q_2) & J \\ J & H_{e2}^D(q_1,q_2) \end{pmatrix}. \tag{4.3}$$

In this formula, the Hamiltonians

$$H_{e1}^D(q_1,q_2) = H_e^M(q_1) + H_g^M(q_2) + (\Delta E_D - \Delta E_M), \tag{4.4}$$

$$H_{e2}^D(q_1,q_2) = H_g^M(q_1) + H_e^M(q_2) + (\Delta E_D - \Delta E_M). \tag{4.5}$$

are employed, where the difference between the energy shifts $\Delta E_D - \Delta E_M$ of dimer and monomer appears. Within the harmonic approximation, the potentials of the monomer units are taken as

$$V_g^M(q_n) = \frac{1}{2}\,\omega^2\, q_n^2 \tag{4.6}$$

$$V_e^M(q_n) = \frac{1}{2}\,\omega^2\,(q_n - q_{e,n})^2 + \Delta E_M \tag{4.7}$$

under the assumption of a different equilibrium distance $q_{e,n}$ in the excited state relative to the ground state. The coupling constant J can be obtained

by a multipole expansion, where only the dipole-dipole-interaction term is included approximately [61, 62]. This leads to the formula

$$J(\vec{R}) = \frac{\vec{\mu}_1 \vec{\mu}_2}{R^3} - 3\frac{(\vec{R}\,\vec{\mu}_1)(\vec{R}\,\vec{\mu}_2)}{R^5} \tag{4.8}$$

with $\vec{R}$ as the difference vector between the centers-of-mass of the monomer units. Furthermore, the monomer transition dipole moments

$$\vec{\mu}_n = \left\langle e(n) \left| \hat{\vec{\mu}}_n \right| g(n) \right\rangle \tag{4.9}$$

appear in this equation, containing the dipole operator $\hat{\vec{\mu}}_n$ of monomer n. By introducing the angles β between the transition dipole moments and α_n between the transition dipole moment $\hat{\vec{\mu}}_n$ and the intermolecular axis, equation (4.8) becomes

$$J(R, \beta, \alpha_1, \alpha_2) = \frac{\mu^2}{R^3}[\cos(\beta) - 3\cos(\alpha_1)\cos(\alpha_2)], \tag{4.10}$$

with $\mu = |\vec{\mu}_n|$. However, the assumptions leading to Eq. (4.10) are often not fulfilled [63]. Better approximations to the interaction can be formulated such as the extended dipole model [64] or methods employing multicentre monopole or multipole expansions [65]. In the Fig. (4.1), the spatial arrangement of the monomer units, which are symbolized as rectangles, is illustrated.

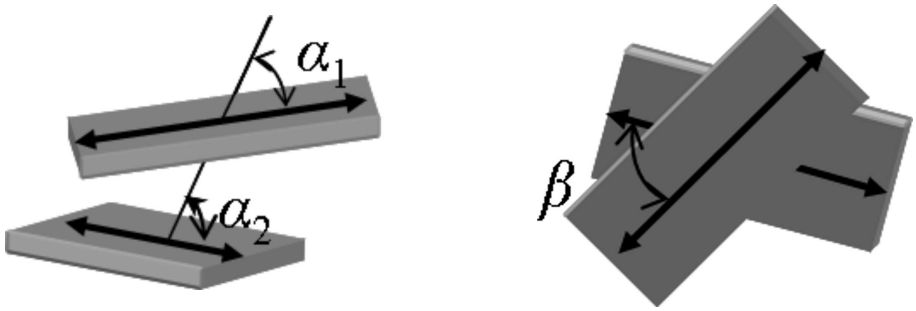

Figure 4.1: *Illustration of the spatial arrangement, where the molecules are symbolized as rectangles and the transition dipole-moments are represented by the arrows.*

For the calculation of dimer-spectra, the angle β between the transition dipole moments is essential. The transition dipole moments are localized in a coordinate system with the y -axis bisecting the angle β in order to determine the interaction contributions of the electric field with the electronic transition dipole-moments in the cases of x - and y - polarized light, see Sec. (A.1). The same holds for the interaction of the magnetic field with the magnetic transition dipole moments, which are defined as [66]

$$\vec{m}_n = -i\frac{D_{eg}}{2c}\left(\vec{a}_n \times \vec{\mu}_n\right), \tag{4.11}$$

where D_{eg} is the difference between the monomer excited and ground state potential curves evaluated at the Franck-Condon-point $q_1 = q_2 = 0$. Thereby $\vec{a}_n$ denotes the position vector of monomer unit (n). The spatial arrangement of electronic and magnetic transition dipole moments is shown in figure (4.2). The wave functions of the dimer have two components:

$$\vec{\mu}_n\psi_g = \psi_g \begin{pmatrix} \vec{\mu}_1\delta_{1n} \\ \vec{\mu}_2\delta_{2n} \end{pmatrix}. \tag{4.12}$$

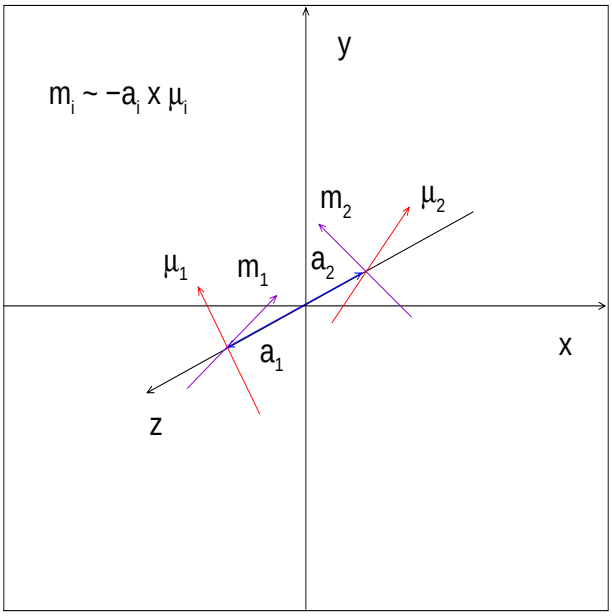

Figure 4.2: *Spatial arrangement of electronic and magnetic transition dipole moments of a dimer.*

For the calculation of the time-correlation function

$$c_{abs}(t) = \vec{\epsilon}\left\{\sum_{(n,m)=1}^{2} \langle\vec{\mu}_n\psi_g|U_e(t)|\vec{\mu}_m\psi_g\rangle\right\}\vec{\epsilon}, \tag{4.13}$$

only the contribution of the above described arrangement has to be regarded, as the contributions of all other orientations vanish in the average, see Sec. (A.1). In the cases of x - and y -polarized light, one has to employ

$$\vec{\epsilon}_x\ \vec{\mu}_n = \mu_n \sin\left(\frac{\beta}{2}\right)(-1)^n \tag{4.14}$$

and

$$\vec{\epsilon}_y\ \vec{\mu}_n = \mu_n \cos\left(\frac{\beta}{2}\right). \tag{4.15}$$

This leads to the time-correlation function

$$c_{abs}(t) = \left\langle \left(\mu_1 \left(-\sin\left(\frac{\beta}{2}\right) + \cos\left(\frac{\beta}{2}\right)\right) + \mu_2 \left(\sin\left(\frac{\beta}{2}\right) + \cos\left(\frac{\beta}{2}\right)\right)\right) \psi_g \right|$$
$$\hat{U}_e\,(t)$$
$$\left| \left(\mu_1 \left(-\sin\left(\frac{\beta}{2}\right) + \cos\left(\frac{\beta}{2}\right)\right) + \mu_2 \left(\sin\left(\frac{\beta}{2}\right) + \cos\left(\frac{\beta}{2}\right)\right)\right) \psi_g \right\rangle . \quad (4.16)$$

Using the sum and difference formulas for trigonometric functions, this expression can be simplified as

$$\begin{aligned} c_{abs}(t) &= \langle \mu_1\ \psi_g \,|\, \hat{U}_e\,(t) \,|(\mu_1\ +\ \mu_2\ \cos(\beta))\ \psi_g\rangle \\ &+ \langle \mu_2\ \psi_g \,|\, \hat{U}_e\,(t) \,|(\mu_1\ \cos(\beta)\ +\ \mu_2)\ \psi_g\rangle\,, \end{aligned} \quad (4.17)$$

where both terms yield the same contribution to the time-correlation function due to symmetry. Under the assumption $|\mu_1| = |\mu_2| = 1$, the result can be written as [12]

$$c_{abs}(t) \sim \left\langle \begin{pmatrix} \psi_g \\ 0 \end{pmatrix} \left|\hat{U}_e(t)\right| \begin{pmatrix} \psi_g \\ \psi_g \cos(\beta) \end{pmatrix} \right\rangle . \quad (4.18)$$

In order to derive a simplified expression for the time-correlation function in the case of CD-spectroscopy, the magnetic transition dipole moments have to be regarded. In analogy to the corresponding expression, which includes the electronic transition dipole moments, the definition

$$\vec{m}_n \psi_g = \psi_g \begin{pmatrix} \vec{m}_1 \delta_{1n} \\ \vec{m}_2 \delta_{2n} \end{pmatrix} \quad (4.19)$$

is used.

Employing the given vectors

$$\vec{\mu}_1 = \mu_1 \begin{pmatrix} -\sin\left(\frac{\beta}{2}\right) \\ \cos\left(\frac{\beta}{2}\right) \\ 0 \end{pmatrix}, \vec{\mu}_2 = \mu_2 \begin{pmatrix} \sin\left(\frac{\beta}{2}\right) \\ \cos\left(\frac{\beta}{2}\right) \\ 0 \end{pmatrix} \tag{4.20}$$

and

$$\vec{a}_1 \sim \begin{pmatrix} 0 \\ 0 \\ 1 \end{pmatrix}, \vec{a}_2 \sim \begin{pmatrix} 0 \\ 0 \\ -1 \end{pmatrix}, \tag{4.21}$$

the magnetic dipole vectors $\vec{m}_n \sim -i\vec{a} \times \vec{\mu}, n = 1, 2$ can be specified as

$$\vec{m}_1 \sim m_1 \begin{pmatrix} \cos\left(\frac{\beta}{2}\right) \\ \sin\left(\frac{\beta}{2}\right) \\ 0 \end{pmatrix}, \vec{m}_2 \sim m_2 \begin{pmatrix} -\cos\left(\frac{\beta}{2}\right) \\ \sin\left(\frac{\beta}{2}\right) \\ 0 \end{pmatrix}, \tag{4.22}$$

Thereby m_1 and m_2 denote the absolute values of the vectors, multiplied with i. If these vectors are inserted within the time-correlation function

$$c_{CD}(t) = \Im \left\{ \left(\vec{k} \times \vec{\epsilon} \right) \left\{ \sum_{(n,m)=1}^{2} a_m \left\langle \vec{\mu}_m \psi_g | U_e(t) | \vec{\mu}_n \psi_g \right\rangle \right\} \vec{\epsilon} \right\}, \tag{4.23}$$

the result

$$\begin{aligned} -i\, c_{CD}(t) &= \left\langle \left(m_1 \left(\cos\left(\frac{\beta}{2}\right) + \sin\left(\frac{\beta}{2}\right) \right) \right) \psi_g \right| \\ &\quad \hat{U}_e(t) \left| \left(\mu_2 \left(\sin\left(\frac{\beta}{2}\right) + \cos\left(\frac{\beta}{2}\right) \right) \right) \psi_g \right\rangle \\ &+ \left\langle \left(m_2 \left(-\cos\left(\frac{\beta}{2}\right) + \sin\left(\frac{\beta}{2}\right) \right) \right) \psi_g \right| \\ &\quad \hat{U}_e(t) \left| \left(\mu_1 \left(-\sin\left(\frac{\beta}{2}\right) + \cos\left(\frac{\beta}{2}\right) \right) \right) \psi_g \right\rangle \end{aligned} \tag{4.24}$$

is obtained, where only cross terms appear, as the vectors of electronic and magnetic transition dipole moment related to the same monomer unit are orthogonal. This expression can be simplified towards

$$\begin{aligned} -i\, c_{CD}(t) &= (1+\sin(\beta))\, \langle m_1\, \psi_g|\, \hat{U}_e\,(t)\, |\mu_2\, \psi_g\rangle \\ &+ (-1+\sin(\beta))\, \langle m_2\, \psi_g|\, \hat{U}_e\,(t)\, |\mu_1\, \psi_g\rangle\,. \end{aligned} \tag{4.25}$$

Taking advantage of the symmetry, it is evident that the matrix elements in both summands yield the same contribution.
Under the assumption $|\mu_1| = |\mu_2| = |m_1| = |m_2| = 1$, the final result can be written as

$$c_{CD}(t) \sim \sin(\beta) \left\langle \begin{pmatrix} \psi_g \\ 0 \end{pmatrix} \left| \hat{U}_e(t) \right| \begin{pmatrix} 0 \\ \psi_g \end{pmatrix} \right\rangle. \tag{4.26}$$

In the case of emission-spectra, the coupled vibrational ground state

$$\vec{\psi_e} = \begin{pmatrix} \psi_{e,1} \\ \psi_{e,2} \end{pmatrix} \tag{4.27}$$

has to be calculated first. Furthermore, the definition

$$(\vec{\mu}_1 + \vec{\mu}_2)\, \vec{\psi_e} = \vec{\mu}_1 \psi_{e,1} + \vec{\mu}_2 \psi_{e,2} \tag{4.28}$$

takes place. Accordingly, the corresponding time-correlation function

$$c_{em}(t) = \vec{\epsilon} \left\{ \sum_{(n,m)=1}^{2} \left\langle \vec{\psi_e} \vec{\mu}_n | U_g(t) | \vec{\mu}_m \vec{\psi_e} \right\rangle \right\} \vec{\epsilon} \tag{4.29}$$

becomes

$$c_{em}(t) = \langle \psi_{e1}\, |U_g(t)|\, \psi_{e,1}\rangle + \cos(\beta)\, \langle \psi_{e1}\, |U_g(t)|\, \psi_{e,2}\rangle \tag{4.30}$$

after some simplification steps.

Larger aggregates like trimers and tertamers can be treated in a similar way as the dimer. For each monomer unit one vibrational degree of freedom is taken into account. The ground state of the aggregate with N monomers $|g\rangle = |g(1), ..., g(N)\rangle$ is (to a good approximation) separable because of the weak interaction between the monomer units (see the dimer case). The respective Hamiltonian then is

$$\hat{H}_g\left(q_1, ..., q_N\right) = |g\rangle \left[\sum_{n=1}^{N} \hat{H}_g^M\left(q_n\right)\right] \langle g| \,. \tag{4.31}$$

The excitation of the monomer (m) within the aggregate through photon absorption leads to the representation

$$|e, n\rangle = |g(1), ..., e(n), ..., g(N)\rangle \,, \tag{4.32}$$

where there are N of these states, which are degenerated [61]. As in the case of the dimer, the excited states are coupled to each other. According to the coupling scheme, a distinction is made between linear and cyclic aggregates. While linear aggregates only exhibit couplings between consecutive monomer units, cyclic aggregates additionally posses a coupling between the first and the last monomer unit of the aggregate. The common Hamiltonian for an aggregate consisting of N monomer units reads

$$\hat{H} = \begin{pmatrix} \hat{H}_{e,1} & J & 0 & . & 0 & J\delta_{j,c} \\ J & \hat{H}_{e,2} & J & 0 & . & 0 \\ 0 & J & . & . & . & . \\ . & . & . & . & . & . \\ 0 & . & . & . & . & J \\ J\delta_{j,c} & 0 & . & 0 & J & \hat{H}_{e,N} \end{pmatrix}, \; j = c, l, \tag{4.33}$$

depending on whether the coupling scheme is linear (l) or cyclic (c).

In order to calculate spectra of an aggregate with N monomer units, the formulas

$$c_{abs}(t) = \vec{\epsilon}\left\{\sum_{(n,m)=1}^{N}\langle\vec{\mu}_n\psi_g|U_e(t)|\vec{\mu}_m\psi_g\rangle\right\}\vec{\epsilon}, \tag{4.34}$$

$$c_{CD}(t) = \Im\left\{\left(\vec{k}\times\vec{\epsilon}\right)\left\{\sum_{(n,m)=1}^{N}\langle\vec{m}_n\psi_g|U_e(t)|\vec{\mu}_m\psi_g\rangle\right\}\vec{\epsilon}\right\}, \tag{4.35}$$

$$c_{em}(t) = \vec{\epsilon}\left\{\sum_{(n,m)=1}^{N}\left\langle\vec{\mu}_n\vec{\psi}_e|U_g(t)|\vec{\mu}_m\vec{\psi}_e\right\rangle\right\}\vec{\epsilon} \tag{4.36}$$

are used, employing the definitions

$$\vec{\mu}_n\psi_g = \psi_g\begin{pmatrix}\vec{\mu}_1\delta_{1n}\\.\\.\\.\\\vec{\mu}_N\delta_{Nn}\end{pmatrix},\ \vec{m}_n\psi_g = \psi_g\begin{pmatrix}\vec{m}_1\delta_{1n}\\.\\.\\.\\\vec{m}_N\delta_{Nn}\end{pmatrix},\ \vec{\psi}_e = \begin{pmatrix}\psi_{e,1}\\.\\.\\.\\\psi_{e,N}\end{pmatrix} \tag{4.37}$$

and

$$\sum_n \vec{\mu}_n\vec{\psi}_e = \sum_n \vec{\mu}_n\psi_{e,n}. \tag{4.38}$$

In these formulas the notation ψ_g is used for the lowest vibrational eigenfunction in the electronic ground state. The j -th component of the coupled vibrational ground state in the electronic excited state is denoted as $\psi_{e,j}$. In the next step, the contributions of the different polarization directions of the incident light have to be determined. For this aim, the transition dipole moments are again projected into a coordinate system, where the origin coincidences with the center of mass of the aggregate and the transition dipole

moments are placed in the (x,y)-plane. If the angles between the transition dipole moments of next-neighbored monomer units are equal, only one orientation of the coplanar monomer transition dipole moments has to be taken into account. Having determined the x - and y components, the time-correlation functions can be simplified using the sum and difference formulas for trigonometric functions. This leads to the compact analytical expressions

$$c_{abs}(t) = \sum_{(n,m)=1}^{N} \langle \mu_n \psi_g | U_e(t) | \mu_m \psi_g \rangle \cos\left((m-n)\,\beta\right), \tag{4.39}$$

$$\begin{aligned} -i\; c_{CD}(t) &= \sum_{(n,m)=1}^{N} \langle m_n \psi_g | U_e(t) | \mu_m \psi_g \rangle \sin\left((m-n)\,\beta\right), \\ &= \sum_{(n,m)=1}^{N} a_n \langle \mu_n \psi_g | U_e(t) | \mu_m \psi_g \rangle \sin\left((m-n)\,\beta\right), \end{aligned} \tag{4.40}$$

$$c_{em}(t) = \sum_{(n,m)=1}^{N} \langle \mu_n \psi_{e,n} | U_g(t) | \mu_m \psi_{e,m} \rangle \cos\left((m-n)\,\beta\right), \tag{4.41}$$

where β denotes the angle between the transition dipole moments of the monomer units m and n, which is equal for all next neighbor pairs. The trimer case is discussed in more detail in Sec. (A.2).

For the calculation of nonlinear spectra, a double excitation (2-exciton state $|e(1), e(2)\rangle$) with Hamiltonian

$$H_d^D(q_1, q_2) = |e(1), e(2)\rangle \left(H_{e1,e2}^D(q_1, q_2) \right) \langle e(2), e(1)|, \tag{4.42}$$

and eigenstates $|n_d\rangle$ with eigenenergies E_{n_d} has to be regarded in addition to the Hamiltonians of the ground state (Eq. (4.1)) and the singly excited state (Eq. (4.2)). The Hamiltonian of the nuclear motion is thereby defined as

$$H_{e1,e2}^D(q_1, q_2) = H_e^M(q_1) + H_e^M(q_2) + (\Delta E_D - \Delta E_M). \tag{4.43}$$

The eigenenergies $|n_e\rangle$ of the singly excited state Hamiltonian are of the form

$$|n_e\rangle = |\psi_{n_e,1}; e(1), g(2)\rangle + |\psi_{n_e,2}; g(1), e(2)\rangle\,, \tag{4.44}$$

where $\psi_{n_e,j}$ denote the components of the total vibrational wave function in the two electronic states. This leads to the representation of the excited state propagator as

$$\begin{aligned} U_e^D(t) &= \sum_{n_e} |\psi_{n_e,1}; e(1), g(2)\rangle \; e^{-iE_{n_e}t} \; \langle\psi_{n_e,1}; e(1), g(2)| \\ &+ \sum_{n_e} |\psi_{n_e,1}; e(1), g(2)\rangle \; e^{-iE_{n_e}t} \; \langle\psi_{n_e,2}; g(1), e(2)| \\ &+ \sum_{n_e} |\psi_{n_e,2}; g(1), e(2)\rangle \; e^{-iE_{n_e}t} \; \langle\psi_{n_e,1}; e(1), g(2)| \\ &+ \sum_{n_e} |\psi_{n_e,2}; g(1), e(2)\rangle \; e^{-iE_{n_e}t} \; \langle\psi_{n_e,2}; g(1), e(2)|\,. \end{aligned} \tag{4.45}$$

For the doubly excited state, the propagator reads

$$U_d^D(t) = \sum_{n_d} |\psi_{n_d}; e(1), e(2)\rangle \; e^{-iE_{n_d}t} \; \langle\psi_{n_d}; e(1), e(2)|\,. \tag{4.46}$$

The transition dipole vector, which enters into the calculation of the spectra, is of the form

$$\begin{aligned} \vec{\mu} &= |e(1), g(2)\rangle\, \vec{\mu}_{eg}(1)\, \langle g(2), g(1)| + |g(1), e(2)\rangle\, \vec{\mu}_{eg}(2)\, \langle g(2), g(1)| \\ &+ |e(1), e(2)\rangle\, \vec{\mu}_{eg}(1)\, \langle e(2), g(1)| + |e(1), e(2)\rangle\, \vec{\mu}_{eg}(2)\, \langle g(2), e(1)| + cc, \end{aligned} \tag{4.47}$$

where $\vec{\mu}_{eg}(n)$ is the transition dipole moment of monomer (n) and off-resonant transitions from the ground state to the doubly excited state and between the 1-exciton states are not included. Placing the monomer transition dipole moments in the (x,y)-plane with the y-axis bisecting the angle β between

them, the scalar product with the electric field polarization vector having the components $(x, y, 0) = (1, 1, 0)$ yields

$$\begin{aligned}
\vec{\mu} &= |e(1), g(2)\rangle \, \mu_{eg}(1) f_{-}(\beta) \, \langle g(2), g(1)| \\
&+ |g(1), e(2)\rangle \, \mu_{eg}(2) f_{+}(\beta) \, \langle g(2), g(1)| \\
&+ |e(1), e(2)\rangle \, \mu_{eg}(1) f_{-}(\beta) \, \langle e(2), g(1)| \\
&+ |e(1), e(2)\rangle \, \mu_{eg}(2) f_{+}(\beta) \, \langle g(2), e(1)| + cc
\end{aligned} \tag{4.48}$$

with the definitions

$$f_{\pm}(\beta) = \cos\left(\frac{\beta}{2}\right) \pm \sin\left(\frac{\beta}{2}\right). \tag{4.49}$$

Note that the molecule-field interaction depends on the relative angle β between the monomer transition-dipole moments. This has a great influence on the linear absorption-spectra, but also on the 2D-spectra. An energy diagram including the possible excitation pathways is shown in Fig. (4.3).

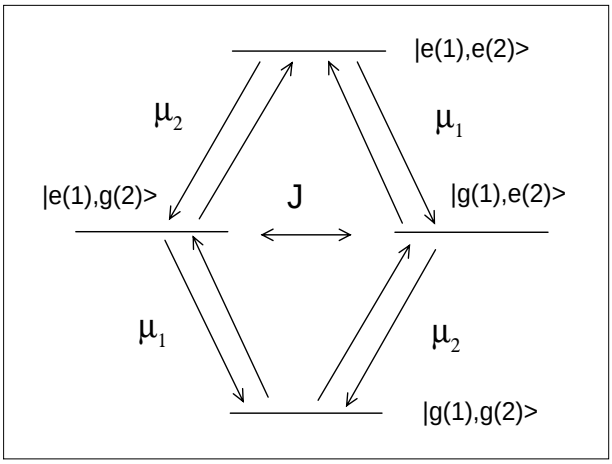

Figure 4.3: *Energy diagram containing the excitation pathways of the dimer model with singly and doubly excited states.*

Besides the terms which contribute to the third-order polarization in the monomer case (in the direction of the laser polarization), additional terms are found for the dimer, so that

$$P^{(3)} = 2\left(\langle\psi\left(21,t\right)|\,\mu\,|\psi\left(3,t\right)\rangle + \langle\psi\left(1,t\right)|\,\mu\,|\psi\left(32,t\right)\rangle\right). \tag{4.50}$$

The same analysis, which resulted in expression Eq. (4.51), can be performed in the present case. This leads to the expression:

$$\begin{aligned} P^{(3)}\left(t,\tau\right) &= 2\left(\frac{i}{2}\right)^3 \sum_{n_e}\sum_{n_g}\sum_{m_e} a\left(\beta,i,n_e,n_g,m_e\right)\tilde{b}\left(i,n_e,n_g,m_e\right) \\ &\quad e^{i\left(E_{n_e}-E_i\right)\tau} e^{i\left(E_{n_g}-E_{m_e}\right)t'} \\ &- 2\left(\frac{i}{2}\right)^3 \sum_{n_e}\sum_{n_d}\sum_{m_e} a\left(\beta,i,n_e,n_d,m_e\right)\tilde{b}\left(i,n_e,n_d,m_e\right) \\ &\quad e^{i\left(E_{n_e}-E_i\right)\tau} e^{i\left(E_{m_e}-E_{n_d}\right)t'}. \end{aligned} \tag{4.51}$$

Here, the coefficients are of a different form because of the presence of the two coupled 1-exciton states. In more detail, one finds:

$$a\left(\beta,i,n_e,n_g,m_e\right) \tag{4.52}$$

$$\begin{aligned} &= \sum_{i,j,k,l=1}^{2} f_+(\beta)^{\delta_{i1}+\delta_{j1}+\delta_{k1}+\delta_{l1}} f_-(\beta)^{\delta_{i2}+\delta_{j2}+\delta_{k2}+\delta_{l2}} \\ &\quad \langle\psi_i|\,\mu(1)\delta_{i1}+\mu(2)\delta_{i2}\left|\psi_{n_{e,1}}\delta_{i1}+\psi_{n_{e,2}}\delta_{i2}\right\rangle \\ &\quad \left\langle\psi_{n_{e,1}}\delta_{j1}+\psi_{n_{e,2}}\delta_{j2}\right|\mu(1)\delta_{j1}+\mu(2)\delta_{j2}\left|\psi_{n_g}\right\rangle \\ &\quad \left\langle\psi_{n_g}\right|\mu(1)\delta_{k1}+\mu(2)\delta_{k2}\left|\psi_{m_{e,1}}\delta_{k1}+\psi_{m_{e,2}}\delta_{k2}\right\rangle \\ &\quad \left\langle\psi_{m_{e,1}}\delta_{l1}+\psi_{m_{e,2}}\delta_{l2}\right|\mu(1)\delta_{l1}+\mu(2)\delta_{l2}\,|\psi_i\rangle \end{aligned} \tag{4.53}$$

and

$$
\begin{aligned}
& a\left(\beta, i, n_e, n_d, m_e\right) && (4.54)\\
= & \sum_{i,j,k,l=1}^{2} f_+(\beta)^{\delta_{i1}+\delta_{j2}+\delta_{k2}+\delta_{l1}} f_-(\beta)^{\delta_{i2}+\delta_{j1}+\delta_{k1}+\delta_{l2}} \\
& \left\langle\psi_i\right| \mu(1)\delta_{i1}+\mu(2)\delta_{i2}\left|\psi_{n_{e,1}}\delta_{i1}+\psi_{n_{e,2}}\delta_{i2}\right\rangle \\
& \left\langle\psi_{n_{e,1}}\delta_{j1}+\psi_{n_{e,2}}\delta_{j2}\right| \mu(1)\delta_{j2}+\mu(2)\delta_{j1}\left|\psi_{n_d}\right\rangle \\
& \left\langle\psi_{n_d}\right| \mu(1)\delta_{k2}+\mu(2)\delta_{k1}\left|\psi_{m_{e,1}}\delta_{k1}+\psi_{m_{e,2}}\delta_{k2}\right\rangle \\
& \left\langle\psi_{m_{e,1}}\delta_{l1}+\psi_{m_{e,2}}\delta_{l2}\right| \mu(1)\delta_{l1}+\mu(2)\delta_{l2}\left|\psi_i\right\rangle && (4.55)
\end{aligned}
$$

The time-integrals for the first term in Eq. (4.51) are identical to the ones given is Eq. (2.54), whereas for the second term (under the assumption of the non-overlapping pulse sequence sketched in Fig. (2.3)) one has

$$
\begin{aligned}
& \tilde{b}\left(i, n_e, n_g, m_e\right)=\int_{-\infty}^{\infty} dt_3^{'} \int_{-\infty}^{t_3^{'}} dt_2^{'} \int_{-\infty}^{\infty} dt_1^{'} \\
& f_1\left(t_1^{'}\right) e^{i\omega t_1^{'}} f_2\left(t_2^{'}\right) e^{-i\omega t_2^{'}} f_3\left(t_3^{'}\right) e^{-i\omega t_3^{'}} \\
& e^{i\left(E_i-E_{ne}\right)t_1^{'}} e^{i\left(E_{me}-E_i\right)t_2^{'}} e^{i\left(E_{n_d}-E_{me}\right)t_3^{'}}. && (4.56)
\end{aligned}
$$

Upon a two-dimensional Fourier transform one then obtains:

$$
\begin{aligned}
S\left(\omega_\tau, \omega_t\right) &= \frac{1}{(2\pi)^2} \int d\tau \int dt\, e^{i\omega_t t} e^{-i\omega_\tau \tau} P^{(3)}\left(t, \tau\right) \\
&= -\frac{i}{4} \sum_{n_e} \sum_{n_g} \sum_{m_e} a\left(\beta, i, n_e, n_g, m_e\right) \tilde{b}\left(i, n_e, n_g, m_e\right) \\
&\quad \delta\left(\omega_t-\left(E_{m_e}-E_{n_g}\right)\right) \delta\left(\omega_\tau-\left(E_{n_e}-E_i\right)\right) \\
&\quad +\frac{i}{4} \sum_{n_e} \sum_{n_d} \sum_{m_e} a\left(\beta, i, n_e, n_d, m_e\right) \tilde{b}\left(i, n_e, n_d, m_e\right) \\
&\quad \delta\left(\omega_t-\left(E_{n_d}-E_{n_e}\right)\right) \delta\left(\omega_\tau-\left(E_{n_e}-E_i\right)\right). && (4.57)
\end{aligned}
$$

By comparison with the monomer expression Eq. (23), it is seen that along the E_τ-direction the formal expressions for the peak positions, which are characterized by the energy differences $(E_{n_e} - E_i)$ between the initial ground state and the intermediate 1-exciton states are equivalent. On the other hand, along E_t one finds contributions, which stem from a coupling between the 1-exciton states and the ground state, and also between the 1-exciton states and the 2-exciton state. It is needless to say that if in the monomer model a second, higher lying electronically excited state is included, there will also be a similar additional term contributing to the spectrum. Furthermore, in the dimer case, the dependence on the orientation angle β (which is hidden in the coefficients $a\,(\beta, i, n_e, n_g, m_e)$) is essential. If the same calculation method as in the monomer case is chosen (see Sec. (2.3)), the Hamiltonian assigned to the index (s)

$$\hat{H}^D_{vib} = \begin{pmatrix} H^D_g(q_1,q_2) & W^{(s)}_{ge}(1) & W^{(s)}_{ge}(2) & 0 \\ W^{(s)}_{eg}(1) & H^D_{e,1}(q_1,q_2) & J & W^{(s)}_{ed}(2) \\ W^{(s)}_{eg}(2) & J & H^D_{e,2}(q_1,q_2) & W^{(s)}_{ed}(1) \\ 0 & W^{(s)}_{de}(2) & W^{(s)}_{de}(1) & H^D_d(q_1,q_2) \end{pmatrix} \tag{4.58}$$

contains the interaction terms

$$W^{(s)}_{nm}(1) = -\mu_{eg}(1)\; f_-(\beta)\; \sum_{n=1}^{3} f_n(t-T_n)\; \cos\left[\omega_n(t-T_n) - \phi_{s,n}\right] \tag{4.59}$$

$$W^{(s)}_{nm}(2) = -\mu_{eg}(2)\; f_+(\beta)\; \sum_{n=1}^{3} f_n(t-T_n)\; \cos\left[\omega_n(t-T_n) - \phi_{s,n}\right] \tag{4.60}$$

In the following, the application of the proposed numerical methods to aggregate systems is discussed.

Chapter 5

Application of a reflection principle to spectroscopic transitions in molecular dimers

For a simplified illustration of absorption phenomena, a reflection principle is suited (see [67, 68]), which establishes a relation between the coordinate dependence of the initial nuclear wave function in the electronic ground state and the spectrum. This approach is applied to absorption spectra of molecular aggregates. The function which provides this map is the excited state potential surface [19] or the difference potential [69] between the ground and excited state potential function. Thus, the analysis of the spectrum allows to obtain a direct view on quantum mechanical probability distributions. The expression for the absorption-spectrum (Eq. (2.12)) can also be written including the propagator $\hat{U}_g(t)$ in the electronic ground state:

$$\sigma(E) \sim \int_{-\infty}^{\infty} dt \exp(iEt)c(t). \tag{5.1}$$

Thereby the time-correlation function $c(t)$ is defined as

$$c(t) = \left\langle \hat{U}_g(t)\hat{\mu}\psi_g | \hat{U}_e(t)\hat{\mu}\psi_g \right\rangle, \tag{5.2}$$

and E denotes the photon energy. The correlation-function contains the initial ground-state wave function ψ_g, multiplied by the projection of the transition dipole-moment on the laser polarization ($\hat{\mu}$). In order to calculate $c(t)$, one has to perform a time-evolution in the ground (g) and excited (e) state with the respective propagators $\hat{U}_n(t) = \exp(-i\hat{H}_n t)$, where $\hat{H}_n$ is the nuclear Hamiltonian in the electronic state (n). Within the reflection approximation, operators of the kinetic energy are neglected leading to

$$c(t) \sim \langle \hat{\mu}\psi_g | \exp(-iD_{e,g}t)\hat{\mu}\psi_g \rangle, \tag{5.3}$$

with the difference of the excited- and ground-state potential $D_{e,g}(\vec{q})$ depending on a set of coordinates $\vec{q} = (q_1, ..., q_n)$. In what follows, the Condon approximation is applied, i. e. all spectra are evaluated employing a coordinate independent transition dipole moment ($\mu = 1$). In order to establish a connection between the ground state wave function and the absorption-spectrum, the former is taken as an (unnormalized) Gaussian centered at the equilibrium configuration $\vec{q} = 0$:

$$\psi_g(\vec{q}) = \exp\left(-\sum_n \beta_n q_n^2\right). \tag{5.4}$$

The difference potential is linearized around the equilibrium position as

$$D_{eg}(\vec{q}) = D_{eg}(0) - \sum_n \left(\frac{\partial D_{eg}(\vec{q})}{\partial q_n}\right)(0)\ q_n = D_0 - \sum_n D_n q_n. \tag{5.5}$$

Under these assumptions, the spectrum takes the simple form

$$\sigma(E) \sim \left(\frac{1}{\beta D}\right)^{\frac{1}{2}} \exp\left(-\frac{(E-D_0)^2}{4D}\right), \tag{5.6}$$

where the abbreviations

$$\beta = \beta_1 * \beta_2 * ... * \beta_n, \; D = \sum_n \frac{D_n^2}{\beta_n} \tag{5.7}$$

are used. The spectrum thus is a Gaussian reflecting the probability density of the ground state wave function [19].

In the following considerations the reflection principle is applied to the dimer problem, where the angle between the transition dipole moments is fixed to $\beta = 90\,^\circ$. In this case, two bands with equal intensity appear in the absorption-spectrum [10, 12]. Fig. (5.1) illustrates spectral features of a monomer/ dimer model system. The upper panels ((a) and (d)) show the monomer spectrum. Here, a spectral resolution of $\Delta E = 68\,\text{meV}$ is used. The latter is introduced by truncating the correlation-function with a Gaussian window function of FWHM (full with at half maximum) ΔT, with $\Delta E \Delta T = 8\ln(2)$ in atomic units ($\hbar = 1$). The resolution is such that the vibrational progression is clearly visible. The dimer spectrum, for a coupling of $J = 0.5\,\text{eV}$, is shown in panel (b) of Fig. (5.1). Due to the strong coupling, the monomer band splits into two separated bands, each exhibiting a vibrational structure. With decreasing resolution ($\Delta E = 181\,\text{meV}$), the vibrational progression is washed out, leading to two unstructured bands. This is also true in the case of a weaker coupling $J = 0.108\,\text{eV}$, as can be taken from the spectra contained in panels (e) and (f). There, the absorption bands overlap, giving rise to a complicated structure if a higher resolution is present (panel (e)). On the other hand, the low-resolution spectrum (panel (f)) exhibits only the broad electronic band structure.

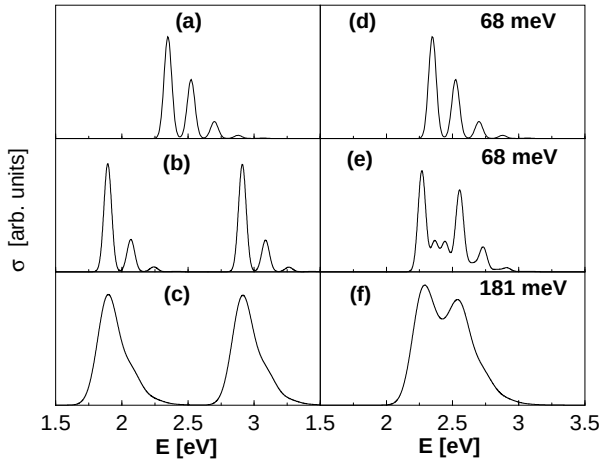

Figure 5.1: *Panels (a) and (d) show the (identical) monomer spectrum. The dimer spectra in panels (b) and (c) are calculated for a coupling element of* $J = 0.5\,\mathrm{eV}$ *and spectral resolutions of* $68\,\mathrm{meV}$ *and* $181\,\mathrm{meV}$*, respectively. The spectra obtained for a weaker coupling of* $J = 0.108\,\mathrm{eV}$ *are displayed in panels (e) and (f).*

In Fig. (5.2), spectra obtained from the numerically exact calculation (solid lines) are compared with those obtained within the reflection approximation dashed lines), where Eq. (5.3) is applied to the adiabatic potentials of the dimer problem (see Eqs. (5.11) and (5.12) below). Results are displayed for two couplings ($J = 0.5\,\mathrm{eV}$, left panels, $J = 0.108\,\mathrm{eV}$, right panels) and different resolutions, as indicated. Because, within the approximate treatment, the kinetic energy of the nuclei is neglected, no vibrational structure is present. Nevertheless, the figure documents that the energetic position of the different bands, and also their overall width is excellently reproduced. In the low resolution case, where the vibrational progression is smeared out, the exactly and approximately determined spectra agree best.

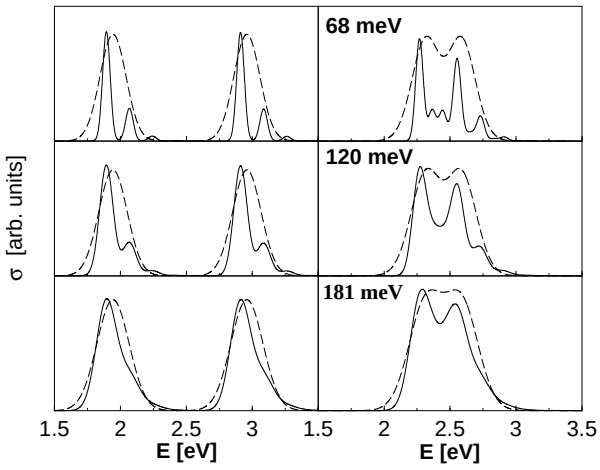

Figure 5.2: *Dimer spectra for a coupling of* $J = 0.5\,\mathrm{eV}$ *(left hand panels) and* $J = 0.108\,\mathrm{eV}$ *(right hand panels). Different resolutions are used, as indicated. Numerically exact spectra (solid lines) are compared to those obtained within the reflection approximation (dashed lines).*

The following considerations aim at an interpretation of the absorption-spectrum in terms of the probability density of the initial state, preferentially as a function of a single coordinate. It is not clear intuitively that this is possible, because the dimer model involves two coupled excited electronic states and two degrees-of-freedom. In order to disentangle this problem, center-of-mass (q_s) and relative (q_r) coordinates are introduced as

$$\begin{pmatrix} q_s \\ q_r \end{pmatrix} = \sqrt{\frac{1}{2}} \begin{pmatrix} 1 & 1 \\ -1 & 1 \end{pmatrix} \begin{pmatrix} q_1 \\ q_2 \end{pmatrix}. \tag{5.8}$$

It has long been known [10] that using this transformation, the coupled two-dimensional dimer problem can be separated into two one-dimensional problems, where only one carries the coupling.

Upon using Eq. (5.8), the excited state Hamiltonian takes the form

$$\hat{H}^D(q_s, q_r) = \begin{pmatrix} \hat{H}^D_+ & J \\ J & \hat{H}^D_- \end{pmatrix}, \tag{5.9}$$

with

$$\begin{aligned} \hat{H}^D_\pm(q_s, q_r) &= \left(\frac{p_s^2}{2} + \frac{p_r^2}{2}\right) \\ &+ \left(\frac{1}{2}\omega^2\left(q_s - \frac{q_e}{\sqrt{2}}\right)^2 + \frac{1}{2}\omega^2\left(q_r \pm \frac{q_e}{\sqrt{2}}\right)^2\right) + \Delta E_e \\ &= \hat{T}(q_s) + \hat{T}(q_r) + V_{e\pm}(q_s, q_r), \end{aligned} \tag{5.10}$$

where $\hat{T}(q_n)$ denotes the kinetic energy operators in the q_m -degree-of-freedom. Next, employing the reflection approximation, the coupled excited state problem is decoupled. The transformation matrix $\hat{A}(q_r)$ diagonalizes the excited state potential matrix and thus also the matrix containing the difference potentials

$$\hat{A}^T \hat{D}_{e,g} \hat{A} = \hat{A}^T \begin{pmatrix} V_{e+} - V_g & J \\ J & V_{e-} - V_g \end{pmatrix} \hat{A} = \begin{pmatrix} D_1^a & 0 \\ 0 & D_2^a \end{pmatrix} \tag{5.11}$$

where $V_g(q_s, q_r)$ is the ground state potential. The adiabatic difference potentials D_n^a are now linearized:

$$D_n^a(q_s, q_r) = D_{n0}^a - D_{ns}^a q_s - D_{nr}^a q_r. \tag{5.12}$$

Here, D_{ns}^a and D_{nr}^a denote the partial derivatives of the adiabatic difference potentials with respect to the variables q_r and q_s, evaluated at the equilibrium position. For the potentials employed in the model, the partial derivatives can be determined analytically yielding $D_{ns}^a = \omega^2 q_e/\sqrt{2}$, whereas D_{nr}^a vanishes.

This yields the simple expression for the absorption-spectrum (see Eq. 5.6):

$$\sigma(E) \sim \sum_{n=1,2} \exp\left(-\frac{(E - D^a_{n0})^2}{4D}\right). \tag{5.13}$$

The constant $D = D^2_{n,s}/\beta_s$ contains only properties corresponding to the center-of-mass degree-of-freedom q_s. Thus, the spectrum originates from two identical bands which, depending on the coupling strength J, are shifted in energy against each other. The derived one-dimensional reflection principle is illustrated in Fig. (5.3), which contains the adiabatic difference potentials as a function of q_s.

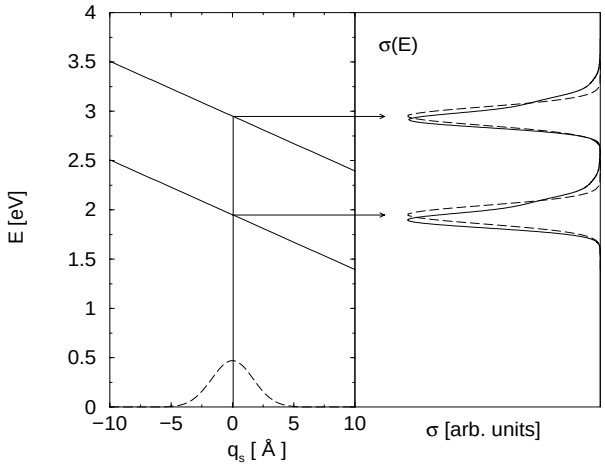

Figure 5.3: *Reflection principle for dimer systems. Shown are the adiabatic difference potentials along the center-of-mass coordinate q_s, together with the respective ground state vibrational density (left panel). Absorption spectra calculated numerically exactly (solid lines) are compared to the ones obtained from the mapping of the density via the difference potentials (dashed lines).*

The ground state density in this coordinate is mapped onto the energy scale via these functions giving rise to two absorption bands (dashed lines) which are in excellent agreement with the numerically exact spectra (solid lines).

One can conclude that the contribution of the relative part only results in a splitting of two energy levels, whereas the center-of-mass part influences the band shape. Furthermore, it is interesting to note that if the frequency ω is given (from a vibrational progression in a measured spectrum), the scheme shown in Fig. (5.3) allows, in principle, to determine the displacement q_e. Under the assumption $\omega_g = \omega_e = \omega$, the difference potential

$$V_e(q_s, 0) - V_g(q_s, 0) = \frac{1}{2}\omega_e^2 \left(q_s - \frac{q_e}{\sqrt{2}} \right)^2 + \Delta E - \frac{1}{2}\omega_g^2 q_s^2 \tag{5.14}$$

becomes

$$V_e(q_s, 0) - V_g(q_s, 0) = -\omega^2 \frac{q_e}{\sqrt{2}} q_s + \frac{1}{2}\omega^2 \frac{q_e^2}{2} + \Delta E. \tag{5.15}$$

Thus, the gradient

$$-D_{n,s} = -\omega^2 \frac{q_e}{\sqrt{2}} \tag{5.16}$$

is found. According to Eq. (5.13), the full width at half maximum w_h of an absorption peak within the reflection principle approximation is given as

$$w_h = \sqrt{\frac{4\ln(2)}{D}} = \frac{\sqrt{4\ln(2)\beta_s}}{D_{n,s}} = \frac{\sqrt{8\ln(2)\beta_s}}{\omega^2 q_e}, \tag{5.17}$$

which yields the displacement

$$q_e = \frac{\sqrt{8\ln(2)\beta_s}}{\omega^2 w_h}. \tag{5.18}$$

This means that the parameter β_s of the ground state Gaussian wave function is needed as well as the vibrational frequency ω and the full width at half maximum w_h in order to obtain the displacement q_e.

Chapter 6

Linear spectra of molecular aggregates

6.1 Geometry dependence of dimer spectra

For an analytical investigation of the geometry dependence of dimer spectra, it is advantageous to use the simplified Hamiltonian

$$\hat{H}_e = \begin{pmatrix} E_d & J \\ J & E_d \end{pmatrix}, \tag{6.1}$$

where E_d and J denote the excited state energy level of the monomer units and the coupling matrix element, respectively. It can be diagonalized using the matrix

$$\hat{A} = \frac{1}{\sqrt{2}} \begin{pmatrix} 1 & 1 \\ -1 & 1 \end{pmatrix}. \tag{6.2}$$

Simplifying the notation by setting $\psi_0 = 1$, the time correlation-function in the case of CD-spectroscopy

$$c_{\mu m}(t) \sim \sin(\beta) \left\langle \mu_2 \psi_i \right| \hat{U}_e(t) \left| \mu_1 \psi_i \right\rangle \tag{6.3}$$

takes the form

$$\begin{aligned} c_{\mu m}(t) &\sim \sin(\beta) \left\langle \hat{A}^T \begin{pmatrix} 0 \\ 1 \end{pmatrix} \middle| \hat{A}^T \hat{U}_e \hat{A} \middle| \hat{A}^T \begin{pmatrix} 1 \\ 0 \end{pmatrix} \right\rangle \\ &= \sin(\beta) \left(\exp\left(-i \left(E_d + J\right) t\right) - \exp\left(-i \left(E_d - J\right) t\right)\right). \end{aligned} \tag{6.4}$$

A Fourier-transform of this expression leads to the result

$$\sigma_{CD}(E) \sim \sin(\beta) \left(\delta\left(E - (E_d + J)\right) - \delta\left(E - (E_d - J)\right)\right). \tag{6.5}$$

This formula predicts two bands with equal intensity proportional to $\sin(\beta)$. However, the lower energy band has a negative sign in the case of a positive coupling matrix element, while the sign of the upper energy band is positive. This is an important difference compared to dimer absorption-spectra, where the simplified model leads to relative intensities of upper and lower band given by the ratio (see Sec. (A.1))

$$I_r = \frac{I_{upper}}{I_{lower}} = \frac{\cos^2\left(\frac{\beta}{2}\right)}{\sin^2\left(\frac{\beta}{2}\right)}. \tag{6.6}$$

The angle dependence of absorption- and CD-spectra, which result from calculations employing the complete dimer Hamiltonian with a constant coupling $J = 0.25\,\mathrm{eV}$, is illustrated in Fig. (6.1).

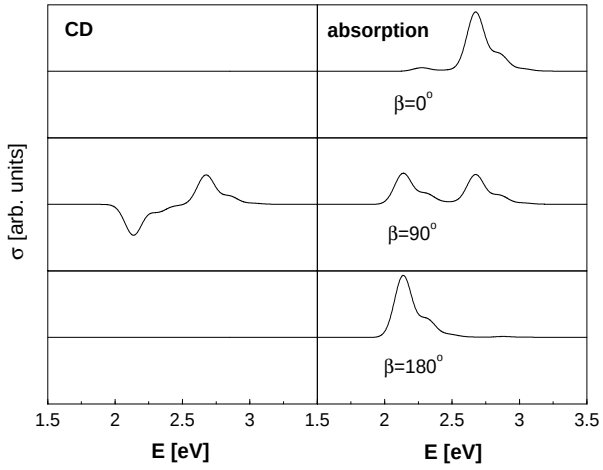

Figure 6.1: *Comparison of absorption- and CD-spectra of the dimer model system ($J = 0.25\,\mathrm{eV}$) for different angles.*

For an angle of $\beta = 0\,^\circ$, the CD spectrum vanishes and only the upper band is excited in the absorption-spectrum. With increasing angle, the CD-spectrum becomes more intensive until it reaches its maximum at $\beta = 90\,^\circ$. However, the form of the CD-spectrum does not change. Furthermore, the relations $\sigma_{CD}(180\,^\circ - \beta) = \sigma_{CD}(\beta)$ and $\sigma_{CD}(360\,^\circ - \beta) = -\sigma_{CD}(\beta)$ are relevant. This means that for $\beta = 180\,^\circ$ the CD-spectrum vanishes and for angles $\beta > 180\,^\circ$ the signs of the bands are inverted. In the case of absorption, the intensity of the lower band increases for $\beta > 0\,^\circ$ until the band intensities are equal at $\beta = 90\,^\circ$. A further increase of the angle leads to a dominance of the lower band until it is excited exclusively at $\beta = 180\,^\circ$. For even larger angles, the relation $\sigma_{abs}(360\,^\circ - \beta) = \sigma_{abs}(\beta)$ is found. Not only the angle, but also the coupling has an important influence on dimer absorption- and CD-spectra. In the case of small coupling constants, vibrational structures and broadening effects make the determination of the relative band intensities difficult, see Fig. (6.2).

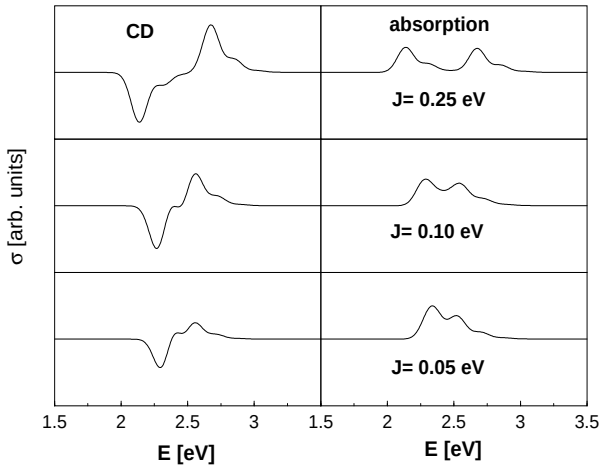

Figure 6.2: *Comparison of absorption- and CD-spectra of the dimer model system ($\beta = 90\,^\circ$) for different coupling constants.*

In contrast to absorption-spectra, the band splitting can easily be extracted from the CD-spectra even in the case of small coupling constants. Thereby the accuracy is limited by the energy resolution. In Fig. (6.3), absorption- and CD-spectra for different values of the coupling element J are shown. The curves in the left and right hand panels differ in their energy resolution $\Delta\epsilon$. First, the separation of the two absorption bands is discussed. For the largest value of J, two bands are detected having extrema separated by a value of twice the coupling element, as expected. A decrease of the coupling shifts the bands closer to each other and already for a value of $J = 0.15\,\mathrm{eV}$ they show a substantial overlap. With increasing overlap, the separation of the maxima seen in the absorption-spectra becomes more difficult. In fact, no clear maximum structure (originating from excitation of the lower energy state) can then be seen. Rather, the spectrum only exhibits a shoulder. On the other hand, the CD-spectra consisting of negative and positive branches clearly show characteristics of two separated bands.

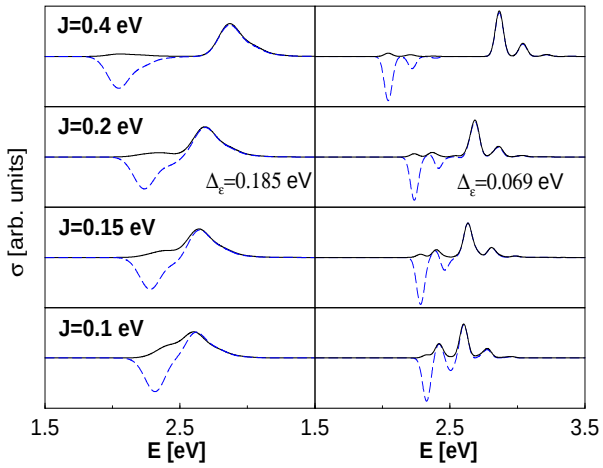

Figure 6.3: *Absorption (solid lines) and CD-spectra (dashed lines) calculated for different coupling J, as indicated. The curves in the left and right hand panels were obtained with a spectral resolution of* $\Delta\epsilon = 0.185\,\mathrm{eV}$ *and* $\Delta\epsilon = 0.069\,\mathrm{eV}$*, respectively.*

Increasing the resolution to $\Delta\epsilon = 0.069\,\mathrm{eV}$ results in a vibrational progression on each of the two bands. Again, for the largest coupling, the separation of the respective vibrational peaks can be used to extract a reliable value of the coupling element. This procedure becomes increasingly difficult with decreasing J. It is obvious that with increasing overlap between the absorption bands the intensity ratio I_r is modified. In particular, the relative magnitude of the low energy band is enhanced. This is clearly documented in Fig. (6.4), which contains absorption-spectra calculated with a resolution of $\Delta\epsilon = 0.139\,\mathrm{eV}$. Already for a coupling value of $J = 0.1\,\mathrm{eV}$, I_r assumes a value which is about 7 times smaller than the value extracted from the $J = 0.4\,\mathrm{eV}$ curve. This leads to an angle larger than $70\,^\circ$, which differs essentially from the real value of $30\,^\circ$. For a smaller coupling, two peaks of equal height ($J = 0.05\,\mathrm{eV}$) are found and then the peak at lower energy becomes even larger than the next one. Here, however, one has to be careful, because

for coupling values below $J = 0.09\,\mathrm{eV}$, the electronic level splitting becomes comparable to the vibrational spacing present in the model system. This is seen if comparing the dimer spectra to the monomer spectrum (obtained for $J = 0.0\,\mathrm{eV}$), which is included as a dotted line in the lower panel of Fig. (6.4). In the limit of an uncoupled system, the CD-spectrum vanishes.

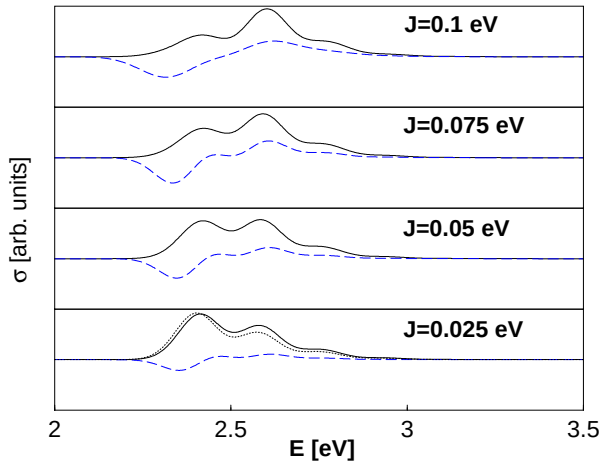

Figure 6.4: *Absorption (solid lines) and CD-spectra (dashed lines) calculated for different coupling J. The absorption-spectra evolve into the monomer spectrum (dotted line in the lower panel) in the case of small coupling.*

Finally, some investigations on the geometry dependence of the dimer emission-spectrum are taken into account. According to Eq. (4.30), the emission-spectrum of the dimer is expected to disappear within the simplified model if the coupled ground state within the electronic excited state is given as

$$\vec{\psi}_{e,0} = \sqrt{\frac{1}{2}} \begin{pmatrix} 1 \\ -1 \end{pmatrix}. \tag{6.7}$$

The maximal intensity of the emission-spectrum is expected for an angle of $\beta = 180\,^{\circ}$. In Fig. (6.5), the results of the calculations employing the complete dimer model are shown.

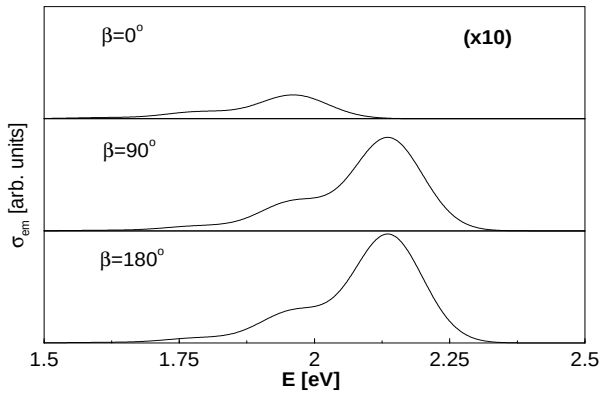

Figure 6.5: *Comparison of emission-spectra of the dimer model system ($J = 0.25\,\mathrm{eV}$) for different angles.*

As the emission takes place from the energetically lowest coupled eigenstate within the electronically excited state, which consists of two components with opposite sign, the spectrum is red-shifted with respect to the monomer reference. For $\beta = 180\,^\circ$ (lower panel), the emission-spectrum has the highest intensity, in the case of $\beta = 90\,^\circ$ (middle panel) it is a little smaller. Although for $\beta = 0\,^\circ$ no emission-spectrum is expected from the simplified model, the transition is not strictly forbidden if vibrations are included and the components of the initial wave function are shifted relative to each other with respect to the nuclear coordinates. In this case a very small emission-spectrum (upper panel, multiplied by a factor of 10) is obtained. The apparent redshift can be explained as follows: Upon symmetry, the overlap integrals of the initial wave functions with the vibrational ground state of the electronic ground state have the same absolute value and opposite sign and therefore cancel each other out. Accordingly, the peak assigned to the corresponding transition does not appear in the emission-spectrum. Thus, the first peak with remarkable intensity belongs to the transition to the first excited vibrational eigenstate.

6.2 Geometry dependence of trimer spectra

In the following section, the influence of geometrical parameters on trimer spectra is investigated. Thereby the capability of the trimer model system in terms of interpreting measured aggregate spectra is discussed. Depending on the form of the excited state Hamiltonian

$$\hat{H}_j = \begin{pmatrix} \hat{H}_1(q_1,q_2,q_3) & J & J\delta_{j,c} \\ J & \hat{H}_2(q_1,q_2,q_3) & J \\ J\delta_{j,c} & J & \hat{H}_3(q_1,q_2,q_3) \end{pmatrix}, \tag{6.8}$$

the trimer system is characterized as linear ($j = l$) or cyclic ($j = c$). In order to reduce the numerical effort, the three-dimensional problem is split up into a one-dimensional and a coupled two-dimensional problem. This is carried out by the coordinate transformation

$$\begin{pmatrix} q_1' \\ q_2' \\ q_3' \end{pmatrix} = \begin{pmatrix} \sqrt{\frac{1}{3}} & \sqrt{\frac{1}{3}} & \sqrt{\frac{1}{3}} \\ \sqrt{\frac{1}{6}} & -\sqrt{\frac{2}{3}} & \sqrt{\frac{1}{6}} \\ \sqrt{\frac{1}{2}} & 0 & \sqrt{\frac{1}{2}} \end{pmatrix} \begin{pmatrix} q_1 \\ q_2 \\ q_3 \end{pmatrix}, \tag{6.9}$$

leading to the Hamiltonian ($j = l, c$, for the linear or cyclic configuration, respectively)

$$\hat{H}_j(q_1',q_2',q_3') = \begin{pmatrix} H_S & 0 & 0 \\ 0 & H_S & 0 \\ 0 & 0 & H_S \end{pmatrix} + \begin{pmatrix} H_{R,1} & J & J\delta_{j,c} \\ J & H_{R,2} & J \\ J\delta_{j,c} & J & H_{R,3} \end{pmatrix}, \tag{6.10}$$

where the 'center of mass' Hamiltonian is

$$H_S(q_1') = \frac{1}{2}p_1'^2 + \frac{1}{2}\omega^2 \left(q_1' - \sqrt{\frac{1}{3}}q_e \right)^2 + \Delta E \tag{6.11}$$

with p'_1 being the momentum operator in the q'_1 degree of freedom. The coupled two-dimensional problem contains the Hamiltonians

$$\begin{aligned} H_{R,1}(q'_2, q'_3) &= \frac{1}{2}(p'^2_2 + p'^2_3) \\ &+ \frac{1}{2}\omega^2 \left(\left(q'_2 - \sqrt{\frac{1}{6}} q_e \right)^2 + \left(q'_3 - \sqrt{\frac{1}{2}} q_e \right)^2 \right) \qquad (6.12) \\ H_{R,2}(q'_2, q'_3) &= \frac{1}{2}(p'^2_2 + p'^2_3) + \frac{1}{2}\omega^2 \left(\left(q'_2 + \sqrt{\frac{2}{3}} q_e \right)^2 + q'^2_3 \right) \qquad (6.13) \\ H_{R,3}(q'_2, q'_3) &= \frac{1}{2}(p'^2_2 + p'^2_3) \\ &+ \frac{1}{2}\omega^2 \left(\left(q'_2 - \sqrt{\frac{1}{6}} q_e \right)^2 + \left(q'_3 + \sqrt{\frac{1}{2}} q_e \right)^2 \right). \qquad (6.14) \end{aligned}$$

In order to understand the geometry-dependent spectroscopic properties, a simplified model is employed, where the potentials are replaced by constant energy levels E_t. The Hamiltonian for the cyclic configuration can be diagonalized using the matrix

$$\hat{A}_c = \begin{pmatrix} -\sqrt{\frac{1}{6}} & \sqrt{\frac{1}{2}} & -\sqrt{\frac{1}{3}} \\ \sqrt{\frac{2}{3}} & 0 & \sqrt{\frac{1}{3}} \\ -\sqrt{\frac{1}{6}} & -\sqrt{\frac{1}{2}} & \sqrt{\frac{1}{3}} \end{pmatrix}. \qquad (6.15)$$

This leads to the eigenvalues $E_{1,c} = E_{2,c} = E_t - J$ and $E_{3,c} = E_t + 2J$. In what follows, all monomer transition dipole-moments $\vec{\mu}_n$ are supposed to be arranged in the (x, y)-plane, so that the projection on the laser polarization vector $\vec{\epsilon} = \vec{\epsilon}_x + \vec{\epsilon}_y$ is

$$\vec{\epsilon}\vec{\mu} = \vec{\epsilon}(\vec{\mu}_1 + \vec{\mu}_2 + \vec{\mu}_3) = \sum_{n=1}^{3} |e, n\rangle \, f_n \, \langle g| \,, \qquad (6.16)$$

where the definitions

$$\begin{aligned} f_1 &= \cos(\beta) - \sin(\beta) \\ f_2 &= 1 \\ f_3 &= \cos(\gamma) + \sin(\gamma). \end{aligned} \tag{6.17}$$

take place. In what follows, the considerations are restricted to the (likely) case, where the orientation angles of two coupled monomer transition dipole-moments are equal, i. e. $\gamma = \beta$. The correlation-function in the case of absorption then is of the form

$$\begin{aligned} c_{abs}(t) &= \left\langle \hat{A}_c^T \begin{pmatrix} f_1\psi_0 \\ f_2\psi_0 \\ f_3\psi_0 \end{pmatrix} \middle| \hat{A}_c^T \hat{U}_e \hat{A}_c \middle| \hat{A}_c^T \begin{pmatrix} f_1\psi_0 \\ f_2\psi_0 \\ f_3\psi_0 \end{pmatrix} \right\rangle \\ &= \sum_{n=1}^{3} I_{n,c} \exp\left(-iE_{n,c}t\right) \end{aligned} \tag{6.18}$$

with the definitions

$$\begin{aligned} I_{1,c} &= \left| -\sqrt{\frac{1}{6}}\left(f_1 + f_3\right) + \sqrt{\frac{2}{3}} f_2 \right|^2 \\ I_{2,c} &= \left| \sqrt{\frac{1}{2}}\left(f_1 + f_2\right) \right|^2 \\ I_{3,c} &= \left| \sqrt{\frac{1}{3}}\left(f_1 + f_2 + f_3\right) \right|^2 . \end{aligned} \tag{6.19}$$

The absorption-spectrum is obtained by the Fourier-transform of the correlation-function leading to

$$\sigma_{abs}(E) \sim \delta(E - (E_{1,c} - E_0))(I_{1,c} + I_{2,c}) + \delta(E - (E_{3,c} - E_0))I_{3,c}, \tag{6.20}$$

where the fact has been used that the lower two levels $E_{1,c}$, $E_{2,c}$ are degenerated. While the intensity of the energetically lower band is given by the sum of the first two terms, the intensity of the energetically higher band is related to the third term of the expressions

$$\begin{aligned} I_{1,c} &= 1 + \frac{1}{3}\cos(2\beta) - \frac{4}{3}\cos(\beta) \\ I_{2,c} &= 1 - \cos(2\beta) \\ I_{3,c} &= 1 + \frac{2}{3}\cos(2\beta) + \frac{4}{3}\cos(\beta). \end{aligned} \tag{6.21}$$

From these equations it is obvious that the absorption-spectrum sensitively depends on the relative orientation of the monomer transition dipole-moments. In contrast, the signs and intensities of the electronic bands in the CD-spectrum can be predicted using the results

$$\begin{aligned} I_{1,c} &= -\frac{2}{3}\sin(\beta) + \frac{1}{3}\sin(2\beta) \\ I_{2,c} &= -\sin(2\beta) \\ I_{3,c} &= \frac{2}{3}\sin(\beta) + \frac{2}{3}\sin(2\beta). \end{aligned} \tag{6.22}$$

The case of emission is easy to treat because a separable ground state Hamiltonian is assumed. Replacing the latter by an energy $E_{0,g}$ and following the steps outlined above, the emission-spectrum can be written as

$$\begin{aligned} \sigma_{em}(E) &\sim \delta(E_{0,e} - (E_{0,g} + E))(1 + 2\cos(2\beta)\,\langle\psi_{0,e,1}|\psi_{0,e,3}\rangle \\ &+ 2\cos(\beta)\,\langle\psi_{0,e,1}|\psi_{0,e,2}\rangle + 2\cos(\beta)\,\langle\psi_{0,e,2}|\psi_{0,e,3}\rangle). \end{aligned} \tag{6.23}$$

The analysis of the geometry dependence of the spectra presented for the cyclic trimer can be performed in a similar way for the linear configuration. There, the Hamiltonian is diagonalized employing the transformation matrix

$$\hat{A} = \begin{pmatrix} \frac{1}{2} & \sqrt{\frac{1}{2}} & -\frac{1}{2} \\ \sqrt{\frac{1}{2}} & 0 & \sqrt{\frac{1}{2}} \\ \frac{1}{2} & -\sqrt{\frac{1}{2}} & -\frac{1}{2} \end{pmatrix}. \tag{6.24}$$

This leads to the eigenvalues $E_{1,l} = E_t + \sqrt{J}$, $E_{2,l} = 0$ and $E_{3,l} = E_t - \sqrt{J}$. The angular averaged absorption-spectrum reads

$$\sigma_{abs}(E) \sim \sum_{n=1}^{3} I_{n,l}\delta(E - (E_{n,l} - E_0)) \tag{6.25}$$

with the relative band intensities

$$\begin{aligned} I_{1,l} &= 1 + \frac{1}{2}\cos(2\beta) + \sqrt{2}\cos(\beta) \\ I_{2,l} &= 1 - \cos(2\beta) \\ I_{3,l} &= 1 + \frac{1}{2}\cos(2\beta) - \sqrt{2}\cos(\beta). \end{aligned} \tag{6.26}$$

In the case of CD-spectra, the result

$$\begin{aligned} I_{1,l} &= \sqrt{\frac{1}{2}}\sin(\beta) + \frac{1}{2}\sin(2\beta) \\ I_{2,l} &= -\sin(2\beta) \\ I_{3,l} &= -\sqrt{\frac{1}{2}}\sin(\beta) + \frac{1}{2}\sin(2\beta) \end{aligned} \tag{6.27}$$

is obtained. The expression for the emission-spectrum is identical to the one derived for the cyclic geometry, see Eq. (6.23), where the coupled vibrational wave functions in the electronic excited state are different because of the changed coupling scheme. In the results of the numerical calculations, which are proposed in the following, the complete nuclear dynamics in the coupled excited state potentials is included.

The absorption properties are the first issue to discuss. In Fig. (6.6), absorption-spectra for both trimer configurations obtained for a coupling element of $J = 0.4\,\mathrm{eV}$ are shown.

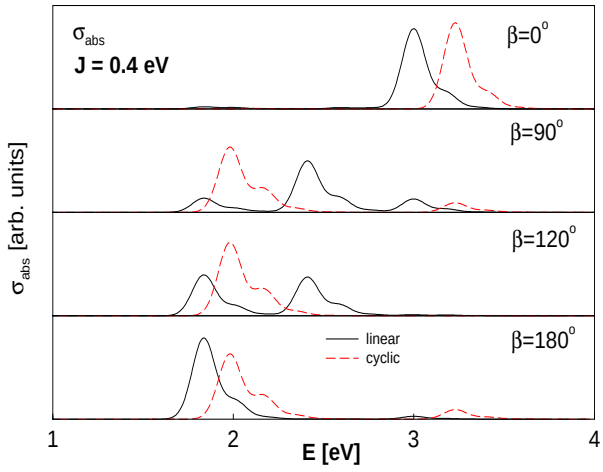

Figure 6.6: *Absorption spectra calculated for a coupling strength of* $J = 0.4\,\mathrm{eV}$ *and various orientation angles* β*, as indicated. Results for the cyclic (dashed lines) and linear (solid lines) configuration are compared.*

The spectra are calculated in low resolution. Therefore, the correlation-functions are convoluted with a Gaussian window function of full width at half maximum of $\tau_w = 24.3\,\mathrm{fs}$. For the cyclic trimer, one expects two absorption bands. Because of the degeneracy at lower energies (for a positive coupling J), the lower band results from a summation over the intensity profiles $I_{1,c}$ and $I_{2,c}$. However, here the transition dipole-moment geometry comes into play. Fig. (6.6) documents that for a parallel orientation ($\beta = 0\,^\circ$, upper panel, dashed line) a single absorption band with a diffuse vibrational structure at higher energies appears. This can be understood by inspection of Eq.(6.21), which shows that the two overlapping bands at the smaller energy, having intensities of $I_{1,c}$, $I_{2,c}$ are identically zero. Changing the angle to $\beta = 90\,^\circ$ has a dramatic effect: now the upper band looses intensity and

the second band around 2 eV appears. The intensity ratio $\frac{I_{1,c}+I_{2,c}}{I_{3,c}}$ is about 7.5, which is slightly lower than estimated from the simple model leading to the analytical expression for the intensities. Of course, such deviations are to be expected because of the Franck-Condon factors corresponding to the various transitions. It is as well possible that the lower band is exclusively present, which is the case for an orientation of $\beta = 120\,^\circ$. Finally, the spectrum for the anti-parallel orientation ($\beta = 180\,^\circ$) is identical to the one for the $\beta = 90\,^\circ$ case, which follows directly from Eqs. (6.21). As a result, the absorption-spectra of the cyclic trimer depend sensitively on the transition-dipole geometry. The same holds for the linear configuration. The respective spectra are included in Fig. (6.6) for the same orientation angles. In this case, the former analysis shows that, in general, one has to expect three absorption bands of different intensity. However, the orientations with $\beta = 0\,^\circ$ and $180\,^\circ$ result in single bands at larger and lower energies, respectively. In each case, the other two bands are of such small intensity that they are not likely to be detected in an experiment. On the other hand, for $\beta = 120\,^\circ$ one finds a double-band spectrum and only the case with the perpendicular orientation ($\beta = 90\,^\circ$) exhibits three absorption bands. All these features are explained in applying the expressions given in Eqs. (6.26). This directly hints at the question if geometric information can be obtained from a measured trimer absorption-spectrum. The following example, where the angles are fixed to values of $80\,^\circ$, illustrates that this is feasible, in principle. The absorption-spectrum, which then serves as a starting point for the inversion procedure, is shown in Fig. (6.7).

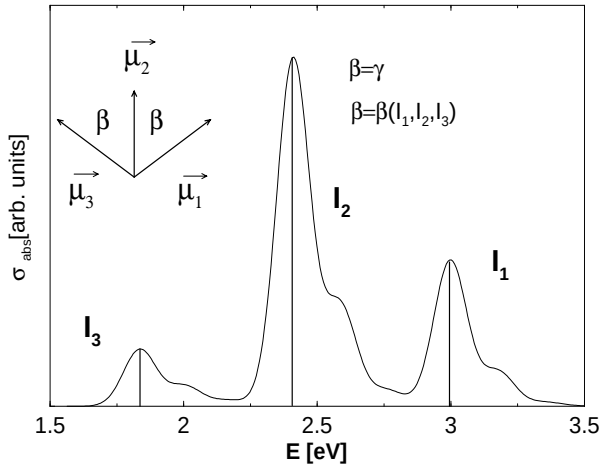

Figure 6.7: *Absorption spectra calculated for a coupling strength of* $J = 0.4\,\mathrm{eV}$ *and various orientation angles* β*, as indicated. Results for the cyclic (dashed lines) and linear (solid lines) configuration are compared.*

The figure indicates the determination of the angle . Because it is a function of the band intensities I_n, its value can be extracted. From Eqs. (6.26), the functional dependence

$$\cos(\beta) = \frac{3}{2\sqrt{2}} \frac{I_1 - I_3}{I_1 + I_2 + I_3} \tag{6.28}$$

is found (for $\beta = \gamma$). From the spectrum, the values of $I_3 = 57.2$, $I_2 = 348.4$, and $I_1 = 146.1$ are taken, which yield a value of $\beta = 80.2\,^\circ$, in perfect agreement with the input data. Note that another likely configuration is defined by $\beta = -\gamma$. In this case, however, the intensity I_2 vanishes, so that no central absorption band exists and the situation is well distinguishable from the former one. A comparison of the two coupling schemes shows that they result in quite different absorption-spectra. This leads to the conclusion that - except for the case where three clearly separated bands are found - it is not possible to determine if the system is a of cyclic or linear geometry.

This is even more critical if one considers the case of a smaller coupling constant J. Fig. (6.8) contains spectra calculated for a value of $J = 0.1\,\mathrm{eV}$.

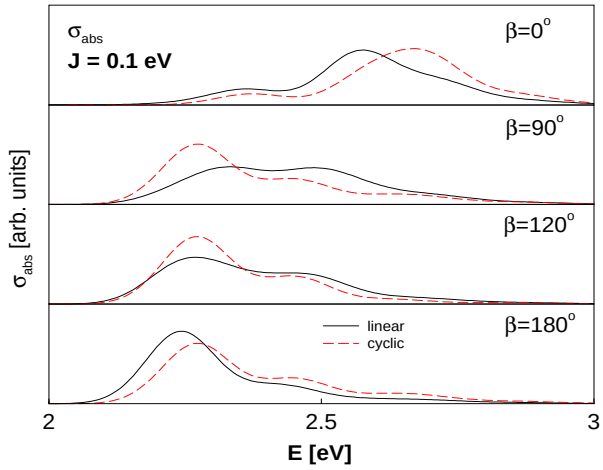

Figure 6.8: *Absorption spectra calculated for a coupling strength of* $J = 0.1\,\mathrm{eV}$ *and various orientation angles* β*, as indicated. Results for the cyclic (dashed lines) and linear (solid lines) configuration are compared.*

As the band splitting is directly correlated with the coupling strength, the band separation is small and the bands overlap. As a consequence, the spectra for the cyclic and linear configuration become more alike, so that the absorption properties alone do not allow to extract information on the structure of the aggregate in the case of a small coupling strength. CD-spectra of trimer systems also show an extensive angle dependence. Some cases are illustrated in Fig. (6.9).

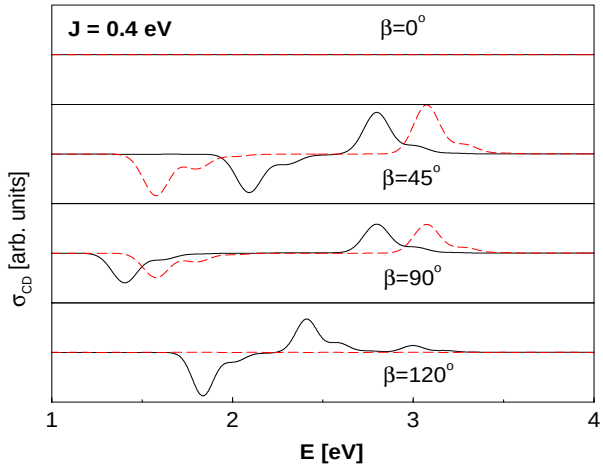

Figure 6.9: *CD-spectra of the linear (solid lines) and cyclic (dashed lines) trimer calculated for a coupling strength of* $J = 0.4\,\mathrm{eV}$ *and various orientation angles* β*, as indicated.*

The case of a linear coupling scheme is discussed first. For $\beta = 0\,^\circ$, no CD-spectrum is obtained. An increase of the angle ($\beta = 45\,^\circ$) leads to an excitation of the middle and the upper band, where the first has a negative, the latter a positive sign. In the case of $\beta = 90\,^\circ$, the middle band vanishes and at the same time the negative lower band appears. At $\beta = 120\,^\circ$, the upper band is replaced by the positive middle band. With a further increase of the angle up to $\beta = 180\,^\circ$, the CD-spectrum vanishes. For even larger angles, the formula $\sigma_{CD}(360\,^\circ - \beta) = -\sigma_{CD}(\beta)$ can be used. If a cyclic coupling scheme is employed, some differences to the linear case are found, see Fig. (6.9). While for $\beta = 0\,^\circ$ and $\beta = 120\,^\circ$ the CD-spectrum disappears, the lower and the upper band appear with negative and positive sign, respectively, for angles in between. A further increase of the angle leads to inverted signs of the peaks, until the CD-spectrum vanishes again at $\beta = 180\,^\circ$. The formula given above in order to predict CD-spectra of linear trimers for angles $\beta > 180\,^\circ$ can also be used in the case of a cyclic coupling scheme.

In the following, emission-spectra are discussed. In Fig. (6.10), angle dependent spectra calculated for a coupling strength of $J = 0.4\,\mathrm{eV}$ are shown. As expected, the spectra are red-shifted as compared to the absorption profiles. For both coupling configurations different intensities are found. Nevertheless, in contrast to the absorption case, the spectra for the linear (solid lines) and cyclic trimer (dashed lines) are similar in their profile for the same orientation geometry. Of course, due to the different energetic positions of the bands in the two cases, they are shifted with respect to each other on the energy scale. The results summarized in Fig. (6.10) can be rationalized employing the simplified considerations, which led to Eq. (6.23).

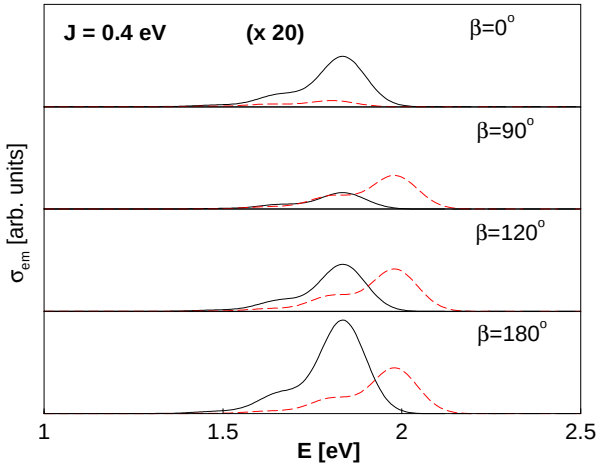

Figure 6.10: *Emission spectra for the cyclic (dashed lines) and linear (solid lines) configuration employing different orientation angles β.*

As an example, the intensity dependence of the spectrum on the orientation geometry for the linear trimer is discussed. There, the excited state ground state vector is given as

$$\begin{pmatrix} \psi_{0,e,1} \\ \psi_{0,e,2} \\ \psi_{0,e,3} \end{pmatrix} = \begin{pmatrix} -\frac{1}{2} \\ \sqrt{\frac{1}{2}} \\ -\frac{1}{2} \end{pmatrix}. \tag{6.29}$$

The emission-spectrum of Eq. (6.23) then reduces to

$$\sigma_{em}(E) \sim \delta(E_{0,e} - (E_{0,g} + E)) \left(1 + \frac{1}{2}\cos(2\beta) - \sqrt{2}\cos(\beta)\right). \tag{6.30}$$

The expression in the brackets yields numbers of 0.086 (0 °), 0.5 (90 °), 1.46 (120 °), and 2.914 (180 °). Similar ratios between the maxima of spectra for different orientations can be taken from Fig. (6.10) (note that the spectrum for the $\beta = 0\,°$ is scaled by a factor of 20). As is the case for absorption, the emission-spectra for both trimer configurations becomes more alike if a weaker excited state coupling exists. This is documented in Fig. (6.11), which collects curves calculated for a value of $J = 0.1\,\mathrm{eV}$.

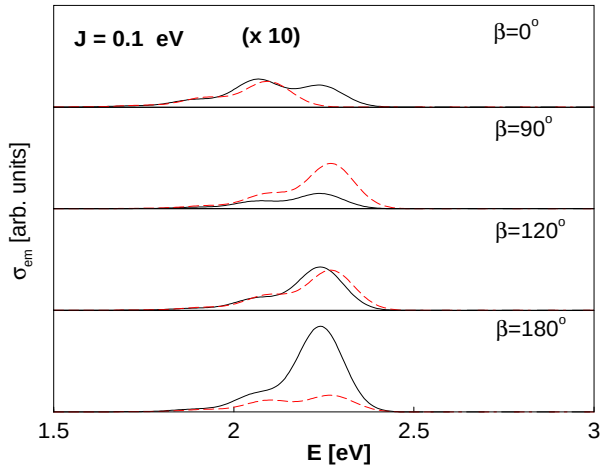

Figure 6.11: *Same as previous figure, but for a coupling of* $J = 0.1\,\mathrm{eV}$.

An interesting case is found for an orientation of the transition dipole-moments, where the angle β equals $45\,^{\circ}$. In this case, the emission to the ground state is dipole-forbidden and only weakly allowed by the involvement of vibrations. This means that the excited state has a long lifetime, so that the decay via a radiative transition is unfavored compared to other processes like an intersystem crossing eventually giving rise to a time-delayed phosphorescence.

6.3 CD-spectroscopy and quantum dynamics

In this section, the time-dependence of time correlation-functions is analyzed in order to find an interpretation in terms of the quantum nuclear motion. The absolute values of the correlation-functions for the case of CD- and absorption-spectroscopy, which correspond to the spectra in Fig. (6.2), are displayed in Fig. (6.12).

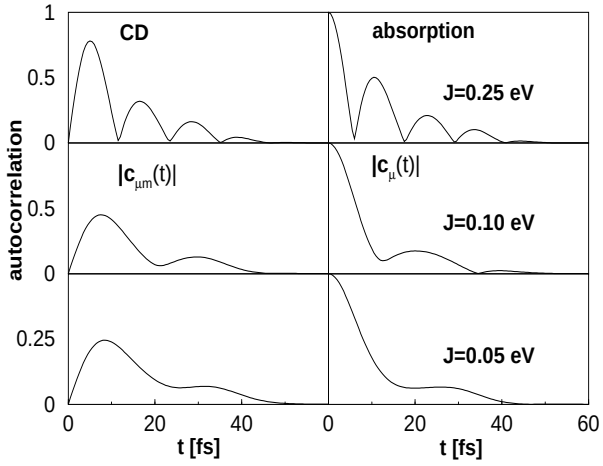

Figure 6.12: *Modulus of the time correlation-functions for CD ($c_{\mu m}$) and absorption- (c_μ) spectroscopy. The functions are damped with a Gaussian window function.*

Although the excited state dynamics is the same in both cases, upon the different projection a different time-dependence is observed (see Eq. (4.26)). In particular, one finds that $c_\mu(0)$ is real and nonzero, whereas $c_{\mu m}(0)$ is identical to zero. In the case of absorption, the decay of the correlation-functions at early times measures the separation of the wave packet in the excited state from its initial position (see Eq. (4.17) and Refs. [19, 70, 71]). On the other hand, in the CD case, one has an initial increase, which characterizes how much of the first wave-packet component has reached the second one.

A comparison of the time correlation-function to the population

$$P_2(t) = \langle \psi_{e2}(\vec{q},t) | \psi_{e2}(\vec{q},t) \rangle \tag{6.31}$$

and energy

$$E_2(t) = \langle \psi_{e2}(\vec{q},t) | \, \hat{H}_{e2}(\vec{q}) \, | \psi_{e2}(\vec{q},t) \rangle \tag{6.32}$$

in component 2 is shown in Fig. (6.13).

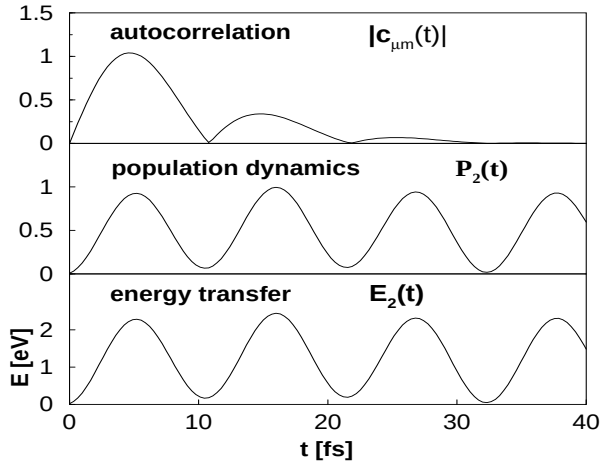

Figure 6.13: *Upper panel: modulus of the time correlation-function obtained from the Fourier transform of the CD-spectrum. Below, the population in the excited state configuration $M_1 - M_2^*$ (middle panel) and the energy of this configuration (lower panel) is shown.*

As indicated by the general formula for the time-correlation function of the dimer in the case of CD-spectroscopy (see Eq. (6.3)), the CD-effect can be related to the excitation transfer dynamics, where energy deposited in the excited state configuration $M_1^* - M_2$ is transfered to the second one $M_1 - M_2^*$. According to the 2-level expression from Eq. (6.4), the oscillation period can be related to the difference between the energy levels. The calculated value

of $T = 11.456\,\mathrm{fs}$ for a coupling constant of $J = -0.1805\,\mathrm{eV}$ agrees well with the result taken from the graph. For a trimer system, the expression

$$\begin{aligned} c_{\mu m}(t) &\sim \sin(\beta) \left\langle \mu_2 \psi_i \right| \hat{U}_e(t) \left| \mu_1 \psi_i \right\rangle + \sin(2\beta) \left\langle \mu_3 \psi_i \right| \hat{U}_e(t) \left| \mu_1 \psi_i \right\rangle \\ &= \left\langle 2 \right| \left| 1 \right\rangle_t + \left\langle 3 \right| \left| 1 \right\rangle_t . \end{aligned} \tag{6.33}$$

is found. Using the simplified model, this expression can be written as

$$\begin{aligned} c_{\mu m}(t) &\sim \sin(\beta) \left\langle \hat{A}^T \begin{pmatrix} 0 \\ 1 \\ 0 \end{pmatrix} \middle| \hat{A}^T \hat{U}_e \hat{A} \middle| \hat{A}^T \begin{pmatrix} 1 \\ 0 \\ 0 \end{pmatrix} \right\rangle \\ &+ \sin(2\beta) \left\langle \hat{A}^T \begin{pmatrix} 0 \\ 0 \\ 1 \end{pmatrix} \middle| \hat{A}^T \hat{U}_e \hat{A} \middle| \hat{A}^T \begin{pmatrix} 1 \\ 0 \\ 0 \end{pmatrix} \right\rangle \\ &\sim \sin(\beta) \sqrt{\frac{1}{8}} \left(\exp\left(-iE_{1,l}t\right) - \exp\left(-iE_{3,l}t\right) \right) \\ &+ \sin(2\beta) \left(\frac{1}{4} \exp\left(-iE_{1,l}t\right) - \frac{1}{2} \exp\left(-iE_{2,l}t\right) + \frac{1}{4} \exp\left(-iE_{3,l}t\right) \right), \end{aligned} \tag{6.34}$$

where the eigenvalues of the linear trimer system are given in Sec. (6.2). Thus, the trimer correlation-function shows a more complex dependence on the orientation angle than it is found for the dimer. There are two terms that contribute, where the first $\left\langle 2 \right| \left| 1 \right\rangle_t$ resembles the one encountered in the dimer case. It measures the energy transfer between the configurations $M_1^* - M_2 - M_3$ and $M_1 - M_2^* - M_3$. The second term $\left\langle 3 \right| \left| 1 \right\rangle_t$ maps the transfer dynamics between $M_1^* - M_2 - M_3$ and $M_1 - M_2 - M_3^*$. Thus, two predominant time scales occur upon the coupling effects, as can be seen in Fig. (6.14).

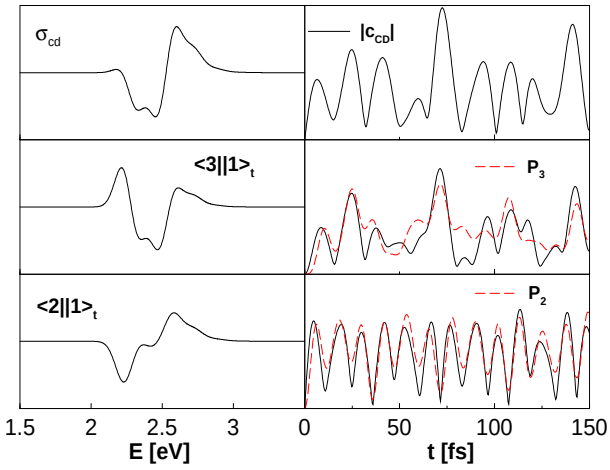

Figure 6.14: *Trimer dynamics. Left panels: total and partial CD-spectra of a trimer system. Right panels: modulus of the time-correlation function (straight lines) corresponding to the spectra on the left hand sides. Also shown are the populations in the configurations* $M_1 - M_2^* - M_3$ *(*$P_2(t)$*) and* $M_1 - M_2 - M_3^*$ *(*$P_3(t)$*) as dashed lines. The correlation-functions and populations are normalized to each other in each case.*

According to Eq. (6.34), the $\langle 2|\,|1\rangle_t$ contribution (lower panel) should exhibit oscillations with a period corresponding to the energy difference of $E_{1,l} - E_{3,l} = 2\sqrt{2}J$ with $J = 0.108\,\mathrm{eV}$. The respective period of about 13.4 fs agrees with the oscillatory patterns seen in the numerical results. Also shown is the population $P_2(t)$ of the $M_1 - M_2^* - M_3$ configuration, which nicely tracks the features of the correlation-function. Regarding the middle right panel of Fig. (6.14), the depicted function $\langle 3|\,|1\rangle_t$ contribution contains terms oscillating with the energy differences $E_{1,l} - E_{3,l} = 13.4\,\mathrm{fs}$ and also with $E_{1,l} - E_{2,l} = E_{2,l} - E_{3,l}$, where the latter has the double period. Note that this simplified analysis, of course, neglects the vibrational degrees of freedom, which induce a further complication in the dynamics. Nevertheless, the numerical results are suitable to illustrate the picture that the population and likewise the

energy, is transferred successively from monomer M_1 via the intermediate monomer M_2 to monomer M_3. The left hand side of Fig. (6.14) contains the total CD-spectrum (upper panel) and also the partial spectra, which are obtained by separate Fourier transform of the two terms contributing to the correlation-function. In the first case, the spectrum resembles the dimer spectrum, whereas the second contribution exhibits a different band structure. The sum of the two spectra then yields the total spectrum (upper panel).

6.4 Spectra of merocyanine dimers

In order to determine the model parameters of a dimer system, the informations from CD- and absorption-spectroscopy can be combined. While the first provides insight into the relative orientations of the monomer transition dipole moments upon the angle dependence of the relative band intensities, the latter allows a more direct view into the electronic excited state coupling. As an example for the application of a theoretical analysis to measured spectra, merocanine dye aggregates are investigated. Molecules of this substance class contain variable donor and acceptor groups, which are connected by a conjugated π-system (see Fig. (6.15)).

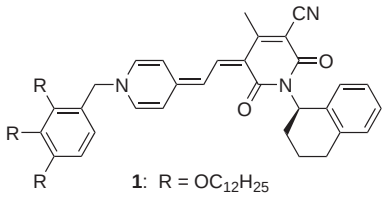

Figure 6.15: *Structure of the chiral merocyanine monomer (M).*

The transition dipole moment is directed from the amide group to the opposite carboxyl group and lies in the plane of the molecule [72]. Electronic excitation induces a molecular vibration, which can be identified with a stretching mode [73]. Upon $\pi - \pi$ -interactions dimer formation takes place within a certain concentration range [74]. CD-spectra of the dimer are only obtained if the substituents of the molecule are chiral. Note that the chiral monomer itself does not exhibit a CD-spectrum. In order to interpret the measured dimer spectra by varying the parameters of the model system in the calculations, the parameters of the monomer model have to be fixed. To do so, the monomer absorption-spectrum is fitted to the measured absorption-spectrum. The result is shown in Fig. (6.16), which compares calculated and measured absorption-spectra.

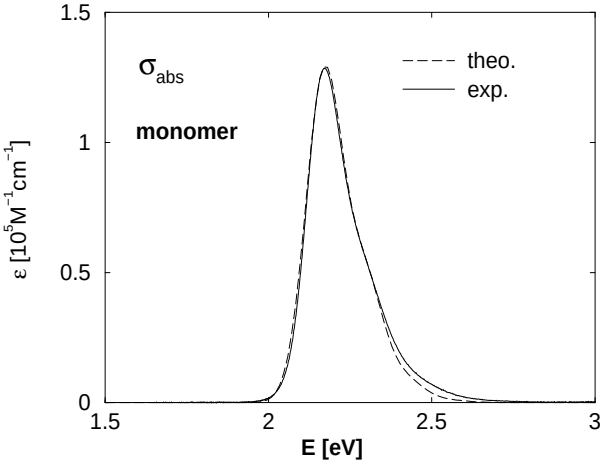

Figure 6.16: *Comparison of measured and calculated absorption-spectrum.*

The absorption band exhibits an asymmetric line-shape with a width of almost 0.5 eV. In order to simulate this finite width, nuclear motion has to be taken into account. Although there are many vibrational modes, which participate in the electronic transition (for a discussion on similar systems see e. g. Ref. [75]), a single vibrational degree of freedom is included. The

monomer potentials are parameterized employing the values of $\omega = 0.125\,\mathrm{eV}$, $q_e = 2.4\,\mathrm{eV}^{-\frac{1}{2}}$ and $\Delta E_M = 2.1648\,\mathrm{eV}$ in Eqs. (4.4). The limited resolution of the experiment is included by truncating the correlation-function $c_\mu(t)$ with a Gaussian window function having a temporal width, which corresponds to a spectral resolution of 0.0697 eV. Within this model, the spectrum is excellently reproduced by theory. Having fixed the monomer potential parameters, the dimer Hamiltonian can be defined. For this aim, the additional parameters for the electronic coupling element J and an energy shift ΔE_D have to be fixed. Also, the transition dipole geometry has to be determined. It was shown above that in the one-exciton model employed here, the dimer spectrum consists of two absorption bands, which are split by (for a two level system) an amount of $\Delta = 2|J|$ and exhibit the relative band intensities given in Eq. (6.6). Regarding the experimentally determined dimer spectrum, which is displayed in Fig. (6.17)(solid line, upper panel), no clear double band structure is found.

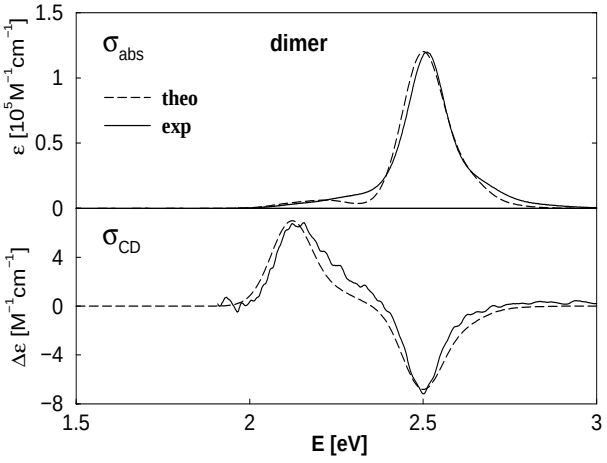

Figure 6.17: *Comparison between measured and calculated absorption- and CD-spectra of merocyanine dimer aggregates.*

Thus, neither the extraction of the magnitude of the coupling element J (from the band splitting) nor the angle β (from the relative band intensity) is possible from these UV/Vis absorption data. In order to proceed, the experimental CD- dimer spectrum, which is displayed in the lower panel of Fig. (6.17) is considered. As the upper energy band has a negative sign, the coupling matrix element is negative (see Eq. (6.5)). From the band splitting a value of $J = -0.1805\,\mathrm{eV}$ can be derived. Fixing the dimer shift to a value of $\Delta E_D = 2.285\,\mathrm{eV}$ and employing a spectral resolution of $0.091\,\mathrm{eV}$, the absolute value yields the simulated CD-spectrum, which is in excellent agreement with experiment. Given the numerical value of J and thus the two band positions, it is now possible to deduce the angle β from the relative band intensities in the absorption-spectrum. Regarding the negative sign of J, which is proportional to $\cos(\beta)$, an angle of $\beta = 161\,^\circ$ is found to yield the best agreement with experiment [74].

6.5 Spectra of perylene bisimide aggregates

As a further application, the theoretical evaluation of absorption- and CD-spectra can be used to investigate the size of perylene bisimide aggregates. The structure of this kind of molecules is displayed in Fig. (6.18).

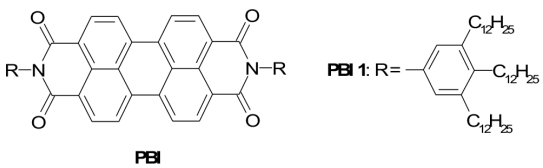

Figure 6.18: *Structure of the perylene bisimide monomer (M).*

Perylene bisimides are an important class of organic dyes [76]. In particular, many pigments are produced on a large scale and their coloristic properties vary from red to maroon and black [77]. Most important, these color changes do not arise from different substituents like in many other classes of dyestuffs but are governed by aggregation effects [4]. Opposite to merocyanines, which only form dimers within a certain concentration range, perylene bisimides build aggregates with a temperature-dependent distribution of size [78]. The monomeric dyes are strongly photo-luminescent but this photoluminescence is often quenched in the aggregated state. For the transition between S_0 and S_1 of the monomer, well-defined vibronic structures are observed in the absorption- as well as in the mirror image fluorescence-spectra [76]. Thereby the transition dipole moment is directed along the long in-plane symmetry axis of the molecule [79]. The vibrational mode taken into account in the model corresponds to a breathing motion of the perylene skeleton [73].
In order to calculate absorption- and CD-spectra, the relevant monomer parameters $\omega_g = \omega_e = 0.175\,\mathrm{eV}$, $q_e = 2.57\,\mathrm{eV}^{-\frac{1}{2}}$ and $\Delta E = 2.35\,\mathrm{eV}$ can be taken from former investigations [80]. From quantum chemical calculations for the dimer, the angle between the transition dipole moments can be fixed as $\beta = 28\,^\circ$ (see Sec. (7)). In order to reproduce the dimer spectrum, a coupling constant of $J = 0.065\,\mathrm{eV}$ is employed, which is slightly smaller than the value determined from ab initio calculations (see Sec. (7)). Furthermore, a spectral resolution of $0.149\,\mathrm{eV}$ is introduced by a Gaussian damping function. For larger aggregates, these values are taken as the angles between next neighbor transition dipole moment vectors and the corresponding coupling matrix elements, respectively. The calculations are performed by the MCTDH-method, see Sec. (3.3). In the evaluation, the relevant question is, how far the employed model is capable to describe the spectral changes which arise from

aggregation effects. The calculated absorption-spectra for different aggregate sizes are shown in Fig. (6.19). For comparison, the absorption-spectra measured at different temperatures are displayed in Fig. (6.20).

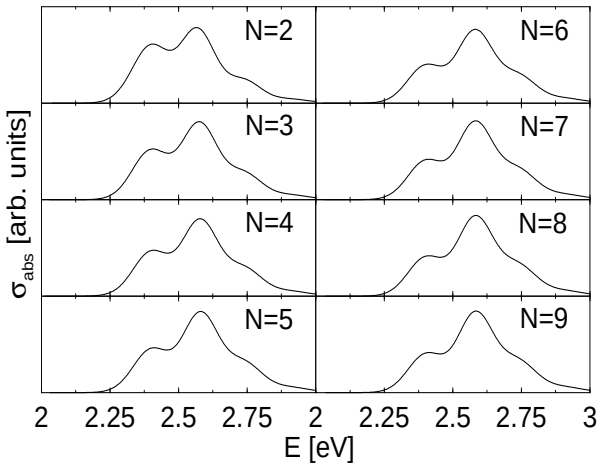

Figure 6.19: *Calculated absorption-spectra for different aggregate sizes.*

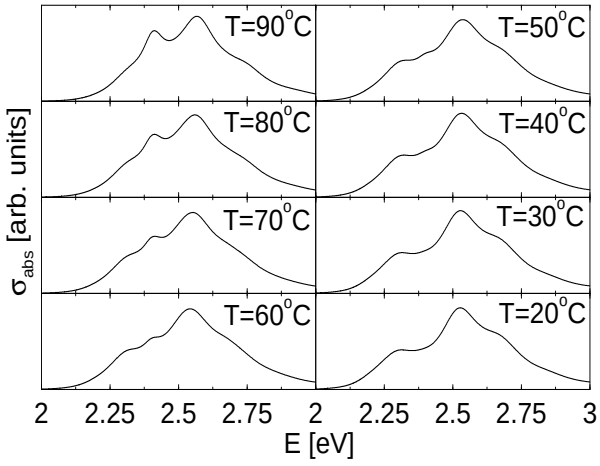

Figure 6.20: *Measured absorption-spectra at different temperatures.*

The relative intensity of the energetically lower band with respect to the energetically higher band decreases both with increasing aggregate size and decreasing temperature. This means that the model calculations reproduce the tendencies of the measured spectra qualitatively, although a quantitative evaluation is very difficult. The same holds for CD-spectra. Theoretical and experimental results are displayed in Fig. (6.21) and Fig. (6.22), respectively.

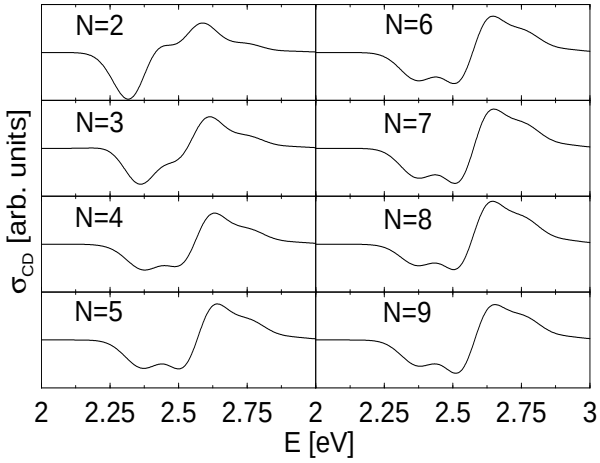

Figure 6.21: *Calculated CD-spectra for different aggregate sizes.*

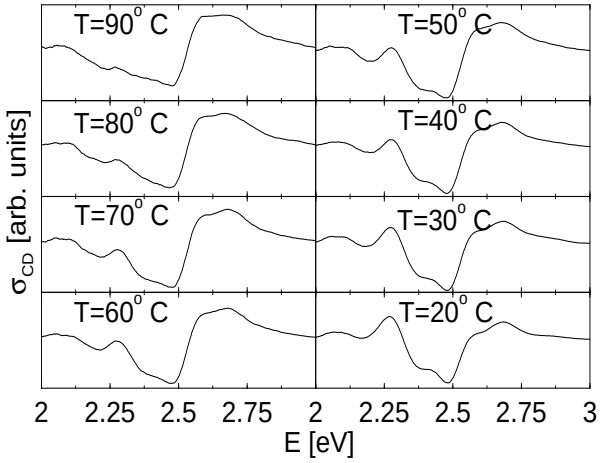

Figure 6.22: *Measured CD-spectra at different temperatures.*

Calculated and measured spectra agree in the change of the sign from the negative to the positive range with increasing energy in the range of $2.25 - 3\,\mathrm{eV}$. Furthermore, the lower band becomes subdivided with increasing aggregate size and decreasing temperature, where the energetically highest sub-band is more pronounced. However, the appearance of the band in the low energy range for low temperatures is not reproduced by the theoretical model. Nevertheless, upon the good agreement of experimental and theoretical results one can conclude that the model captures the relevant aspects of the perylene bisimide aggregates. On the basis of the parameters employed within the dimer model in order to reproduce the measured spectrum at the highest temperature, spectra of higher aggregates can be calculated. The results show a good qualitative agreement with experimental data obtained at lower temperature. This leads to the conclusion that the assumptions concerning numerical values of angles and couplings from the dimer case are also valid for larger aggregates. Furthermore, it is evident that the aggregate size increases with decreasing temperature.

In contrast, in the case of emission-spectra, a redshift is found, which cannot be explained without including a torsional degree of freedom.

Chapter 7

Extended dimer model

As the previous model is not capable to reproduce measured emission spectra, intermolecular degrees of freedom have to be included. Quantum chemical calculations with different intermolecular parameters yield potential energy surfaces, where the angular coordinate θ proves to be most important for the calculation of spectra for topological reasons. Thereby the other parameters are determined from the global minimum position at an intermolecular distance of $R = 3.36\,\text{Å}$, longitudinal and transversal shifts of $X = 0\,\text{Å}$ and $Y = 0\,\text{Å}$, respectively. For the electronic ground state $V_g(\theta)$, the DFT-D approach is used in combination with the BLYP functional [81, 82], where dispersion effects are comprised by adding empirical corrections to the standard density functional energy [83]. The resulting potential curve shown in Fig. (7.1) allows an intuitive interpretation: Because of attractive electrostatic interactions between the terminal carbonyl and nitrogen groups, the minimum is found at an equilibrium torsional angle of about $\theta = 30°$, whereas the sandwich structure $\theta = 0°$ is highly unfavorable. The determination of the potential curves of the excited states within the adiabatic representation $V_{e1}(\theta)$ and $V_{e2}(\theta)$ demands a different procedure. Since time-dependent den-

sity functional theory (TDDFT) with standard functionals is unreliable for the calculation of locally excited states with neutral character [84,85], the excited state potentials are calculated using the time-dependent Hartree-Fock (TD-HF) method. As dispersion effects lack in TD-HF, they are approximated by the ground state results. This approach is consistent with the basic idea of the DFT-D method, in which the parameters are molecule- and state-independent. The energy difference between the PES of the excited states result from the interactions between the transition dipole moments (independent dipole model, see Eq. (4.10)). For the explanation of the detailed form of the potential curves, and in particular the crossing at $\theta = 60°$, higher order effects have to be taken into account by regarding the respective transition densities. In order to obtain a sufficient agreement of the calculated absorption-spectra with measured ones, the splitting of the potential curves has to be decreased within the absorption region. For this aim, the input data for the excited states are multiplied by a factor of $\lambda = 0.6$ and shifted in energy, so that the minimum of the lower potential keeps its position. This procedure yields the potential curves $\tilde{V}_{e1}(\theta)$ and $\tilde{V}_{e2}(\theta)$ which are shown in Fig. (7.1).

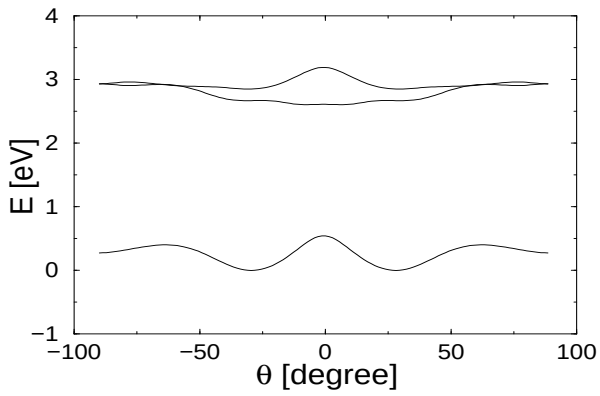

Figure 7.1: *Potentials as a function of the torsional motion coordinate θ.*

Within the diabatic representation, which is essential for the integration of the torsional mode into the dimer model, the excited state potential curve $V_e(\theta) = \frac{1}{2}\left(\tilde{V}_{e1}(\theta) + \tilde{V}_{e2}(\theta)\right)$ enters as well as the angle dependent coupling $J(\theta) = \frac{1}{2}\left(\tilde{V}_{e1}(\theta) - \tilde{V}_{e2}(\theta)\right)$.
The Hamiltonian of the total system in the ground state is given as

$$\hat{H}_g\left(q_1, q_2, \theta\right) = \hat{H}_g^D\left(q_1, q_2\right) + \hat{H}_g\left(\theta\right), \tag{7.1}$$

in the excited state it reads

$$\hat{H}_e\left(q_1, q_2, \theta\right) = \begin{pmatrix} \hat{H}_{e1}^D\left(q_1, q_2\right) + \hat{H}_e\left(\theta\right) & J\left(\theta\right) \\ J\left(\theta\right) & \hat{H}_{e2}^D\left(q_1, q_2\right) + \hat{H}_e\left(\theta\right) \end{pmatrix}. \tag{7.2}$$

Thereby the definitions $\hat{H}_g(\theta) = \hat{T}(\theta) + V_g(\theta)$ and $\hat{H}_e(\theta) = \hat{T}(\theta) + V_e(\theta)$ are employed. As θ denotes an azimuth angle here, the corresponding kinetic energy operator reads $\hat{T}(\theta) = -\frac{1}{2I}\frac{\partial^2}{\partial\theta^2}$, where the definition of the rotational constant I is given below. Furthermore, the transition dipole moments $\mu_{1,ad}(\theta)$ and $\mu_{2,ad}(\theta)$ belonging to the transitions between the ground state and the adiabatic excited state potentials (see Fig. (7.2)) have to be transformed to the diabatic picture using a transformation matrix, which diagonalizes the potential part of the Hamiltonian:

$$\begin{pmatrix} \mu_{1,dia}(\theta) \\ \mu_{2,dia}(\theta) \end{pmatrix} = \frac{1}{\sqrt{2}} \begin{pmatrix} 1 & 1 \\ 1 & -1 \end{pmatrix} \begin{pmatrix} \mu_{1,ad}(\theta) \\ \mu_{2,ad}(\theta) \end{pmatrix}. \tag{7.3}$$

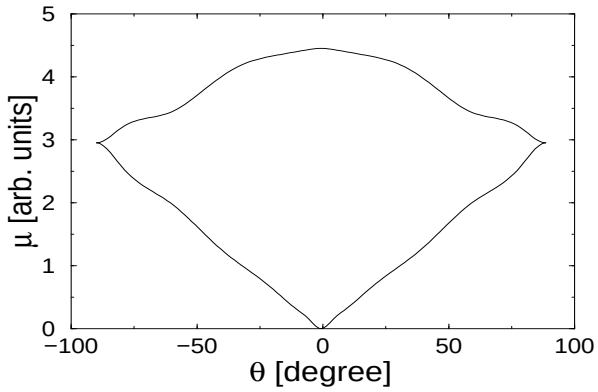

Figure 7.2: *Transition dipole moments with respect to the coordinate θ.*

For the quantum dynamical calculation, the rotational constant, which can formally be identified with a mass m, must be known. It can be determined on the basis of the calculated frequency of the torsional motion $\omega = 1.263\,\mathrm{meV}$ in the ground state. As the prefactor a of the parabolic approximation $V_g(\theta) = a(\theta - \theta_0)^2$ is given as $\frac{1}{2}I\omega^2 = 0.9335\,\mathrm{meV}$, the curvature of the ground state potential at the position of the minimum $\theta_0 = 28.8°$ has to be taken from the existing graph in order to obtain the corresponding rotational constant. In this way, the value $I = 1170.41\,\mathrm{eV}^{-1} \hat{=} 31848\,\mathrm{au} \hat{=} 17.471\,\mathrm{u}$ is found.

Within the following investigations, the influence of the temperature-dependent population of the vibrational eigenstates in the electronic ground and excited state has to be regarded for the calculation of absorption- and emission-spectra, respectively. In the case of absorption, the following procedure is employed: First, the minimum $V_{g,min}$ of the ground state potential surface is determined in order to obtain an energy reference. Then the eigenfunctions $\psi_{i,g,1D}(\theta)$ and $\psi_{j,g,2D}(q_1, q_2)$ with respect to the torsional coordinate and the two vibrational modes are calculated separately. From the corresponding eigenenergies $E_{i,g,1D}$ and $E_{j,g,2D}$, the value of $V_{g,min}$ is subtracted, yielding

the results $\tilde{E}_{i,g,1D}$ and $\tilde{E}_{j,g,2D}$. Afterwards the eigenfunctions and eigenenergies of the total system are composed, where the first consist of the product wave functions

$$\psi_{i,j}(q_1, q_2, \theta) = \psi_{i,g,1D}(\theta)\psi_{j,g,2D}(q_1, q_2), \tag{7.4}$$

while the latter are given by the sum

$$\tilde{E}_{i,j} = \tilde{E}_{i,g,1D} + \tilde{E}_{j,g,2D}. \tag{7.5}$$

On this basis, the time correlation-functions

$$\begin{aligned} c_{i,j}(t) \;=\; & \left\langle \begin{pmatrix} \psi_{i,j}(q_1, q_2, \theta)\mu_{1,dia}(\theta) \\ \psi_{i,j}(q_1, q_2, \theta)\mu_{2,dia}(\theta) \end{pmatrix} \right| \\ & \exp\left(-i\hat{H}_e(q_1, q_2, \theta)t\right) \left| \begin{pmatrix} \psi_{i,j}(q_1, q_2, \theta)\mu_{1,dia}(\theta) \\ \psi_{i,j}(q_1, q_2, \theta)\mu_{2,dia}(\theta) \end{pmatrix} \right\rangle \end{aligned} \tag{7.6}$$

can be calculated, which yield the absorption-spectra

$$\sigma_{abs,i,j}(E) = \int dt \exp\left(i\left(E + \left(\tilde{E}_{i,j} + V_{g,min}\right)\right)t\right) c_{i,j}(t). \tag{7.7}$$

Finally, the total absorption-spectrum is obtained as

$$\sigma_{abs}(E) = \sum_{i,j} \sigma_{abs,i,j}(E) \exp\left(-\frac{\tilde{E}_{i,j}}{kT}\right). \tag{7.8}$$

In order to calculate temperature-dependent emission-spectra in a numerically effective way, the potential part of the excited state Hamiltonian (see Eq. (7.2)) is transformed to the adiabatic picture, where a separate calculation of the eigenfunctions with respect to the torsional coordinate and the two-dimensional space of the vibrational coordinates becomes possible.

First, the value and position of the minimum of the lower adiabatic potential

$V_{e2,ad,min} = V_{e2,ad}(q_{1,min}, q_{2,min}, \theta_{min})$ has to be determined in order to get an energy reference. Then the corresponding value of the ground state potential at the minimum position $V_{g,min} = V_{g,ad}(q_{1,min}, q_{2,min}, \theta_{min})$ is specified. This leads to the energy shift $\Delta E = V_{e2,ad,min} - V_{g,min}$. In the next step, cuts through the potentials $V_{e2,ad}$ and V_g around $(q_{1,min}, q_{2,min}, \theta_{min})$ yield the one-dimensional curves $V_{e2,ad,1D}(\theta)$ and $V_{g,1D}(\theta)$ as well as the two-dimensional surfaces $V_{e2,ad,2D}(q_1, q_2)$ and $V_{g,2D}(q_1, q_2)$.

After the eigenfunctions $\psi_{i,e2,1D}(\theta)$ and $\psi_{j,e2,2D}(q_1, q_2)$ of the one and two-dimensional excited state potentials are calculated, the value $V_{e2,ad,min}$ is subtracted from the corresponding eigenenergies, yielding the energy values $\tilde{E}_{i,e2,1D} = E_{i,e2,1D} - V_{e2,ad,min}$ and $\tilde{E}_{i,e2,2D} = E_{i,e2,2D} - V_{e2,ad,min}$. Then the energy of the product wave function is given as $\tilde{E}_{i,j} = \tilde{E}_{i,e2,1D} + \tilde{E}_{j,e2,2D}$. According to the equations

$$\begin{aligned} c_{i,1D}(t) &= \langle \psi_{i,e2,1D}(\theta)\mu_{2,ad}(\theta)| \exp\left(-i\left(\hat{T}(\theta) + V_{g,1D}(\theta)\right)t\right) \\ &\quad \exp\left(iV_{g,min}t\right) |\mu_{2,ad}(\theta)\psi_{i,e2,1D}(\theta)\rangle \end{aligned} \tag{7.9}$$

and

$$\begin{aligned} c_{j,2D}(t) &= \langle \psi_{j,e2,2D}(q_1, q_2)| \exp\left(-i\left(\hat{T}(q_1, q_2) + V_{g,2D}(q_1, q_2)\right)t\right) \\ &\quad \exp\left(iV_{g,min}t\right) |\psi_{j,e2,2D}(q_1, q_2)\rangle\,, \end{aligned} \tag{7.10}$$

the time correlation-functions are obtained. For the calculation of emission-spectra, the expression

$$\sigma_{em,i,j}(E) = \int dt \exp\left(-i\left(E + \left(\Delta E + \tilde{E}_{i,j}\right)\right)t\right) c_{i,1D}(t)c_{j,2D}(t) \tag{7.11}$$

is used.

Finally, the weighted sum over these spectra

$$\sigma_{em}(E) = \sum_{i,j} \sigma_{em,i,j}(E) E^3 \exp\left(-\frac{\tilde{E}_{i,j}}{kT}\right) \tag{7.12}$$

yields the temperature-dependent emission-spectrum. The subject of the following considerations is the influence of the temperature on absorption- and emission-spectra of the system.

The dimer model without torsional motion is capable to reproduce measured absorption-spectra, but not emission-spectra (see Fig. (7.3)). The extended model aims at a better understanding of the emission properties.

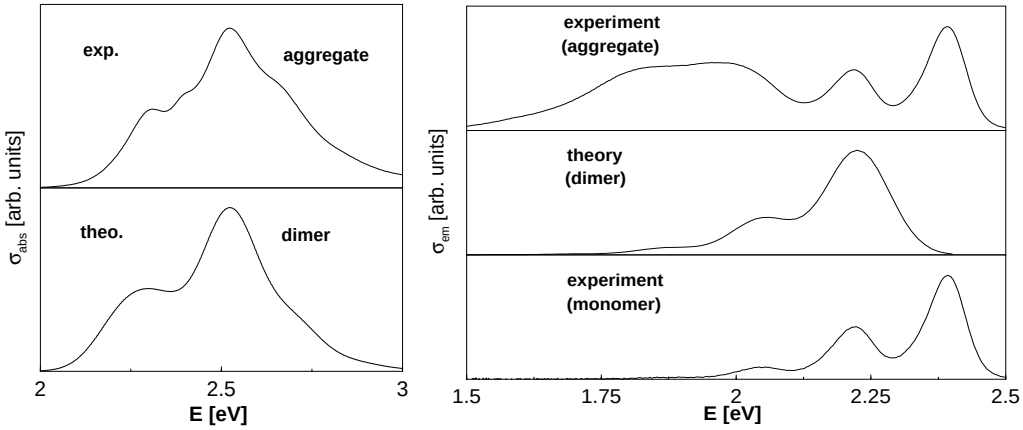

Figure 7.3: *Comparison between measured and calculated absorption- (left) and emission-spectra (right) using the dimer model without torsional motion and the monomer model.*

If only the lowest vibrational states in the extended model are taken into account, one obtains a redshift of the emission-spectrum with respect to the absorption-spectrum, which is however too large (see Fig. (7.4, right hand panel, dashed line)). Furthermore, the broad band appearing in the emission-spectrum can not be explained. Concerning the involvement of higher excited vibrational eigenstates with respect to the torsional degree-of-freedom, there

is a substantial difference between absorption and emission of the model system. On the one hand, their influence is negligible in the case of absorption because of the relatively large difference between the corresponding eigenenergies within $V_g(\theta)$ and therefore the small population of higher eigenstates in thermal equilibrium. According to the reflection principle, the small increase of the curves $V_{e1}(\theta)$ and $V_{e2}(\theta)$ in the region around the minimum of the ground state potential (see Fig. (7.1)) keeps the contribution of the angular component to the total absorption-spectrum small, even if higher excited vibrational eigenstates were populated significantly. The resulting absorption-spectrum is practically identical with the one, which is obtained from the simplified dimer model neglecting the torsional motion (see Fig. (7.4), left side). On the other hand, in the case of emission, the temperature-dependent population distribution of the vibrational eigenfunctions within $V_{e2,ad,1D}(\theta)$ implies a larger contribution of the increasingly delocalized higher eigenstates upon the energetically dense progression of the eigenenergies. The reflection of the initial wave functions at the potential curve $V_g(\theta)$ (see Fig. (7.1)) on the energy axis covers a wide range, as the curve is very steep within the emission region. The energetical position of the emission-spectrum is correlated to the density distribution of the excited state wave functions. These considerations allow to understand the result shown in Fig. (7.4) (right side, solid line) basically.

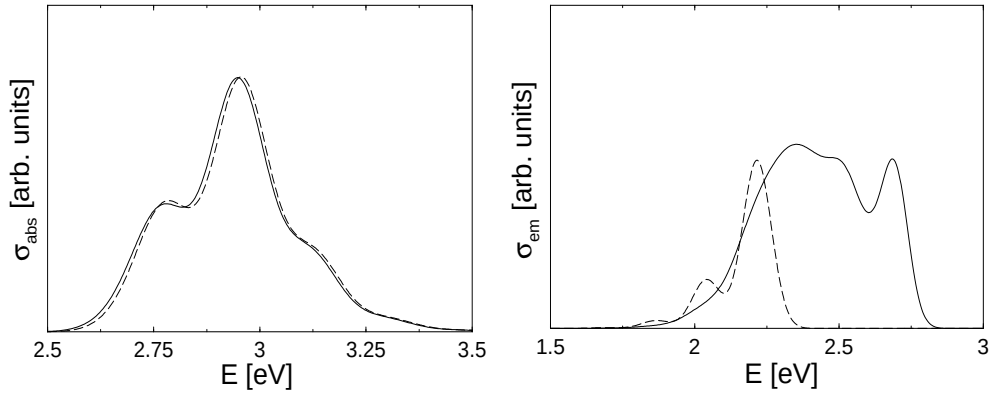

Figure 7.4: *Absorption (left) and emission-spectra (right) of the extended dimer model at* $T = 0\,\mathrm{K}$ *(dashed line) and* $T = 300\,\mathrm{K}$ *(solid line).*

An even more comprehensive explanation for the characteristic features is given on the basis of the following considerations. The peak appearing at an energy of 2.2 eV in the calculated emission-spectrum is related to the topology of the excited state potential energy surface with respect to the torsional angle. Within a classical approach, the spectrum can be written as [19]

$$\sigma(E) = E^3 \sum_i |\mu(\theta_i)|^2 \exp\left(-\frac{\epsilon}{kT}\right). \tag{7.13}$$

Here the sum is over all roots θ_i of the equation $D(\theta) - E = 0$, where $D(\theta)$ denotes the difference between the lower adiabatic excited state and ground state potential curves. The energy ϵ appearing in the Boltzmann factor is taken relative to the potential minimum ($V_{e2,min}$) in the excited state. In Fig. (7.5), upper panel, classical and quantum mechanical emission-spectrum are compared, where only the torsional degree-of-freedom is taken into account and the temperature is set to $T = 300\,\mathrm{K}$. Also shown is the energy-dependent weighting function (7.13), which determines the intensity of the emission band (middle panel). The lower panel of the same figure shows the difference

potential. It is seen that for energies lower than 2.1 eV, two angle values contribute to the spectrum with equal weights, whereas for larger energies, there are six angle values yielding a contribution. Taking the particular form of the weighting function into account (middle panel of Fig. (7.5)), it is clear that the broad band at lower energies (two contributions) is followed by the more intense peak resulting from the multiple contributions stemming from different angles θ_i. The classically obtained spectrum decreases to zero for energies larger than 2.34 eV because the difference potential does not assume these values. At this point, there is a pronounced maximum which in scattering processes is known as a rainbow [86]. Comparing the classically obtained spectrum to the quantum one shows that the developed classical picture is overall correct. Quantum mechanics leads to a diminished intensity of the 2.2 eV peak, which is a general trend as found, e. g. in the calculation of scattering [86] or photodissociation cross-sections (see Ref. [19]). In going from the one-dimensional quantum spectrum to the one including the monomer vibrations (Fig. (7.4), left hand panel), it is seen that the relative peak height (at 2.2 eV) decreases. It is then to be expected that the inclusion of other internal degrees of freedom decreases the peak intensity even further. Note that the same trend is observed if the temperature is decreased, so that the higher energy parts of the excited state potential are not accessed.

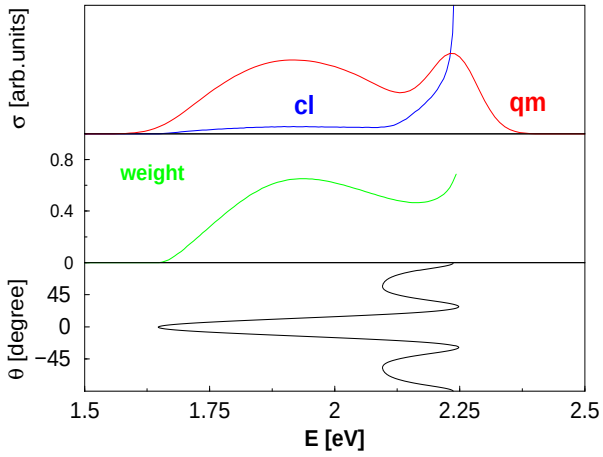

Figure 7.5: *Upper panel: emission-spectra calculated at a temperature of* $T = 300\,\mathrm{K}$ *within a one-dimensional model involving the torsional degree of freedom. Classically and quantum mechanically calculated spectra are shown on an arbitrary scale. The middle panel contains the weighting function* $(\sum_i |\mu(\theta_i)|^2)$ *entering into the classical expression for the emission-spectrum. Lower panel: difference potential between the excited and ground electronic states, which participate in the emission process.*

In order to compare the calculated spectra to the measured ones, an energy shift has to be applied, as the relative energetic distance between the quantum chemically calculated potential curves is not reliable. Therefore, it is feasible to adapt it to the existing data. If the position of the calculated absorption-spectrum is shifted towards the measured one and the same shift operation is applied to the temperature-dependent emission-spectrum, the latter shows an excellent agreement with the experimental data (see Fig. (7.6)).

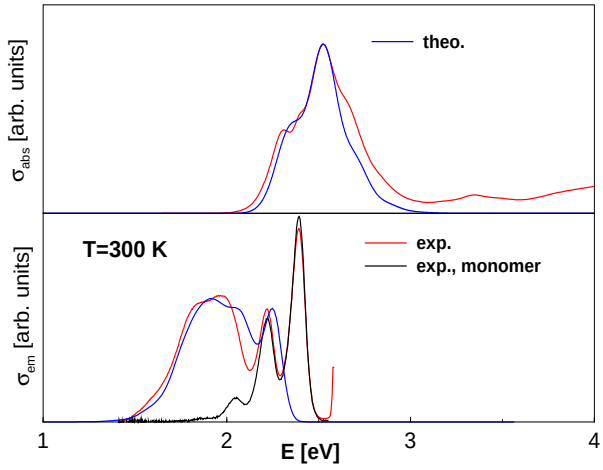

Figure 7.6: *Comparison between experimental data and calculated, energetically shifted spectra of the extended dimer model at* $T = 300\,\mathrm{K}$.

Summing up the results, one can conclude that the intermolecular torsional degree of freedom can be neglected in the case of absorption- and CD- spectroscopy, but not in the case of emission-spectroscopy.

Chapter 8

Calculation of 2D-spectra

8.1 Two-dimensional monomer spectra

Using the monomer-model, the general properties of two-dimensional spectra can be illustrated, see [41, 87]. If no additional multiplication of the polarization with a factor of i is performed, the real and imaginary parts of the Fourier-transformed signal can be identified with the dispersive and absorptive part of the spectrum, respectively [43]. While the dispersive properties of matter interacting with incident light influence the propagation velocity of the electromagnetic field depending on the photon energy, the absorptive properties are accountable for damping effects. Both quantities are connected by introducing a complex refraction index. The real part of the 2D-spectrum consists of butterfly-shaped peaks with a nodal plane along the diagonal direction, the imaginary part exhibits Gaussian-shaped peaks (see Fig. (8.1) and Eq. (2.57)). In what follows, only the imaginary part will be regarded.

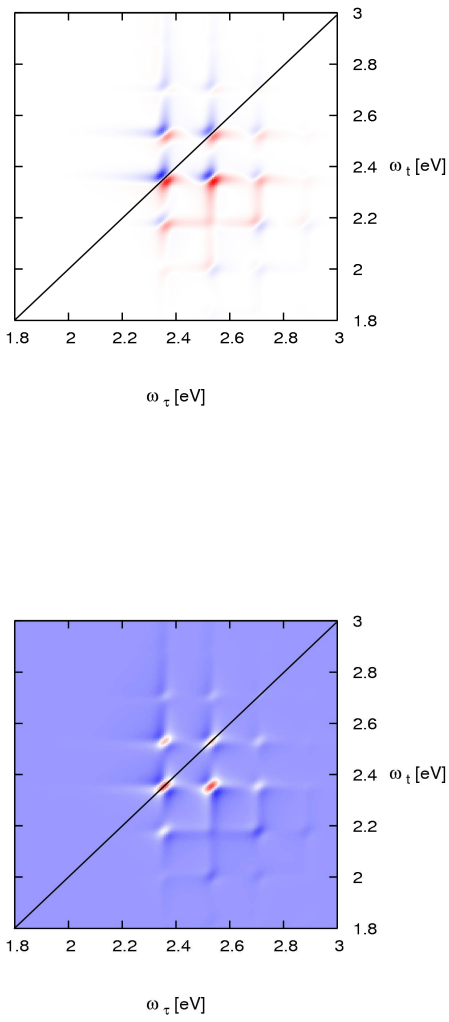

Figure 8.1: *Real (upper panel) and imaginary part (lower panel) of the monomer 2D-spectrum* ($\Delta\omega = 0.033\,\mathrm{eV}$).

In the numerical calculation, the parameters of the monomer model are taken from former investigations (see Sec. (6.4)), taking the vibrational ground state in $|g\rangle$ as the initial state. The maximum molecule-field coupling obtained at the maximum of the Gaussian envelope functions is arbitrarily set to a value of 0.01 eV. The field envelopes have a width (full width at half maximum) of $\Delta T = 5.4\,\mathrm{fs}$, and a carrier photon energy of $\omega = 2.35\,\mathrm{eV}$ is employed. For the calculation of the 2D-spectra, times (t,τ) ranging from -170 to 170 fs are included. Thereby negative times t (polarization is determined before the central time of the pulses $\vec{E}_2, \vec{E}_3$) and negative delay-time (pulses $\vec{E}_2, \vec{E}_3$ arrive before pulse $\vec{E}_1$) are taken into account in order to include pulse overlap contributions. However, excluding these effects yields to almost identical signals. Furthermore, a spectral resolution of $\Delta\omega = 0.033\,\mathrm{eV}$ is introduced by a Gaussian damping function. An entire set of peaks appears and the respective energies can be identified in regarding Eq. (2.56). Along the ω_τ -direction, the peak with the lowest energy occurs at the $i = 0, n_e = 0$ transition. With increasing energy ω_τ, two more peaks with non-negligible intensity appear, which correspond to $i = 0 - n_e = 1, 2$ transitions. Thus, the excited state level structure can be investigated. The most intensive diagonal peak is located at a frequency, which corresponds to the energy shift between the electronic ground and excited state. It can be identified with the $i = 0, n_e = 0$ transition. With increasing photon energy, a progression of equally spaced peaks corresponding to $i = 0 - n_e = 1, 2$ transitions is observed in both directions. Thereby diagonal peaks ($\omega_t = \omega_\tau$) and cross peaks ($\omega_t \neq \omega_\tau$) can be distinguished. Furthermore, in ω_t -direction also a progression down to lower energies with respect to the $i = 0, n_e = 0$ transition appears. An explanation for these features is given on the basis of Fig (8.2).

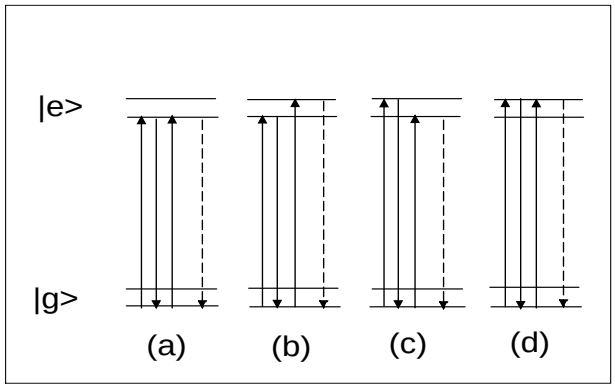

Figure 8.2: *Excitation schemes including three transitions in an electronic two level system with two additional vibrational eigenstates, respectively.*

In each case, the length of the first arrow from the left side can be identified with the ω_τ -frequency. For simplicity, the second transition (second arrow) is supposed to end up at the lowest vibrational eigenstate. The third arrow symbolizes another transition to the excited state, from where a photon with frequency ω_t is emitted upon a transition back to the initial state (dashed arrow). In Fig (8.3) the structure of the 2D-Spectrum is sketched.

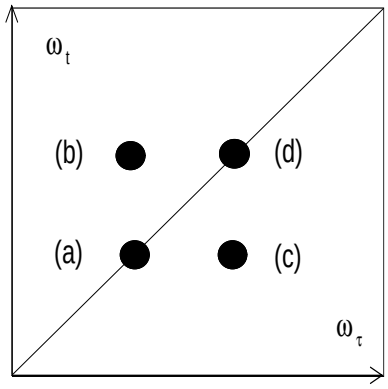

Figure 8.3: *Structure of a two-dimensional spectrum with the peaks assigned to the transitions indicated in Fig. (8.2).*

While the diagonal peaks (a) and (d) can be related to the peaks in a linear absorption spectrum by projecting them onto the ω_τ - or ω_t -axis, the cross peaks (b) and (c) hint to transitions between the electronic ground state and different vibrational levels of the excited state. If the arrow which represents the second transition ends up at a higher vibrational eigenstate of the electronic ground state, additional peaks with $\omega_t < \Delta E$ appear. Though in ω_τ -direction the lower limit is given by ΔE.
If an energetic resolution of $\Delta\omega = 0.11\,\mathrm{eV}$ is employed, which corresponds to the value found for linear absorption spectra of perylene bisimide [80], a more realistic 2D-spectrum is predicted, see Fig. (8.4).

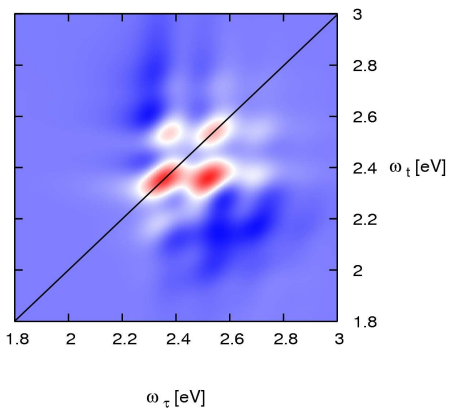

Figure 8.4: *Two-dimensional monomer spectrum* ($\Delta\omega = 0.11\,\mathrm{eV}$).

Note that the broadening is taken into account only phenomenologically. A more proper theoretical treatment needs, e. g., the solution of the Liouville-von Neumann equation [44].

8.2 Two-dimensional dimer spectra

For the investigation of two-dimensional dimer spectra, the coupling element is taken as $J = 0.25\,\mathrm{eV}$ at first. As the molecule-field interaction in the case of a dimer depends critically on the angle β between the monomer transition dipole-moments, the three characteristic geometries $\beta = 0\,^\circ, 90\,^\circ$ and $180\,^\circ$ are investigated. The excitation schemes depicted in Fig. (8.5) and Fig. (8.6) show the electronic level structure of a dimer. Depending on the relative orientation of the monomer transition dipole-moments, different electronic states are coupled by the external field. In particular, for angles of $\beta = 0\,^\circ$ and $\beta = 180\,^\circ$, only the upper/lower intermediate states are accessible, so that the corresponding bands appear in the linear absorption spectra exclusively. The case of $\beta = 90\,^\circ$ represents the intermediate situation where both 1-exciton states are excited with equal probability.

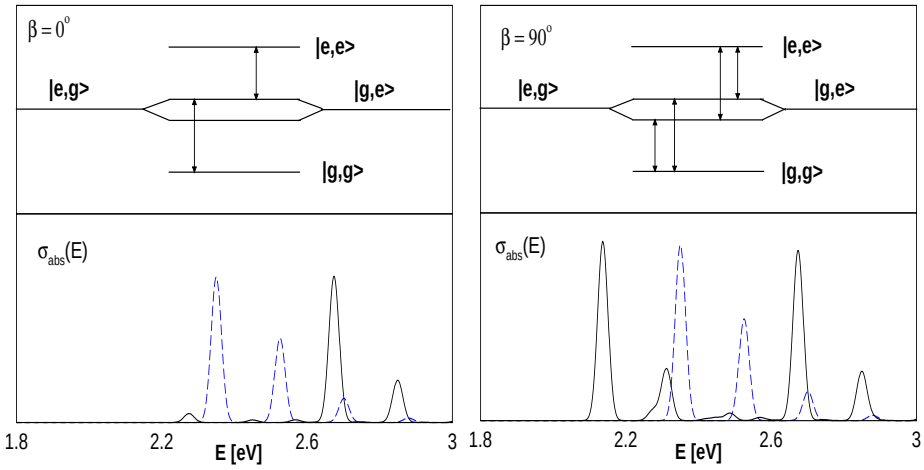

Figure 8.5: *Transition schemes and dimer absorption spectra (solid line) for the case of $\beta = 0\,^\circ$ (left side) and $\beta = 90\,^\circ$ (right side). The monomer absorption spectrum is also shown (blue line).*

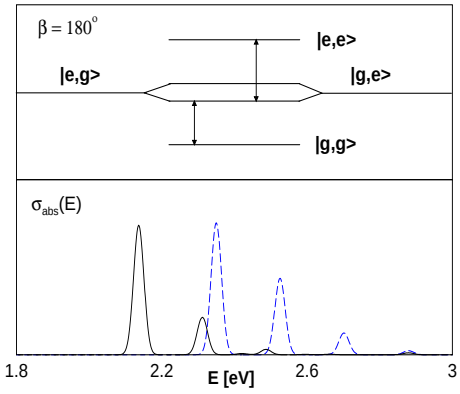

Figure 8.6: *Transition scheme and dimer absorption spectrum (solid line) for the case of* $\beta = 180\,^\circ$. *The monomer absorption spectrum is also shown (blue line).*

The transition schemes in Fig. (8.5) and Fig. (8.6) show a situation, where the electric fields couple the electronic ground state $|g, g\rangle$ with the accessible 1-exciton states $|n, e\rangle$ and the latter with the 2-exciton state $|e, e\rangle$, respectively. As in the case of $\beta = 0\,^\circ$ only transitions to the upper band of the singly excited states are possible, one would expect only such diagonal peaks in the 2D-spectrum which are shifted to higher energies. The transition scheme from the left side of Fig. (8.7) can be understood as a combination of stimulated emission and ground state bleaching. The corresponding peaks have negative values (indicated by the color red), which is characteristic for such processes [88]. This contribution can be related to the first term in Eq. (4.50). Additional cross peaks at lower ω_t -values stem from transitions between singly and doubly excited states. In the panel on the right side of Fig. (8.7), the black arrow symbolizes the transition from the ground state to the upper 1-exciton state, which is induced by the first pulse and is related to the bra-vector $\left\langle \vec{\psi} \right|$. On the other hand, the red and the blue arrow illustrate the successive application of the excitation formalism containing the second and

the third pulse to the ket-vector $\left|\vec{\psi}\right\rangle$, which leads to a transition to the upper band of the singly excited state and subsequently to the doubly excited state. This kind of process is called excited state absorption and leads to positive peaks (indicated by the color blue). A transition between bra- and ket-state, which gives rise to the signal, is indicated by the green, dashed arrow. The formal expression for this contribution is given by the second term in Eq. (4.50).

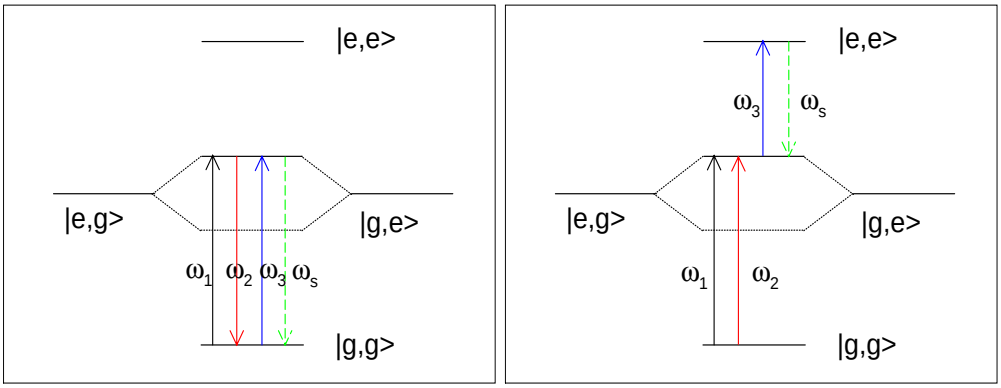

Figure 8.7: *Transition schemes leading to the upper diagonal peak group (left side) and to a cross peak group at lower ω_t (right side), respectively.*

The 2D-spectra shown in the upper and lower panel of Fig. (8.8) are obtained for a dimer model system without and with vibrations, respectively. This allows to investigate the influence of the electronic level structure without including vibrations. The deviations of the 2D-spectrum of the complete model system compared to the the results for the simplified model stem from connection between vibrational and electronic excitation (exciton-phonon-coupling).

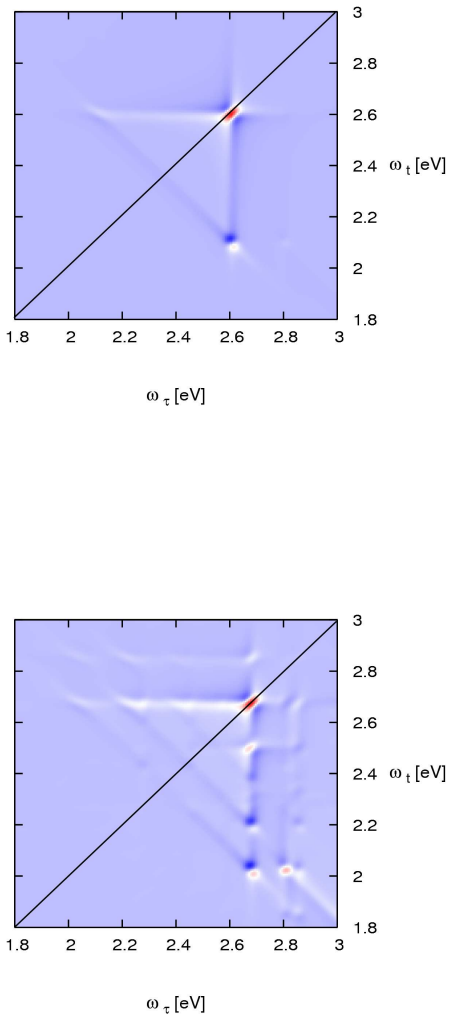

Figure 8.8: *Two-dimensional dimer spectra* ($J = 0.25\,\mathrm{eV}$, $\beta = 0\,^\circ$, $\Delta\omega = 0.033\,\mathrm{eV}$) *without and with vibrations are shown in the upper and lower panel, respectively.*

As indicated by the linear absorption-spectrum, in the case of $\beta = 180°$ only transitions to the lower band of the singly exciton state are possible. The transition scheme which leads to a diagonal peak group in the upper half of the band splitting energy range is illustrated in the left hand panel of Fig. (8.9). Again, stimulated emission and ground state bleaching are involved and, therefore, the corresponding peaks have a negative sign. In order to outline the transition scheme, which gives rise to cross peaks at higher ω_t -values, the right hand panel of Fig. (8.9) is shown. This is an excited state absorption process, which leads to positive peaks. Again, the processes illustrated on the left and the right side correspond to the first and the second term in Eq. (4.50)

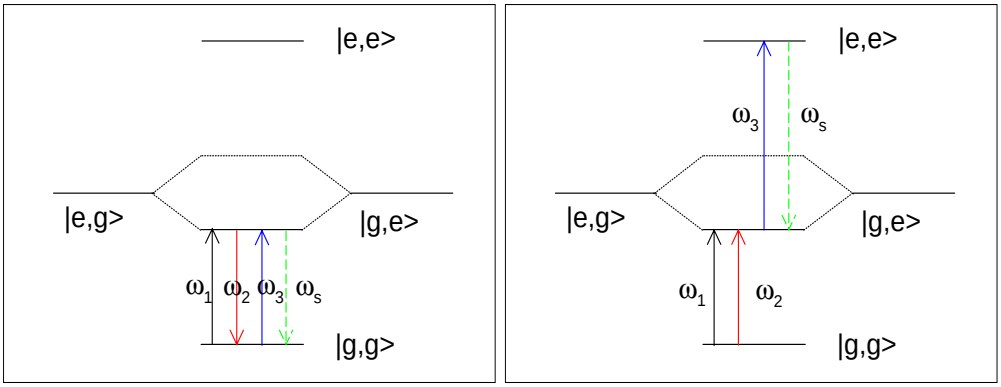

Figure 8.9: *Transition schemes leading to the lower diagonal peak group (left side) and to a cross peak group at higher ω_t (right side), respectively.*

In analogy to Fig. (8.8), the corresponding 2D-spectra are shown in Fig. (8.10).

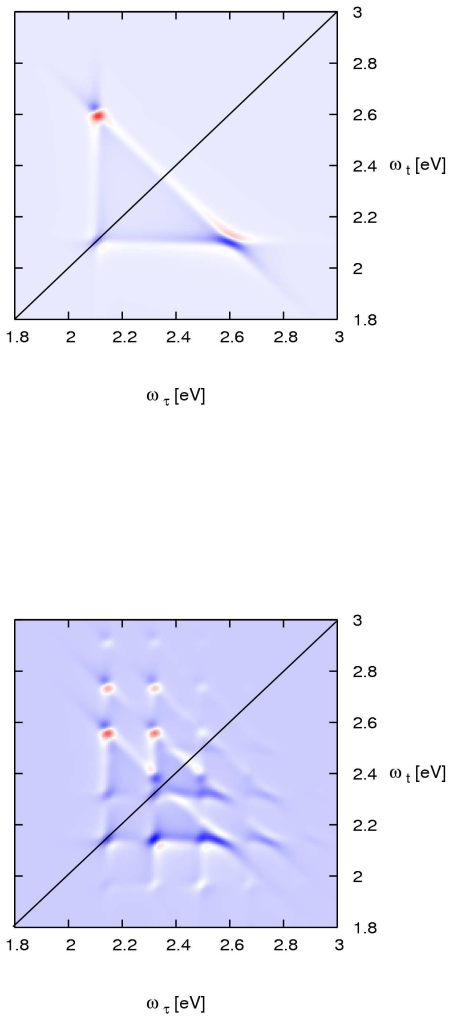

Figure 8.10: *Two-dimensional dimer spectra ($J = 0.25\,\mathrm{eV}$, $\beta = 180\,^\circ$, $\Delta\omega = 0.033\,\mathrm{eV}$) without and with vibrations are shown in the upper and lower panel, respectively.*

In the case of orthogonal dipole moments ($\beta = 90\,^\circ$), the 2D-spectrum is expected to be a mixture of the spectra evolving from the two cases discussed above. Note, however, that here all vibrational states in all electronic states are coupled coherently so that the mixture is not meant to be an incoherent sum of the different signals. If the vibrational degrees of freedom are ignored, the 4-level calculation yields a spectrum with diagonal and cross peaks. A comparison between the spectra obtained from the simplified electronic level model in Fig. (8.11) and the complete spectrum in Fig. (8.12) demonstrates that a resolved vibrational progression results in a complicated pattern, which is not facile to interpret.

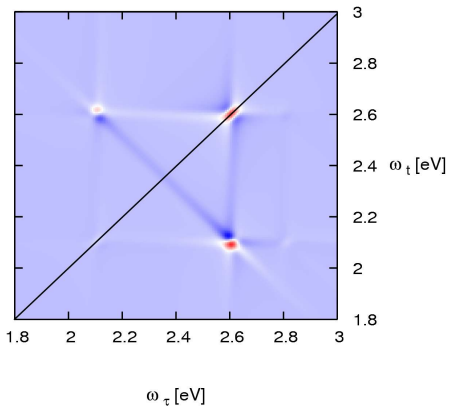

Figure 8.11: *Two-dimensional dimer spectrum ($J = 0.25\,\mathrm{eV}$, $\beta = 90\,^\circ$, $\Delta\omega = 0.033\,\mathrm{eV}$) without vibrations.*

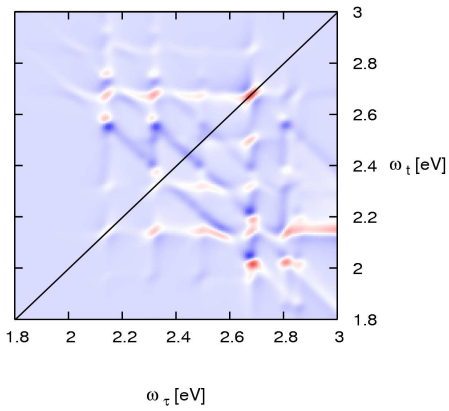

Figure 8.12: *Two-dimensional dimer spectrum ($J = 0.25\,\mathrm{eV}$, $\beta = 90\,^\circ$, $\Delta\omega = 0.033\,\mathrm{eV}$) with vibrations.*

Finally a model adapted to the PBI dimer aggregates is regarded, where a coupling element of $J = 0.092\,\mathrm{eV}$ and an orientation angle of $\beta = 27.5\,^\circ$ is employed. This corresponds to a case, where both absorption bands are excited, the one at lower energies being about half as intense as the one at higher energies. Two-dimensional spectra for the case of low resolution ($0.033\,\mathrm{eV}$) and higher resolution ($0.196\,\mathrm{eV}$) are compared in Figs. (8.13) and (8.14), respectively. In the first case, the spacing between vibrational peaks ($0.175\,\mathrm{eV}$ in the zeroth order picture) is comparable to the electronic level splitting ($0.184\,\mathrm{eV}$ eV) between the 1-exciton states. This makes it difficult to extract the coupling element. If the resolution is decreased, the vibrational progressions can no longer be resolved. The 2D-spectrum then exhibits a diffuse structure. Nevertheless, besides the diagonal peak around $2.5\,\mathrm{eV}$, there is a cross-peak roughly at $\omega_t = 2.15\,\mathrm{eV}$. If this peak is associated with a tran-

sition between the higher 1-exciton state and the 2-exciton state, a coupling element of $J = 0.175\,\mathrm{eV}$ is deduced. The reason for this deviation from the real value is rooted in the vibrationally broadened and strongly overlapping bands which makes the conventional method (rested on the simple four-level picture) fail (see the discussion given in Sec. (6.1)).

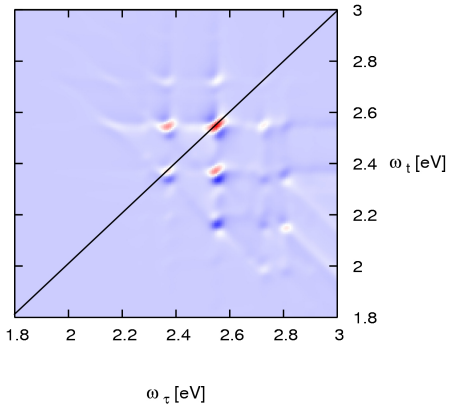

Figure 8.13: *Two-dimensional dimer spectrum ($J = 0.092\,\mathrm{eV}$, $\beta = 27.5\,^{\circ}$, $\Delta\omega = 0.033\,\mathrm{eV}$).*

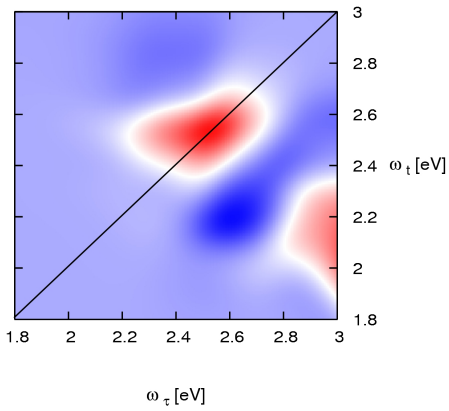

Figure 8.14: *Two-dimensional dimer spectrum* ($J = 0.092\,\mathrm{eV}$, $\beta = 27.5\,^\circ$, $\Delta\omega = 0.196\,\mathrm{eV}$*).*

Chapter 9

Outlook

An interesting topic for future research is the investigation of relaxation effects with respect to the intermolecular torsional coordinate by means of two-dimensional spectroscopy. For this aim, an appropriated relaxation algorithm has to be included in the calculation. By keeping the delay between the second and the third pulse constant on the picosecond time scale, relaxation effects can also be monitored in the experiment. A variation of the relaxation parameters in the calculations in order to reproduce measured spectra allows an interpretation of experimental results in terms of the underlying quantum dynamics. If an experimental spectrum is reproduced by calculations, the latter allow an insight into the wave-packet motion on an ultrafast time scale. In this context, also energetically low charge transfer potentials can be included. The data from quantum chemical calculations are already available and a diabatization of the potential curves has been performed. From such investigations, it can be figured out, to which extent charge transfer processes are involved in the excited state dynamics.
Furthermore, the theoretical analysis of spectroscopic properties of large aggregates such as supramolecular rings and helices could improve the under-

standing of excitation processes in these systems. If the structure of e. g. a ring of merocyanine units is known from molecular modeling calculations, the relevant parameters can be extracted using vector geometry. In the case of helices, vibrations can be neglected, and under this simplification, such systems can be traced back to the less complex model of a ring. In order to get information about the exciton migration along the stack, nonlinear spectroscopy using circular polarized light might be a helpful tool.

Chapter 10

Conclusion

In this work, the spectroscopic properties of molecular aggregates have been investigated. It was aimed to characterize the aggregates by means of electronic spectroscopy. Thereby absorption-, emission-, CD- and two-dimensional nonlinear spectra were regarded in order to obtain information about the geometrical arrangement of the transition dipole moments and the coupling between different excited configurations.

Initially, the reflexion principle as an approximation method was discussed, which yields the absorption spectrum as a map of the ground-state wave function. By applying the reflexion principle on the dimer problem, it was shown that an intuitive interpretation can be found. If a separation ansatz is employed, the center-of-mass and relative part are independent. Then one finds that the relative part causes a band splitting, while the center-of-mass part is related to the line shape.

Afterwards, the dependence of linear absorption-, emission- and CD-spectra on the relative orientation of the monomer units was discussed. In the case of dimers, absorption- and CD-spectroscopy prove to be complementary investigation methods in a sense. While the first allows to determine the angle

between the transition dipole moments, the latter yields more accessible information about the coupling. In view of trimers and larger aggregates, linear and cyclic coupling scheme can be distinguished, where the relative intensity of the electronic bands emerges from a simplified model. The dependence of absorption- and CD-spectra on the angle between the transition dipole moments and the coupling was investigated by means of numerical calculations. Under certain assumptions, it is possible to draw conclusions about the relative orientation of the transition dipole moments from the band intensities. Compared to the absorption-spectra, a redshift is found in the fluorescence spectra, as the emission takes place from the coupled vibrational ground state in the energetically lowest band of the electronic excited state. Upon the involvement of vibrations, even dipole-forbidden transitions become weakly allowed, where the long radiative lifetime favors competing processes like *intersystem crossing*, which can lead to time-delayed phosphorescence, eventually.

The time-dependent approach, which was employed in this work, has the advantage that population and energy transfer processes can be investigated. Thereby the spectrum is obtained as the Fourier-transform of the time-correlation function, which corresponds to the projection of the propagated wave function onto the initial wave function. The connection between time-correlation function and spectrum is particularly recognizable in the case of CD-spectroscopy.

As an application, the relative orientation of the transition dipole moments in the merocyanine dimer was determined by the combined evaluation of absorption- and CD-spectra. Afterwards, the temperature dependence of perylene bisimide absorption- and CD-spectra was discussed. On the basis of calculations up to an aggregate size of 9 monomer units, it could be

concluded that the relative orientation of the transition dipole moments is continued in analogy to the dimer case and that the average aggregate size becomes smaller with decreasing temperature.

On the other hand, it was not possible to explain the large redshift of the emission-spectra on the basis of the previously employed model. If an additional intermolecular torsional coordinate is introduced though, a better agreement with the experimental data is obtained. The employed potentials stem from quantum chemical calculations. In order to calculate absorption- and emission-spectra, a thermal average is required, where the vibrational eigenfunctions of the ground state and the lower adiabatic excited state potential have to be weighted with the corresponding Boltzmann-factors. While in the case of absorption-spectra practically no difference is found compared to the model system without an intermolecular torsional coordinate, the emission-spectrum exhibits a band broadening and a remarkable redshift. Considering the topology of the potentials, one finds a large increase of the ground state potential around the minimum, which results in strongly localized vibrational eigenfunctions, large spacings between the corresponding eigenenergies and therefore small population of the higher excited eigenstates. In connection with the flat curvature of the excited state potentials, this leads to an energetically narrow absorption band according to the reflexion principle. Thus, the contribution of the torsional degree of freedom to the total spectrum is small. In the case of emission, though, especially the thermally excited vibrational wave functions in the lower adiabatic electronic excited state potential are strongly delocalized, so that the reflexion on the ground state potential, which exhibits a steep progression within the emission region, covers a broad energy range. The redshift of the emission-spectrum can be explained from the relatively small potential difference within the Franck-

Condon region.

Finally, calculations of vibronic 2D-spectra were performed. As opposed to the frequently employed density matrix formalism, the use of wave functions allows for a direct interpretation of the dynamics. Two-dimensional optical spectroscopy is based on the induction of a third-order polarization in a molecular system by three laser pulses, where the direction of the signal determines, which resonant transitions are induced by the respective laser pulses. By varying the delay time τ between the first and the second pulse as well as the acquisition time t after the third pulse, two dimensions are obtained, which are related to the energy variables ω_τ and ω_t by Fourier transform. The 2D-spectrum is complex valued and consists of a reflective and an absorptive part. It contains, in general, diagonal and cross peaks, where the first yield no additional information compared to linear absorption-spectra, whereas the latter reflect additional couplings between ground and excited state vibronic levels. With the cross peaks, transfer processes become visible, which is especially interesting in the case of electronic couplings. As an application, monomer and dimer spectra were investigated by means of 2D-spectroscopy.

Upon the nonlinear spectroscopic technique, the dimer model has to be extended by introducing a doubly excited state. The angle β between the transition dipole moments determines, which peaks appear in the 2D-spectrum, if the coupling is fixed. Therefore the cases $\beta = 0\,^\circ$, $\beta = 90\,^\circ$ and $\beta = 180\,^\circ$ were investigated. On the one hand, a negative sign of the peaks hints to *ground state bleaching* and *stimulated emission*, on the other hand a positive sign indicates *excited state absorption*. In the latter case the doubly excited state is populated. For $\beta = 0\,^\circ$, only diagonal peaks related to the upper band and furthermore a group of cross peaks in the lower right area appear.

In the case of $\beta = 180\,^\circ$ one only obtains diagonal peaks related to the lower band and cross peaks with a negative sign above and with a positive sign below the diagonal. For an angle of $\beta = 90\,^\circ$, the interpretation of the resulting spectrum is difficult, as the previously mentioned cases enter there in terms of a coherent mixing.

Chapter 11

Zusammenfassung

In dieser Arbeit wurden die spektroskopischen Eigenschaften molekularer Aggregate untersucht. Das Ziel bestand darin, die Aggregate mittels elektronischer Spektroskopie zu charakterisieren. Dabei wurden Absorptions-, Emissions– , CD- und nichtlineare zweidimensionale Spektroskopie einbezogen, um Informationen über die geometrische Anordnung der Monomer-Einheiten sowie die Kopplung zwischen verschiedenen angeregten Konfigurationen zu erhalten.

Zunächst wurde als Näherungsmethode das sogenannte Reflexionsprinzip diskutiert, welches das Absorptionsspektrum als Abbild der Grundzustandswellenfunktion liefert. Durch Anwendung des Reflexionsprinzips auf das Dimer-Problem wurde eine anschauliche Interpretation der betreffenden Absorptionsspektren erhalten. Führt man einen Separationsansatz durch und trennt Schwerpunkts- und Relativanteil voneinander, so stellt man fest, dass im Rahmen der Näherung der Relativanteil ausschließlich eine Aufspaltung in separate Banden bewirkt, der Schwerpunktsanteil hingegen Einfluss auf die Bandenform hat.

Anschließend wurde die Abhängigkeit der linearen Absorptions-, Emissions-

und CD-Spektren von der relativen Orientierung der Monomer-Einheiten diskutiert. Im Fall von Dimeren erweisen sich Absorptions- und CD-Spektroskopie als in gewissem Sinn komplementäre Untersuchungsmethoden, wobei letztere Aufschluss über die Kopplung gibt, während sich aus den Absorptionsspektren der Winkel zwischen den Übergangsdipolmomenten der beiden Monomer-Einheiten einfacher bestimmen lässt. In Hinblick auf Trimere und größere Aggregate lassen sich ein lineares und ein zyklisches Kopplungsmuster unterscheiden, wobei die Intensität der elektronischen Banden aus einem vereinfachten Modell abgeschätzt werden kann. Anhand der numerischen Rechnungen wurde die Winkel- und Kopplungsabhänigkeit von Absorptions- und CD-Spektren untersucht. Unter bestimmten Annahmen ist es prinzipiell möglich, wie beim Dimer aus den relativen Bandenintensitäten Rückschlüsse auf die relative Orientierung der Monomer-Einheiten zu ziehen. Bei den Fluoreszenzspektren lässt sich eine Rotverschiebung gegenüber den Absorptionsspektren feststellen, da die Emission aus dem gekoppelten Schwingungsgrundzustand des energetisch niedrigsten Bandes im elektronisch angeregten Zustand erfolgt. Aufgrund der Schwingungsbeteiligung sind auch Dipol-verbotene Übergänge im Allgemeinen schwach erlaubt, wobei die große Lebensdauer im angeregten Zustand Konkurrenzprozesse wie *intersystem crossing* ermöglicht, was unter Umständen zu einer zeitlich verzögerten Phosphoreszenz führen kann.

Die in dieser Arbeit verwendete zeitabhängige Betrachtungsweise zeichnet sich dadurch aus, dass sich Populations- und Energietransferprozesse untersuchen lassen. Dabei wird das Spektrum durch Fouriertransformation einer Autokorrelationsfunktion berechnet, welche der Projektion der zeitlich entwickelten Wellenfunktion auf die Startwellenfunktion entspricht. Besonders deutlich kommt der Zusammenhang von Anregungstransfer und Spektrum

im Fall der CD-Spektroskopie zum Ausdruck.

Als Anwendungsbeispiel der Modellsysteme für Molekülaggregate wurde zunächst die relative Orientierung der Übergangsdipolmomente im Merocyanin-Dimer durch kombinierte Auswertung von Absorptions- und CD-Spektren bestimmt. Anschließend wurde die Temperaturabhängigkeit der Absorptions- und CD-Spektren von Perylenbisimiden untersucht. Anhand von Berechnungen bis zu einer Aggregatgröße von 9 Monomer-Einheiten konnte die Schlussfolgerung gezogen werden, dass die relative Orientierung der Übergangsdipolmomente in Analogie zum Dimer fortgesetzt wird und dass die mittlere Aggregatgröße mit sinkender Temperatur abnimmt.

Dagegen war es auf der Basis des bisher verwendeten Modells im Fall von Perylenbisimiden nicht möglich, die starke Rotverschiebung des gemessenen Emissionsspektrums zu erklären. Führt man jedoch zusätzlich eine intermolekulare Torsionskoordinate ein, so zeigt sich eine bessere Übereinstimmung mit den experimentellen Daten. Die verwendeten Potentiale wurden quantenchemisch bestimmt. Bei der Berechnung von Absorptions- und Emissionsspektren ist eine thermische Mittelung erforderlich, indem die Schwingungseigenfunktionen im Grundzustands- sowie im unteren adiabatischen Potential mit den entsprechenden Boltzmannfaktoren gewichtet werden. Während im Fall der Absorption praktisch kein Unterschied zu den Ergebnissen der Rechnungen für das Modellsystem ohne intermolekulare Torsionskoordinate besteht, zeigt sich im Emissionsspektrum eine Verbreiterung sowie eine deutliche Rotverschiebung. Betrachtet man den Potentialverlauf, so stellt man fest, dass das Grundzustandspotential im Bereich des Minimums steil verläuft und demzufolge auch die thermisch höher angeregten Wellenfunktionen stark lokalisiert sind. Darüber hinaus sind die höheren Schwingungseigenzustände aufgrund der relativ geringen Zustandsdichte ohnehin nur

schwach besetzt. Dies führt in Verbindung mit dem flachen Verlauf der Potentiale des angeregten Zustandes nach dem Reflexionsprinzip zu einer energetisch schmalen Absorptionsbande und somit zu einem geringen Beitrag der entsprechenden Mode zum Gesamtspektrum. Bei der Emission hingegen sind im unteren adiabatischen Potential des elektronisch angeregten Zustandes insbesondere die thermisch höher angeregten Wellenfunktionen stark delokalisiert, so dass deren Reflexion am Grundzustandspotential einen breiten Energiebereich abdeckt. Die Rotverschiebung des Emissionsspektrums lässt sich aus der relativ geringen Potentialdifferenz in der Franck-Condon-Region erklären.

Zuletzt wurden die Ergebnisse der Berechnung von vibronischen 2D-Spektren vorgestellt. Im Gegensatz zu dem sonst häufig verwendeten Dichtematrix-Formalismus ermöglicht die Verwendung von Wellenfunktionen eine direkte Interpretation der zeitlichen Dynamik. Die zweidimensionale optische Spektroskopie beruht auf der Induktion einer Polarisation dritter Ordnung in einem molekularen System durch drei eingestrahlte Laserpulse, wobei über die Detektionsrichtung festgelegt wird, welche resonanten Übergänge durch die jeweiligen Pulse herbeigeführt werden können. Durch Variation der Verzögerungszeit τ zwischen erstem und zweitem Puls sowie der Akquisitionszeit t nach Durchlaufen der Pulssequenz erhält man zwei Dimensionen, welche nach Fouriertransformation durch die Energievariablen ω_τ und ω_t beschrieben werden. Das 2D-Spektrum ist komplexwertig und setzt sich aus gebrochenem und absorbiertem Anteil zusammen. Es enthält im Allgemeinen Diagonal- und Crosspeaks, wobei die zuerst genannten keine zusätzliche Information gegenüber den Banden im linearen Absorptionsspektrum bieten, während letztere auf zusätzliche Kopplungen zwischen den vibronischen Niveaus von Grundzustand und angeregtem Zustand zurückzuführen sind. Anhand der

Crosspeaks werden Transferprozesse sichtbar gemacht, was insbesondere bei Auftreten elektronischer Kopplungen von Interesse ist.

Als Anwendung wurden die Modellsysteme für Monomer und Dimer mittels berechneter 2D-Spektren untersucht. Aufgrund der nichtlinearen Spektroskopietechnik muss das Dimer-Modell um einen doppelt angeregten Zustand erweitert werden. Der Winkel β zwischen den Übergangsdipolmomenten bestimmt bei vorgegebener Kopplung, welche Peaks im 2D-Spektrum auftreten. Daher wurden die Spezialfälle eines Winkels von $\beta = 0\,^\circ$, $\beta = 90\,^\circ$ und $\beta = 180\,^\circ$ untersucht. Anhand der Vorzeichen der Peaks erkennt man, dass einerseits *ground state bleaching* und *stimulated emission* (negatives Vorzeichen), andererseits aber auch *excited state absorption* -Prozesse (positives Vorzeichen) beteiligt sind. Bei letzteren wird der doppelt angeregte Zustand bevölkert. Im Fall $\beta = 0\,^\circ$ treten nur zum oberen Band gehörige Diagonalpeaks sowie eine Gruppe von Crosspeaks in der rechten unteren Hälfte auf. Für $\beta = 180\,^\circ$ erhält man nur zum unteren Band gehörige Diagonalpeaks sowie Crosspeaks, deren Vorzeichen oberhalb der Diagonale negativ, unterhalb der Diagonale positiv ist. Bei einem Winkel von $\beta = 90\,^\circ$ lässt sich das Ergebnis schwer interpretieren, da hier die beiden zuvor genannten Fälle in Form einer kohärenten Mischung eingehen.

Appendix A

A.1 Orientational average using the example of the dimer

For a simplified dimer system, which includes two coupled excited levels, the Hamiltonian reads

$$\hat{H}_e = \begin{pmatrix} E_d & J \\ J & E_d \end{pmatrix}. \tag{A.1}$$

In this formula, E_d and J denote the excited state energy level of the monomer units and the coupling matrix element, respectively. It can be diagonalized using the matrix

$$\hat{A} = \frac{1}{\sqrt{2}} \begin{pmatrix} 1 & 1 \\ -1 & 1 \end{pmatrix}. \tag{A.2}$$

Therefore, the time-correlation function can be written as

$$c_\mu(t) = \left\langle \hat{A}^T \vec{v} \right| \hat{A}^T \hat{U}_e \hat{A} \left| \hat{A}^T \vec{v} \right\rangle, \tag{A.3}$$

where

$$\vec{v} = \begin{pmatrix} f_1 \\ f_2 \end{pmatrix} = \begin{pmatrix} \left(\cos\left(\phi - \frac{\beta}{2}\right) + \sin\left(\phi - \frac{\beta}{2}\right)\right)\sin(\theta) \\ \left(\cos\left(\phi + \frac{\beta}{2}\right) + \sin\left(\phi + \frac{\beta}{2}\right)\right)\sin(\theta) \end{pmatrix} \tag{A.4}$$

includes the orientation of the dimer within the coordinate system, which is characterized by the angles ϕ and θ. The first describes rotations within the (x, y)-plane, whereas the latter indicates out-of-plane rotations around the x -axis. It is equal to zero if the symmetry plane of the dimer is parallel to the z -axis. Altogether, the result

$$c_\mu(t) = \frac{1}{2}\left((f_1 + f_2)^2 \exp(iJt) + (f_1 - f_2)^2 \exp(-iJt)\right) \tag{A.5}$$

is obtained. This means that the intensity of transitions to the upper band is given as

$$I_+ = \int_0^\pi d\theta \sin(\theta) \int_0^{2\pi} d\phi \, \frac{1}{2}(f_1 + f_2)^2, \tag{A.6}$$

while the intensity of transitions to the lower band reads

$$I_- = \int_0^\pi d\theta \sin(\theta) \int_0^{2\pi} d\phi \, \frac{1}{2}(f_1 - f_2)^2. \tag{A.7}$$

This leads to the expressions

$$\begin{aligned} I_\pm = {} & \frac{1}{2}\int_0^\pi d\theta \sin^3(\theta) \int_0^{2\pi} d\phi \\ & \left(\cos^2\left(\phi - \frac{\beta}{2}\right) \pm 2\cos\left(\phi - \frac{\beta}{2}\right)\sin\left(\phi - \frac{\beta}{2}\right) + \sin^2\left(\phi - \frac{\beta}{2}\right)\right. \\ & + \cos\left(\phi - \frac{\beta}{2}\right)\cos\left(\phi + \frac{\beta}{2}\right) \pm \cos\left(\phi - \frac{\beta}{2}\right)\sin\left(\phi + \frac{\beta}{2}\right) \\ & \pm \sin\left(\phi - \frac{\beta}{2}\right)\cos\left(\phi + \frac{\beta}{2}\right) + \sin\left(\phi - \frac{\beta}{2}\right)\sin\left(\phi + \frac{\beta}{2}\right) \\ & \left. + \cos^2\left(\phi + \frac{\beta}{2}\right) \pm 2\cos\left(\phi + \frac{\beta}{2}\right)\sin\left(\phi + \frac{\beta}{2}\right) + \sin^2\left(\phi + \frac{\beta}{2}\right)\right) \end{aligned} \tag{A.8}$$

For the evaluation of this expression, the following formulas are used:

$$\int_0^{\pi} d\theta \sin^3(\theta) = \frac{4}{3}, \tag{A.9}$$

$$\begin{aligned} \int_0^{2\pi} d\phi \cos^2\left(\phi - \frac{\beta}{2}\right) &= \int_0^{2\pi} d\phi \sin^2\left(\phi - \frac{\beta}{2}\right) \\ = \int_0^{2\pi} d\phi \sin^2\left(\phi + \frac{\beta}{2}\right) &= \int_0^{2\pi} d\phi \cos^2\left(\phi + \frac{\beta}{2}\right) = \pi, \end{aligned} \tag{A.10}$$

$$\begin{aligned} &\int_0^{2\pi} d\phi \cos\left(\phi - \frac{\beta}{2}\right) \sin\left(\phi - \frac{\beta}{2}\right) \\ &= \int_0^{2\pi} d\phi \cos\left(\phi + \frac{\beta}{2}\right) \sin\left(\phi + \frac{\beta}{2}\right) = 0, \end{aligned} \tag{A.11}$$

$$\int_0^{2\pi} d\phi \cos\left(\phi - \frac{\beta}{2}\right) \cos\left(\phi + \frac{\beta}{2}\right) = \pi \cos(\beta), \tag{A.12}$$

$$\int_0^{2\pi} d\phi \cos\left(\phi - \frac{\beta}{2}\right) \sin\left(\phi + \frac{\beta}{2}\right) = \pi \sin(\beta), \tag{A.13}$$

$$\int_0^{2\pi} d\phi \sin\left(\phi - \frac{\beta}{2}\right) \cos\left(\phi + \frac{\beta}{2}\right) = -\pi \sin(\beta), \tag{A.14}$$

$$\int_0^{2\pi} d\phi \sin\left(\phi - \frac{\beta}{2}\right) \cos\left(\phi + \frac{\beta}{2}\right) = \pi \cos(\beta). \tag{A.15}$$

This leads to the result

$$I_{\pm} = \frac{2}{3} 4\pi \left(1 \pm \cos(\beta)\right). \tag{A.16}$$

Employing the formulas

$$\cos(\beta) = \cos^2\left(\frac{\beta}{2}\right) - \sin^2\left(\frac{\beta}{2}\right) \tag{A.17}$$

and

$$1 = \cos^2\left(\frac{\beta}{2}\right) + \sin^2\left(\frac{\beta}{2}\right), \tag{A.18}$$

the relative intensities are given as

$$\frac{I_+}{I_-} = \frac{\cos^2\left(\frac{\beta}{2}\right)}{\sin^2\left(\frac{\beta}{2}\right)} = \frac{\left(f_1^2\left(\phi = 0, \theta = 0\right) + f_2^2\left(\phi = 0, \theta = 0\right)\right)}{\left(f_1^2\left(\phi = 0, \theta = 0\right) - f_2^2\left(\phi = 0, \theta = 0\right)\right)}. \tag{A.19}$$

Thus, just one orientation ($\phi = 0°$, $\theta = 90°$) has to be taken into account, as this yields the same ratio of the peak intensities as the rotational average.

A.2 Time-correlation functions of the trimer

In order to calculate the time-correlation functions entering into the equations of absorption-, emission- and CD-spectra, the trimer is placed in a $(x,\, y,\, z)$ -coordinate system. Thereby the transition dipole moment of the monomer unit in the middle lies at $z = 0$ and is parallel to the y -axis, whereas the outer monomer units are shifted along the positive and negative z -direction, respectively. Furthermore, the transition dipole moments of the latter are rotated in the $(x,\, y)$ -plane, so that $\vec{\mu}_1$ and $\vec{\mu}_2$ draw an angle β, while the angle between $\vec{\mu}_2$ and $\vec{\mu}_3$ is denoted as γ, see Fig. (A.1).

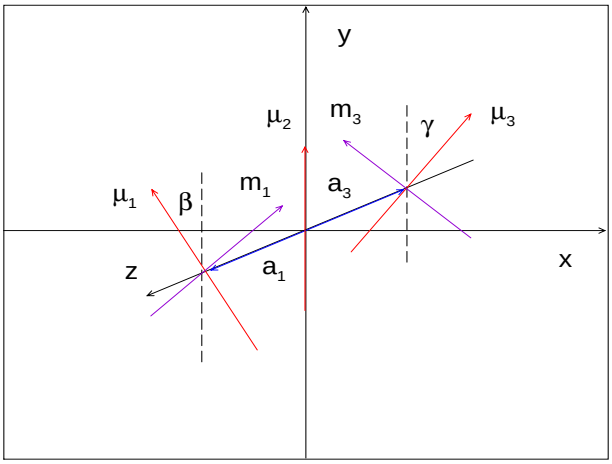

Figure A.1: *Orientation of the trimer transition dipole moments within the (x, y, z)-coordinate system.*

The relevant vectorial quantities read

$$\vec{\mu}_1 = \mu_1 \begin{pmatrix} -\sin(\beta) \\ \cos(\beta) \\ 0 \end{pmatrix}, \vec{\mu}_2 = \mu_2 \begin{pmatrix} 0 \\ 1 \\ 0 \end{pmatrix}, \vec{\mu}_3 = \mu_3 \begin{pmatrix} \sin(\gamma) \\ \cos(\gamma) \\ 0 \end{pmatrix}, \qquad \text{(A.20)}$$

$$\vec{a}_1 = a_1 \begin{pmatrix} 0 \\ 0 \\ 1 \end{pmatrix}, \vec{a}_2 = \begin{pmatrix} 0 \\ 0 \\ 0 \end{pmatrix}, \vec{a}_3 = a_3 \begin{pmatrix} 0 \\ 0 \\ -1 \end{pmatrix}, \tag{A.21}$$

$$\vec{m}_1 = ia_1\mu_1 \begin{pmatrix} \cos(\beta) \\ \sin(\beta) \\ 0 \end{pmatrix}, \vec{m}_2 = \begin{pmatrix} 0 \\ 0 \\ 0 \end{pmatrix}, \vec{m}_3 = ia_3\mu_3 \begin{pmatrix} -\cos(\gamma) \\ \sin(\gamma) \\ 0 \end{pmatrix}. \tag{A.22}$$

Thus, the decomposition of the time-correlation functions into the x - and y -components yields the results

$$c_{abs,x} = \left\langle \begin{pmatrix} -\sin(\beta)\,\mu_1 \\ 0 \\ \sin(\gamma)\,\mu_3 \end{pmatrix} \psi_g \middle| \hat{U}_e(t) \middle| \begin{pmatrix} -\sin(\beta)\,\mu_1 \\ 0 \\ \sin(\gamma)\,\mu_3 \end{pmatrix} \psi_g \right\rangle, \tag{A.23}$$

$$c_{abs,y} = \left\langle \begin{pmatrix} \cos(\beta)\,\mu_1 \\ \mu_2 \\ \cos(\gamma)\,\mu_3 \end{pmatrix} \psi_g \middle| \hat{U}_e(t) \middle| \begin{pmatrix} \cos(\beta)\,\mu_1 \\ \mu_2 \\ \cos(\gamma)\,\mu_3 \end{pmatrix} \psi_g \right\rangle, \tag{A.24}$$

$$c_{CD,x} = i \left\langle \begin{pmatrix} \cos(\beta)\,a_1\mu_1 \\ 0 \\ -\cos(\gamma)\,a_3\mu_3 \end{pmatrix} \psi_g \middle| \hat{U}_e(t) \middle| \begin{pmatrix} -\sin(\beta)\,\mu_1 \\ 0 \\ \sin(\gamma)\,\mu_3 \end{pmatrix} \psi_g \right\rangle, \tag{A.25}$$

$$c_{CD,y} = i \left\langle \begin{pmatrix} \sin(\beta)\,a_1\mu_1 \\ 0 \\ \sin(\gamma)\,a_3\mu_3 \end{pmatrix} \psi_g \middle| \hat{U}_e(t) \middle| \begin{pmatrix} \cos(\beta)\,\mu_1 \\ \mu_2 \\ \cos(\gamma)\,\mu_3 \end{pmatrix} \psi_g \right\rangle, \tag{A.26}$$

$$\begin{aligned} c_{em,x} &= \langle(-\sin(\beta)\,\mu_1\psi_{e,1} + \sin(\gamma)\,\mu_3\psi_{e,3})|\,\hat{U}_g(t) \\ &\quad |(-\sin(\beta)\,\mu_1\psi_{e,1} + \sin(\gamma)\,\mu_3\psi_{e,3})\rangle\,, \end{aligned} \tag{A.27}$$

$$\begin{aligned} c_{em,y} &= \langle(\cos(\beta)\,\mu_1\psi_{e,1} + \mu_2\psi_{e,2} + \cos(\gamma)\,\mu_3\psi_{e,3})|\,\hat{U}_g(t) \\ &\quad |(\cos(\beta)\,\mu_1\psi_{e,1} + \mu_2\psi_{e,2} + \cos(\gamma)\,\mu_3\psi_{e,3})\rangle\,. \end{aligned} \tag{A.28}$$

Within these equations, ψ_g denotes the vibrational ground state in the electronic ground state potential and the components of the coupled vibrational ground state wave functions in the electronic excited state are written as $\psi_{e,j},\ 1 \leq j \leq 3$. Altogether, in the case of absorption the total correlation function reads

$$\begin{aligned} c_{abs} &= c_{abs,x} + c_{abs,y} \\ &= \sin^2(\beta)\,\langle\mu_1\psi_g|\,\hat{U}_e(t)\,|\mu_1\psi_g\rangle - \sin(\beta)\sin(\gamma)\,\langle\mu_1\psi_g|\,\hat{U}_e(t)\,|\mu_3\psi_g\rangle \\ &\quad - \sin(\beta)\sin(\gamma)\,\langle\mu_3\psi_g|\,\hat{U}_e(t)\,|\mu_1\psi_g\rangle + \sin^2(\gamma)\,\langle\mu_3\psi_g|\,\hat{U}_e(t)\,|\mu_3\psi_g\rangle \\ &\quad + \cos^2(\beta)\,\langle\mu_1\psi_g|\,\hat{U}_e(t)\,|\mu_1\psi_g\rangle + \cos(\beta)\,\langle\mu_1\psi_g|\,\hat{U}_e(t)\,|\mu_2\psi_g\rangle \\ &\quad + \cos(\beta)\cos(\gamma)\,\langle\mu_1\psi_g|\,\hat{U}_e(t)\,|\mu_2\psi_g\rangle + \cos(\beta)\,\langle\mu_2\psi_g|\,\hat{U}_e(t)\,|\mu_1\psi_g\rangle \\ &\quad + \langle\mu_2\psi_g|\,\hat{U}_e(t)\,|\mu_2\psi_g\rangle + \cos(\gamma)\,\langle\mu_2\psi_g|\,\hat{U}_e(t)\,|\mu_3\psi_g\rangle \\ &\quad + \cos(\beta)\cos(\gamma)\,\langle\mu_3\psi_g|\,\hat{U}_e(t)\,|\mu_1\psi_g\rangle + \cos(\gamma)\,\langle\mu_3\psi_g|\,\hat{U}_e(t)\,|\mu_2\psi_g\rangle \\ &\quad + \cos^2(\gamma)\,\langle\mu_3\psi_g|\,\hat{U}_e(t)\,|\mu_3\psi_g\rangle\,. \end{aligned} \tag{A.29}$$

Under the assumption $\beta = \gamma$ and using the formulas $\cos^2(\phi) + \sin^2(\phi) = 1$ and $\cos^2(\phi) - \sin^2(\phi) = \cos(2\phi)$, the result

$$c_{abs}(t) = \sum_{(n,m)=1}^{3} \langle\mu_n\psi_g|U_e(t)|\mu_m\psi_g\rangle\cos((m-n)\,\beta) \tag{A.30}$$

is obtained. The expanded expression for the time-correlation function in the case of CD is given as

$$
\begin{aligned}
-ic_{CD} &= -ic_{CD,x} - ic_{CD,y} \\
&= -\sin(\beta)\cos(\beta)\, a_1 \langle \mu_1\psi_g| \hat{U}_e(t) |\mu_1\psi_g\rangle \\
&+ \sin(\beta)\cos(\gamma)\, a_3 \langle \mu_3\psi_g| \hat{U}_e(t) |\mu_1\psi_g\rangle \\
&+ \sin(\gamma)\cos(\beta)\, a_1 \langle \mu_1\psi_g| \hat{U}_e(t) |\mu_3\psi_g\rangle \\
&- \sin(\gamma)\cos(\gamma)\, a_3 \langle \mu_3\psi_g| \hat{U}_e(t) |\mu_3\psi_g\rangle \\
&+ \cos(\beta)\sin(\beta)\, a_1 \langle \mu_1\psi_g| \hat{U}_e(t) |\mu_1\psi_g\rangle \\
&+ \cos(\beta)\sin(\gamma)\, a_3 \langle \mu_3\psi_g| \hat{U}_e(t) |\mu_1\psi_g\rangle \\
&+ \sin(\beta)\, a_1 \langle \mu_1\psi_g| \hat{U}_e(t) |\mu_2\psi_g\rangle \\
&+ \sin(\gamma)\, a_3 \langle \mu_3\psi_g| \hat{U}_e(t) |\mu_2\psi_g\rangle \\
&+ \cos(\gamma)\sin(\beta)\, a_1 \langle \mu_1\psi_g| \hat{U}_e(t) |\mu_3\psi_g\rangle \\
&+ \cos(\gamma)\sin(\gamma)\, a_3 \langle \mu_3\psi_g| \hat{U}_e(t) |\mu_3\psi_g\rangle . \qquad \text{(A.31)}
\end{aligned}
$$

Employing the formula $2\cos(\phi)\sin(\phi) = \sin(2\phi)$ and assuming $\beta = \gamma$ yields the result

$$
-ic_{CD} = \sum_{(n,m)=1}^{3} a_n \langle \mu_n\psi_g|U_e(t)|\mu_m\psi_g\rangle \sin((m-n)\beta) \qquad \text{(A.32)}
$$

Finally, in the case of emission the total correlation function reads

$$
\begin{aligned}
c_{em} &= c_{abs,x} + c_{abs,y} \\
&= \sin^2(\beta) \langle \mu_1\psi_{e,1}| \hat{U}_e(t) |\mu_1\psi_{e,1}\rangle \\
&- \sin(\beta)\sin(\gamma) \langle \mu_1\psi_{e,1}| \hat{U}_e(t) |\mu_3\psi_{e,3}\rangle \\
&- \sin(\beta)\sin(\gamma) \langle \mu_3\psi_{e,3}| \hat{U}_e(t) |\mu_1\psi_{e,1}\rangle \\
&+ \sin^2(\gamma) \langle \mu_3\psi_{e,3}| \hat{U}_e(t) |\mu_3\psi_{e,3}\rangle \\
&+ \cos^2(\beta) \langle \mu_1\psi_{e,1}| \hat{U}_e(t) |\mu_1\psi_{e,1}\rangle
\end{aligned}
$$

$$
\begin{aligned}
&+ \quad \cos(\beta) \langle \mu_1 \psi_{e,1} | \hat{U}_e(t) | \mu_2 \psi_{e,2} \rangle \\
&+ \quad \cos(\beta) \cos(\gamma) \langle \mu_1 \psi_{e,1} | \hat{U}_e(t) | \mu_2 \psi_{e,2} \rangle \\
&+ \quad \cos(\beta) \langle \mu_2 \psi_{e,2} | \hat{U}_e(t) | \mu_1 \psi_{e,1} \rangle \\
&+ \quad \langle \mu_2 \psi_{e,2} | \hat{U}_e(t) | \mu_2 \psi_{e,2} \rangle \\
&+ \quad \cos(\gamma) \langle \mu_2 \psi_{e,2} | \hat{U}_e(t) | \mu_3 \psi_{e,3} \rangle \\
&+ \quad \cos(\beta) \cos(\gamma) \langle \mu_3 \psi_{e,3} | \hat{U}_e(t) | \mu_1 \psi_{e,1} \rangle \\
&+ \quad \cos(\gamma) \langle \mu_3 \psi_{e,3} | \hat{U}_e(t) | \mu_2 \psi_{e,2} \rangle \\
&+ \quad \cos^2(\gamma) \langle \mu_3 \psi_{e,3} | \hat{U}_e(t) | \mu_3 \psi_{e,3} \rangle . \qquad \text{(A.33)}
\end{aligned}
$$

Taking the assumptions and equations introduced above into account, the formula for the emission-spectrum reads

$$
c_{em}(t) = \sum_{(n,m)=1}^{N} \langle \mu_n \psi_{e,n} | U_g(t) | \mu_m \psi_{e,m} \rangle \cos((m-n)\beta) . \qquad \text{(A.34)}
$$

A.3 Alternative method for the calculation of four-wave mixing signals and two dimensional spectra

In the following section, the method proposed by Egorova, Gelin and Domcke [44, 55] adapted to a wave function description is given. Starting from the time dependent Schrödinger equation

$$i\frac{\partial}{\partial t}\left|\vec{\psi}\left(\lambda_1,\lambda_2,\lambda_3,t\right)\right\rangle = \left(\hat{H}_0+\hat{H}_{int}\left(\lambda_1,\lambda_2,\lambda_3,t\right)\right)\left|\vec{\psi}\left(\lambda_1,\lambda_2,\lambda_3,t\right)\right\rangle \quad \text{(A.35)}$$

with

$$\hat{H}_0 = \begin{pmatrix} \hat{H}_g & 0 \\ 0 & \hat{H}_e \end{pmatrix}, \quad \text{(A.36)}$$

$$\begin{aligned}\hat{H}_{int}\left(\lambda_1,\lambda_2,\lambda_3,t\right) = &-\left(X+X^+\right)\sum_{i=1}^{3}\lambda_i E_i\left(t-T_i\right)\exp\left(-i\left(\omega_i t-\vec{k}_i\vec{x}\right)\right)\\ &-\left(X+X^+\right)\sum_{i=1}^{3}\lambda_i E_i\left(t-T_i\right)\exp\left(+i\left(\omega_i t-\vec{k}_i\vec{x}\right)\right)\end{aligned} \quad \text{(A.37)}$$

and

$$\vec{\psi}\left(\lambda_1,\lambda_2,\lambda_3,t\right) = \begin{pmatrix} \left|\psi_g\left(\lambda_1,\lambda_2,\lambda_3,t\right)\right\rangle \\ \left|\psi_e\left(\lambda_1,\lambda_2,\lambda_3,t\right)\right\rangle \end{pmatrix} = \hat{U}\left(\lambda_1,\lambda_2,\lambda_3,t\right)\begin{pmatrix} \left|\psi_0\right\rangle \\ 0 \end{pmatrix}, \quad \text{(A.38)}$$

the extraction of the signal appearing in the direction

$$\vec{k}_s = -\vec{k}_1+\vec{k}_2+\vec{k}_3. \quad \text{(A.39)}$$

is required. For this aim, only the corresponding parts of the interaction Hamiltonian are taken into account, so it can be reduced to

$$\begin{aligned}\hat{H}_{int}\left(\lambda_1,\lambda_2,\lambda_3,t\right) &= -\lambda_1 E_1\left(t-T_1\right)\exp\left(+i\left(\omega_1 t-\vec{k}_1\vec{x}\right)\right)X\\ &-\lambda_2 E_2\left(t-T_2\right)\exp\left(-i\left(\omega_2 t-\vec{k}_2\vec{x}\right)\right)X^+\\ &-\lambda_3 E_3\left(t-T_3\right)\exp\left(-i\left(\omega_3 t-\vec{k}_3\vec{x}\right)\right)X^+,\end{aligned} \tag{A.40}$$

where the transition operator is defined as

$$X=\begin{pmatrix}0 & 1\\ 0 & 0\end{pmatrix}. \tag{A.41}$$

If the rotating wave approximation is not employed, the operators X and X^+, respectively, have to be replaced by $(X+X^+)$.

The wave function can be expanded into the Taylor series

$$\left|\vec{\psi}\left(\lambda_1,\lambda_2,\lambda_3,t\right)\right\rangle=\sum_{i,j,k=0}^{\infty}\lambda_1^i\lambda_2^j\lambda_3^k\left|\vec{\psi}^{ijk}\left(0,0,0,t\right)\right\rangle. \tag{A.42}$$

As the expansion with respect to λ_2 and λ_3 results in

$$\begin{aligned}\left|\vec{\psi}\left(\lambda_1,\lambda_2,\lambda_3,t\right)\right\rangle &= \left|\vec{\psi}^{00}\left(\lambda_1,0,0,t\right)\right\rangle+\lambda_2\left|\vec{\psi}^{10}\left(\lambda_1,0,0,t\right)\right\rangle\\ &+\lambda_3\left|\vec{\psi}^{01}\left(\lambda_1,0,0,t\right)\right\rangle+\lambda_2^2\left|\vec{\psi}^{20}\left(\lambda_1,0,0,t\right)\right\rangle\\ &+\lambda_3^2\left|\vec{\psi}^{02}\left(\lambda_1,0,0,t\right)\right\rangle+\lambda_2\lambda_3\left|\vec{\psi}^{11}\left(0,0,0,t\right)\right\rangle\\ &+O\left(\lambda_2^k\lambda_3^m\right),k+m>2,\end{aligned} \tag{A.43}$$

one finds

$$\lambda_2\lambda_3\left|\vec{\psi}^{11}\left(\lambda_1,0,0,t\right)\right\rangle=\left|\vec{\psi}\left(\lambda_1,\lambda_2,\lambda_3,t\right)\right\rangle+\left|\vec{\psi}\left(\lambda_1,0,0,,t\right)\right\rangle$$

$$
\begin{aligned}
&- \left|\vec{\psi}\left(\lambda_1, 0, \lambda_3, t\right)\right\rangle - \left|\vec{\psi}\left(\lambda_1, \lambda_2, 0, t\right)\right\rangle \\
&+ O\left(\lambda_2^k \lambda_3^m\right), k + m > 2. \qquad \text{(A.44)}
\end{aligned}
$$

In the next step, the Talor series with respect to λ_1

$$
\left|\vec{\psi}^{11}\left(\lambda_1, 0, 0, t\right)\right\rangle = \left|\vec{\psi}^{011}\left(0, 0, 0, t\right)\right\rangle + \lambda_1 \left|\vec{\psi}^{111}\left(0, 0, 0, t\right)\right\rangle + O\left(\lambda_1^2\right) \qquad \text{(A.45)}
$$

is considered, which leads to the result

$$
\lambda_1 \left|\vec{\psi}^{111}\left(0, 0, 0, t\right)\right\rangle = \left|\vec{\psi}^{11}\left(\lambda_1, 0, 0, t\right)\right\rangle - \left|\vec{\psi}^{11}\left(0, 0, 0, t\right)\right\rangle + O\left(\lambda_1^2\right). \qquad \text{(A.46)}
$$

Altogether the formula

$$
\begin{aligned}
&\lambda_1\lambda_2\lambda_3 \left|\vec{\psi}^{111}\left(0, 0, 0, t\right)\right\rangle = \left|\vec{\psi}\left(\lambda_1, \lambda_2, \lambda_3, t\right)\right\rangle + \left|\vec{\psi}\left(\lambda_1, 0, 0, t\right)\right\rangle \\
&- \left|\vec{\psi}\left(\lambda_1, 0, \lambda_3, t\right)\right\rangle - \left|\vec{\psi}\left(\lambda_1, \lambda_2, 0, t\right)\right\rangle \\
&- \left|\vec{\psi}\left(0, \lambda_2, \lambda_3, t\right)\right\rangle - \left|\vec{\psi}\left(0, 0, 0, t\right)\right\rangle \\
&+ \left|\vec{\psi}\left(0, 0, \lambda_3, t\right)\right\rangle + \left|\vec{\psi}\left(0, \lambda_2, 0, t\right)\right\rangle \\
&+ O\left(\lambda_1^n \lambda_2^k \lambda_3^m\right), n + m + k > 3 \qquad \text{(A.47)}
\end{aligned}
$$

is obtained.

With respect to the calculation of the third order polarization, this term is the only contribution to the total wave function, that has to be regarded. Thus, the resulting expression for the third order polarization reads

$$
\begin{aligned}
&\mathcal{P}\left(\lambda_1, \lambda_2, \lambda_3, t\right) \sim \left\langle \vec{\psi}\left(\lambda_1, \lambda_2, \lambda_3, t\right) |X| \, \vec{\psi}\left(\lambda_1, \lambda_2, \lambda_3, t\right)\right\rangle \\
&= \left\langle \vec{\psi}_{12^+3^+} - \vec{\psi}_{12^+} - \vec{\psi}_{13^+} + \vec{\psi}_1 - \vec{\psi}_{2^+3^+} + \vec{\psi}_{2^+} + \vec{\psi}_{3^+} - \vec{\psi}_0 \right| \\
&X \left|\vec{\psi}_{12^+3^+} - \vec{\psi}_{12^+} - \vec{\psi}_{13^+} + \vec{\psi}_1 - \vec{\psi}_{2^+3^+} + \vec{\psi}_{2^+} + \vec{\psi}_{3^+} - \vec{\psi}_0\right\rangle, \qquad \text{(A.48)}
\end{aligned}
$$

where the notation

$$\begin{aligned}
\left|\vec{\psi}_{12^+3^+}\right\rangle &= \left|\vec{\psi}\left(\lambda_1,\lambda_2,\lambda_3,t\right)\right\rangle \\
\left|\vec{\psi}_{12^+}\right\rangle &= \left|\vec{\psi}\left(\lambda_1,\lambda_2,0,t\right)\right\rangle \\
\left|\vec{\psi}_{13^+}\right\rangle &= \left|\vec{\psi}\left(\lambda_1,0,\lambda_3,t\right)\right\rangle \\
\left|\vec{\psi}_{1}\right\rangle &= \left|\vec{\psi}\left(\lambda_1,0,0,t\right)\right\rangle \\
\left|\vec{\psi}_{2^+3^+}\right\rangle &= \left|\vec{\psi}\left(0,\lambda_2,\lambda_3,t\right)\right\rangle \\
\left|\vec{\psi}_{2^+}\right\rangle &= \left|\vec{\psi}\left(0,\lambda_2,0,t\right)\right\rangle \\
\left|\vec{\psi}_{3^+}\right\rangle &= \left|\vec{\psi}\left(0,0,\lambda_3,t\right)\right\rangle \\
\left|\vec{\psi}_{0}\right\rangle &= \left|\vec{\psi}\left(0,0,0,t\right)\right\rangle
\end{aligned} \tag{A.49}$$

is used.

In order to solve the time dependent Schrödinger equation for the i -th wave function $\vec{\psi}_i\left(t\right), 1 \leq i \leq 8$, a specific interaction Hamiltonian $\hat{H}_{int,i}\left(t\right)$ is employed with

$$\begin{aligned}
\hat{H}_{int,1} &= -V_1(t) - V_2^+(t) - V_3^+(t) \\
\hat{H}_{int,2} &= -V_1(t) - V_2^+(t) \\
\hat{H}_{int,3} &= -V_1(t) - V_3^+(t) \\
\hat{H}_{int,4} &= -V_1(t) \\
\hat{H}_{int,5} &= -V_2^+(t) - V_3^+(t) \\
\hat{H}_{int,6} &= -V_2^+(t) \\
\hat{H}_{int,7} &= -V_3^+(t) \\
\hat{H}_{int,8} &= 0.
\end{aligned} \tag{A.50}$$

In this context, the pulse operators are denoted as

$$V_i(t) = \lambda_i \exp(i\omega_i t) E_i(t - T_i) X. \tag{A.51}$$

As the time evolution operator is not unitary, the conjugate transposed interaction Hamiltonian is needed for the propagation of the bra-vectors. Taking the condition

$$\mathcal{P}(\lambda_1, \lambda_2, \lambda_3, t) \sim \lambda_1\lambda_2\lambda_3 + O\left(\lambda_1^n \lambda_2^k \lambda_3^m\right), n + k + m > 3 \tag{A.52}$$

into account, only those matrix elements from the expansion of Eq. (A.48) have to be regarded, which contain each $\lambda_i, 1 \leq i \leq 3$ exactly once.
Therefore Eq. (A.48) can be simplified to

$$\begin{aligned}\mathcal{P}(\lambda_1, \lambda_2, \lambda_3, t) \sim &\left\langle \vec{\psi}_0 \right| X \left| \vec{\psi}_{12^+3^+} \right\rangle + \left\langle \vec{\psi}_{12^+} \right| X \left| \vec{\psi}_{3^+} \right\rangle \\ &+ \left\langle \vec{\psi}_{13^+} \right| X \left| \vec{\psi}_{2^+} \right\rangle + \left\langle \vec{\psi}_{2^+3^+} \right| X \left| \vec{\psi}_1 \right\rangle,\end{aligned} \tag{A.53}$$

where the first term corresponds to the contribution $\left\langle \vec{\psi}^{(0)} \right| X \left| \vec{\psi}^{(3)} \right\rangle$ and the remaining terms can be identified with the expression $\left\langle \vec{\psi}^{(2)} \right| X \left| \vec{\psi}^{(1)} \right\rangle$ appearing in the perturbative expansion of the third order polarization

$$P(t) = \mathcal{P}(t) + \mathcal{P}^*(t) = \sum_{n=0}^{3} \left\langle \vec{\psi}^{(n)} \right| X \left| \vec{\psi}^{(3-n)} \right\rangle. \tag{A.54}$$

While the term $\left\langle \vec{\psi}_{2^+3^+} \right| X \left| \vec{\psi}_1 \right\rangle = 0$ can be neglected, some corrections to the other terms are required to project out the contributions of lower order to the polarization.

This leads to the final result

$$P(\lambda_1,\lambda_2,\lambda_3,t) \sim \left\langle \vec{\psi}_0 \right| X \left| \vec{\psi}_{12^+3^+} - \vec{\psi}_{12^+} - \vec{\psi}_{13^+} \right\rangle + \left\langle \vec{\psi}_{12^+} - \vec{\psi}_0 \right| X \left| \vec{\psi}_{3^+} \right\rangle + \left\langle \vec{\psi}_{13^+} - \vec{\psi}_0 \right| X \left| \vec{\psi}_{2^+} \right\rangle . \tag{A.55}$$

In order to calculate two dimensional spectra, the delay between the central times of the first two pulses $\tau = T_2 - T_1$ is varied, while the delay between the second and the third pulse $T = T_3 - T_2$ is kept constant. Finally, a two dimensional Fourier-transformation yields the spectrum

$$S(\omega_\tau,\omega_t,T) = \int d\tau \int dt \exp\left(-i\omega_\tau\tau\right) \exp\left(i\omega_t t\right) \mathcal{P}\left(t,\tau,T\right). \tag{A.56}$$

Note that this method tends to numerical instabilities, as the interaction Hamiltonians are not Hermitian, and the propagators therefore are not unitary. In the case of the monomer, these effects do not become noticeable yet. As in the case of the dimer four electronic states are involved, the convergence strongly depends on the pulse intensity, where both too small and too large numerical values are problematic. As a result, one can conclude that the proposed method has advantages compared to the procedure proposed in Sec. (2) concerning the numerical effort (8 instead of 12 propagations), but is less appropriate for the calculation of nonlinear spectra of systems with more than two electronic levels such as molecular aggregates.

Bibliography

[1] M. Schwörer and H. C. Wolf, *Organische molekulare Festkörper, Einführung in die Physik von π-Systemen* (Wiley-VCH, Weinheim, 2005).

[2] F. Yang, M. Shtein, and S. R. Forrest, Nature Materials **4**, 37 (2005).

[3] C. W. Tang, Appl. Phys. Lett. **48**, 183 (1986).

[4] P. Peumans, S. Uchida, and S. R. Forrest, Nature **425**, 158 (2003).

[5] F. Würthner, Chem. Commun. , 1564 (2004).

[6] G. Stock and W. Domcke, Adv. Chem. Phys. **100**, 1 (1997).

[7] E. T. Kobayashi, *J-Aggregates* (World Scientific, Singapore, 1996).

[8] E. G. McRea and M. Kasha, *in: Physical Processes in Radiation Biology (L. Augenstein, B. Rosenberg, S. F. Mason (Eds.)* (Academic Press, New York, 1963, p. 23).

[9] R. L. Fulton and M. Gouterman, J. Chem. Phys. **35**, 1059 (1961).

[10] R. L. Fulton and M. Gouterman, J. Chem. Phys. **41**, 2280 (1964).

[11] P. O. J. Scherer and S. F. Fischer, Chem. Phys. **86**, 269 (1984).

[12] A. Eisfeld, L. Braun, W. T. Strunz, J. S. Briggs, J. Beck, V. Engel, J. Chem. Phys. **122**, 134103 (2005).

[13] P. Meystre and M. Sargent III, *Elements of Quantum Optics* (Springer, Berlin, 1991).

[14] H. Eiermann and M. Wagner, J. Chem. Phys. **105**, 6713 (1996).

[15] J. S. Briggs and A. Herzenberg, Mol. Phys. **21**, 865 (1971).

[16] A. Eisfeld and J. S. Briggs, Chem. Phys. **281**, 61 (2002).

[17] A. Eisfeld and J. S. Briggs, Chem. Phys. **324**, 376 (2006).

[18] E. J. Heller, Acc. Chem. Res. **14**, 368 (1981).

[19] R. Schinke, *Photodissociation Dynamics* (Cambridge University Press, Cambridge, 1993).

[20] N. E. Henriksen, Adv. Chem. Phys. **91**, 433 (1995).

[21] J. Manz, *in: Femtochemistry and Femtobiology: Ultrafast Reaction Dynamics at Atomic-Scale Resolution, V. Sundström (Ed.)* (Imperial College Press, London, 1996).

[22] N. Harada and K. Nakanishi, Acc. Chem. Res. **5**, 257 (1972).

[23] L. Barron, *Molecular Light Scattering and Optical Activity* (Cambridge University Press, Cambridge, 2004).

[24] E. U. Condon, Rev. Mod. Phys. **9**, 432 (1937).

[25] D. J. Caldwell and H. Eyring, *The Theory of Optical Activity* (Wiley, New York, 1971).

[26] S. Abbate, G. Longhi, K. Kwon, and A. Moscowitz, J. Chem. Phys. **108**, 50 (1998).

[27] J. Seibt and V. Engel, J. Chem. Phys. **126**, 074110 (2007).

[28] W. J. D. Beenken, M. Dahlbom, P. Kjellberg, and T. Pullerits, J. Chem. Phys. **117**, 5810 (2002).

[29] M. Bednarz, V. A. Malyshev, and J. Knoester, Phys. Rev. Lett. **91**, 217401 (2003).

[30] W. P. Aue, E. Bartholdi, and R. R. Ernst, J. Chem. Phys. **64**, 2229 (1976).

[31] R. R. Ernst, G. Bodenhausen, and A. Wokaun, *Principles of Nuclear Magnetic Resonance in One and Two Dimensions* (Clarendon Press, Oxford, 1987).

[32] P. Hamm, M. Lim, and R. M. Hochstrasser, J. Phys. Chem. B **102**, 6123 (1998).

[33] M. Khalil, N. Demirdöven, and A. Tokmakoff, J. Phys. Chem. A **107**, 5258 (2003).

[34] J. Brendebeck, J. Helbing, C. Kolano, and P. Hamm, Comput. Phys. Commun. **8**, 1747 (2007).

[35] J. D. Hybl, A. W. Albrecht, S. M. G. Faeder, and D. M. Jonas, Chem. Phys. Lett. **297**, 307 (1998).

[36] P. Tian, D. Keusters, Y. Suzaki, and W. S. Warren, Science **300**, 1553 (2003).

[37] M. L. Cowan, J. P. Ogilvie, and R. J. D. Miller, J. Chem. Phys. **386**, 184 (2004).

[38] T. Brixner, T. Mancal, I. Stiopkin, and G. R. Fleming, J. Chem. Phys. **121**, 4221 (2004).

[39] T. Brixner, J. Stenger, H. M. Vaswani, M. Cho, R. E. Blankenship, G. R. Fleming, Nature **434**, 625 (2005).

[40] W. M. Zhang and S. Mukamel, J. Chem. Phys. **110**, 5011 (1999).

[41] S. Mukamel and D. Abramavicius, Chem. Rev. **104**, 2073 (2004).

[42] D. Abramavicius, B. Palmieri, D. V. Voronine, F. Sanda, S. Mukamel, Chem. Rev. (unpublished).

[43] S. M. G. Faeder and D. M. Jonas, J. Phys. Chem. A **103**, 10489 (1999).

[44] D. Egorova, M. F. Gelin, and W. Domcke, J. Chem. Phys. **126**, 074314 (2007).

[45] V. Szöcs, T. Palszegi, A. Torschano, and H. F. Kauffmann, J. Chem. Phys. **116**, 8218 (2002).

[46] V. Szöcs, T. Palszegi, V. Lukes, J. Spering, F. Milota, W. Jakubetz, H. F. Kauffmann, J. Chem. Phys. **124**, 124511 (2006).

[47] F. Jensen, *Introduction to Computational Chemistry* (John Wiley, New York, 1999).

[48] R. G. Gordon, Adv. Mag. Resonance **3**, 1 (1968).

[49] E. Merzbacher, *Quantum Mechanics* (Wiley, New York, 1998).

[50] V. Engel, R. Schinke, S. Hennig, and H. Metiu, J. Chem. Phys. **92**, 1 (1990).

[51] E. U. Condon, Rev. Mod. Phys. **9**, 432 (1937).

[52] G. Ebel and R. Schinke, J. Chem. Phys. **101**, 1865 (1994).

[53] L. Seidner, G. Stock, and W. Domcke, J. Chem. Phys. **103**, 3998 (1995).

[54] S. Meyer and V. Engel, Appl. Phys. B **71**, 293 (2000).

[55] M. F. Gelin, D. Egorova, and W. Domcke, J. Chem. Phys. **123**, 164112 (2005).

[56] M. D. Feit, J. A. Fleck, and A. Steiger, J. Comput. Phys. **47**, 412 (1982).

[57] J. Alvarellos and H. Metiu, J. Chem. Phys. **88**, 4957 (1988).

[58] J. Stoer, *Numerische Mathematik, Vol II* (Springer, Berlin, 2000).

[59] R. Kosloff and H. Tal-Ezer, Chem. Phys. Lett. **127**, 223 (1986).

[60] M. H. Beck, A. Jäckle, G. A. Worth, and H.-D. Meyer, Phys. Rep. **324**, 1 (2000).

[61] V. May and O. Kühn, *Charge and Energy Transfer Dynamics in Molecular Systems* (Wiley-VCH, Berlin, 2000).

[62] O. Sinanoglu, editor, *Th. Förster in: Modern Quantum Chemistry III* (Academic Press, New York, 1965).

[63] J. N. Murrell and J. Tanaka, Mol. Phys. **7**, 634 (1964).

[64] V. Czikklely, H. D. Försterling, and H. Kuhn, Chem. Phys. Lett. **6**, 207 (1970).

[65] A. J. Stone, *The Theory of Intermolecular Forces* (Cambridge University Press, Oxford, 1996).

[66] O. E. Weigand, J. Chem. Phys. **43**, 71 (1965).

[67] G. Herzberg, *Spectra of Diatomic Molecules* (van Nostrand Reinhold, New York, 1950).

[68] J. Tellinguisen, *in: Photodissociation and Photoionization (K. P. Lawley, Ed.)*, third ed. (Wiley, New York, 1985).

[69] R. S. Mullikan, J. Chem. Phys. **55**, 309 (1971).

[70] E. J. Heller, J. Chem. Phys. **68**, 2066 (1978).

[71] E. J. Heller, J. Chem. Phys. **68**, 3891 (1978).

[72] I. Baraldi, F. Momicchioli, G. Ponterini, and D. Vanossi, Chem. Phys. **238**, 353 (1998).

[73] M. Sadrai, L. Hadel, R. R. Sauers, S. Husain, K. Krogh-Jespersen, J. D. Westbrook, G. R. Bird, J. Chem. Phys. **96**, 7988 (1992).

[74] U. Rösch, S. Yao, R. Wortmann, and F. Würthner, Angew. Chem., Int. Ed. Engl. **45**, 7026 (2006).

[75] K. Ikegamia and M. Lana, Coll. Surf. A **257-258**, 143 (2005).

[76] H. Langhals, Heterocycles **40**, 477 (1995).

[77] W. Herbst and K. Hunger, *Industrial Organic Pigments*, third ed. (Wiley-VCH, Weinheim, 2004).

[78] F. Würthner, C. Thalacker, A. Sautter, W. Schaertl, W. Ibach, O. Hollricher, Chem. Eur. J. **6**, 3871-3885 (2000).

[79] M. Michl and E. W. Thulstrup, *Spectroscopy with Polarized Light. Solute Alignment by Photoselection* (VCH, New York, 1986).

[80] J. Seibt, P. Marquetand, V. Engel, Z. Chen, V. Dehm, F. Würthner, Chem. Phys. **328**, 354 (2006).

[81] A. D. Becke, Phys. Rev. A **38**, 3098 (1988).

[82] C. Lee, W. Yang, and R. G. Parr, Phys. Rev. B **37**, 785 (1988).

[83] S. Grimme, J. Antony, T. Schwabe, and C. Mueck-Lichtenfeld, Org. Biomol. Chem. **5**, 741 (2007).

[84] R. F. Fink, J. Pfister, A. Schneider, H. Zhao, and B. Engels, Chem. Phys. **343**, 353 (2008).

[85] R. F. Fink, J. Pfister, H. Zhao, and B. Engels, Chem. Phys. **346**, 275 (2008).

[86] M. S. Child, *Molecular Collision Theory* (Dover Publications, Mineola, 1996).

[87] M. Cho, Chem. Rev. **108**, 1331 (2008).

[88] D. M. Jonas, Ann. Rev. Phys. Chem. **54**, 425 (2003).

List of publications

The results from this work have been published as:

1. J. Seibt, P. Marquetand, V. Engel, Z. Chen, V. Dehm, F. Wuerthner. On the geometry dependence of molecular dimer spectra with an application to aggregates of perylene bisimide, *Chem. Phys. 328*, *354-362 (2006)*.

2. S. Koller, J. Seibt, P. Marquetand, V. Engel. Application of a reflection principle to spectroscopic transitions in molecular dimers. *Chem. Phys. Lett. 433*, *199 (2006)*.

3. Z. Chen, V. Stepanenko, V. Dehm, P. Prins, L. D. A. Sibelles, J. Seibt, P. Marquetand, V. Engel, F. Wuerthner. Photoluminescence and Conductivity of Self-Assembled π - π Stacks of Perylene Bisimide Dyes, *Chem. Eur. J. 13 (2)*, *436-449 (2007)*.

4. J. Seibt, V. Engel. On the calculation of circular dichroism spectra using quantum wave-packet dynamics with an application to molecular dimers *J. Chem. Phys. 126*, *074110 (2007)*.

5. J. Seibt, V. Dehm, F. Wuerthner, V. Engel. Absorption spectroscopy of molecular trimers *J. Chem. Phys. 126*, *164308 (2007)*.

6. J. Seibt, V. Engel. Wave packet dynamics in molecular dimers *Chem. Phys. 338, 143 (2007).*

7. J. Seibt, A. Lohr, F. Wuerthner, V. Engel. Circular Dichroism and absorption spectroscopy of merocyanine dimer aggregates: molecular properties and exciton transfer dynamics from time-dependent quantum calculations *Phys. Chem. Chem. Phys. 9, 6214 (2007).*

8. J. Seibt, V. Engel. Absorption and emission spectroscopy of molecular trimers: cyclic versus linear geometries *Chem. Phys. 347, 120 (2008).*

9. J. Seibt, V. Dehm, F. Wuerthner, V. Engel. Circular dichroism spectroscopy of small molecular aggregates: Dynamical features and size effects *J. Chem. Phys. 128, 204303 (2008).*

10. J. Seibt, A. Schaumloeffel, C. Lambert, V. Engel. Quantum study of the absorption spectroscopy of bis(triarylamine) radical cations *J. Phys. Chem. A 112, 10178 (2008).*

11. R. Fink, J. Seibt, V. Engel, M. Renz, M. Kaupp, S. Lochbrunner, H.-M. Zhao, J. Pfister, F. Wuerthner, B. Engels. Exciton Trapping in pi-conjugated Materials: A Quantum-Chemistry Based Protocol Applied to Perylene Bisimide Dye Aggregates *J. Am. Chem. Soc. 130, 12858 (2008).*

12. A. Eisfeld, J. Seibt, V. Engel. On the inversion of geometric parameters from absorption and circular dichroism spectroscopy of molecular dimers *Chem. Phys. Lett. 467, 186-190 (2008).*

13. J. Seibt, K. Renziehausen, D. Voronine, V. Engel. Probing the geometry dependence of molecular dimers with 2D-vibronic spectroscopy *J. Chem. Phys. (2009), accepted for publication.*

Danksagung

An erster Stelle möchte ich mich bei Prof. Dr. Volker Engel für die hervorragende Betreuung während meiner Promotion bedanken. Er war jederzeit offen für Fragen und Anregungen, was meine Begeisterung für das Thema stets aufrecht erhielt.
Meinen Eltern bin ich für die Unterstützung während meines Studiums und der Promotion in vielerlei Hinsicht dankbar.
Bei Dr. Philipp Marquetand bedanke ich mich dafür, dass er mir sein umfangreiches Wissen zu diversen Computerprogrammen weitergegeben hat. Den anderen Mitgliedern unserer Arbeitsgruppe, Klaus Renziehausen, Robert Kritzer, Mirjam Falge und Alexander Schubert danke ich für die angenehme Atmosphäre, die gegenseitige Hilfsbereitschaft und die unkomplizierte Aufteilung der anfallenden Aufgaben wie beispielsweise der Betreuung von F-Praktikanten.
Diese brachten immer wieder Abwechselung und neue Impulse, was nicht zuletzt dem Fortschritt der eigenen Arbeit zugute kam. In dieser Hinsicht möchte ich mich auch bei den von mir betreuten Praktikanten Stephan Koller, Sebastian Östreicher, Kolja Theilacker, Kilian Hader und Theresa Winkler sowie bei unserer ehemaligen Diplomandin Anu Schaumlöffel bedanken.
Natürlich gab es auch oft etwas zu feiern, und für solche willkommenen Abwechslungen danke ich den Mitgliedern des Arbeitskreises von Prof. Dr.

Ingo Fischer. Denn Dr. Wolfgang Roth, Dr. Stefan Dümmler, Dr. Raman Maksimenka, Markus Margraf, Michael Schneider, Patrick Hemberger, Christof Schon, Bastian Noller, Juliane Köhler, Christoph Groß, Kathrin Fischer, Michael Steinbauer, Carolin Sobotta, Sonja Lindenmeier und Barbara Buchner trugen entscheidend dazu bei, dass auf unserem Stockwerk keine Langeweile aufkam.

In diesem Zusammenhang möchte ich auch den Leiter des physikalisch-chemischen Praktikums Dr. Colditz nicht unerwähnt lassen, der die Runde am Mittagstisch stets mit anregenden Diskussionen und Anekdoten zu unterhalten wusste.

Und für die Hilfsbereitschaft bei Anträgen, Formalitäten und alltäglichen Problemen möchte ich mich bei unseren Sekretärinnen Frau König und Frau Mühlrath bedanken.